RELATIONSHIPS BETWEEN IMAGE-BASED AND MECHANICAL BONE PROPERTIES WITH PAIN IN KNEE OSTEOARTHRITIS

A Thesis Submitted to the College of
Graduate and Postdoctoral Studies
In Partial Fulfillment of the Requirements
For the Degree of Doctor of Philosophy
In the Division of Biomedical Engineering
University of Saskatchewan
Saskatoon

By

WADENA DELSIE BURNETT

PERMISSION TO USE

In presenting this thesis in partial fulfillment of the requirements for a Postgraduate degree from the University of Saskatchewan, I agree that the Libraries of this University may make it freely available for inspection. I further agree that permission for copying of this thesis/dissertation in any manner, in whole or in part, for scholarly purposes may be granted by the professor or professors who supervised my thesis/dissertation work or, in their absence, by the Head of the Department or the Dean of the College in which my thesis work was done. It is understood that any copying or publication or use of this thesis/dissertation or parts thereof for financial gain shall not be allowed without my written permission. It is also understood that due recognition shall be given to me and to the University of Saskatchewan in any scholarly use which may be made of any material in my thesis.

Requests for permission to copy or to make other uses of materials in this thesis/dissertation in whole or part should be addressed to:

Head of the Division of Biomedical Engineering
Room 2B60, 57 Campus Drive
University of Saskatchewan
Saskatoon, Saskatchewan S7N 5A9
Canada

OR

Dean
College of Graduate and Postdoctoral Studies
University of Saskatchewan
116 Thorvaldson Building, 110 Science Place
Saskatoon, Saskatchewan S7N 5C9
Canada

ABSTRACT

Pain is the predominant symptom of OA, a debilitating disease marked by changes in cartilage and subchondral bone, but pain pathophysiology is poorly understood. Bone is densely innervated and may be linked to OA-related knee pain. Quantitative computed tomography (QCT) is an *in vivo* image-based technique with the potential to quantify bone mineral density (BMD) to explore the role of bone in OA-related pain. When coupled with subject-specific finite element (FE) modeling, it may be possible to clarify the mechanical role of bone in OA-related knee pain.

The objectives of this study were to assess if: 1) tibial subchondral BMD is associated with OA-related nocturnal knee pain using depth-specific QCT image processing, 2) tibial epiphyseal and metaphyseal BMD is associated with OA-related knee pain using a modified depth-specific CT image processing tool, 3) subchondral cyst characteristics are associated with OA-related knee pain, and 4) FE-derived mechanical outcomes at the proximal tibia are associated with OA-related pain.

Lateral focal subchondral BMD was 33% higher in participants with severe nocturnal pain than participants with no nocturnal pain at the 2.5-5mm depth (p=0.028) and 32% higher at 5-10mm from the subchondral surface (p=0.049). At the epiphyseal and metaphyseal depths, higher total pain was associated with lower medial epiphyseal BMD (R^2=-0.40, p=0.002), and lower metaphyseal BMD (R^2=-0.35, p=0.017). At the lateral region, subchondral cyst number (ρ=0.55, p<0.001) and cyst number per proximal tibial volume (ρ=0.52, p<0.001) were both associated with BMD, and lateral cyst number and volume were associated with joint space narrowing (ρ=0.52 to 0.68, p<0.001) and alignment (ρ=0.44 to 0.62, p<0.001). In our FE study, principal compressive stress was associated with nocturnal pain at most lateral regions (ρ=0.33 to 0.50, p<0.05). Principal compressive stress at the lateral region ranged from 47% to 67% higher (p<0.05) in participants with severe nocturnal pain than participants with no pain.

This series of studies suggests that pain in patients with knee OA may be associated with BMD throughout various depths at the proximal tibia as well as FE-based bone mechanical outcomes, such as principal compressive stress. These findings suggest previously unexplored associations between OA-related knee pain and BMD or mechanical outcomes, emphasizing that bone may have a mechanical role in OA-related pain pathogenesis.

ACKNOWLEDGEMENTS

Thank you to my supervisors, Dr. JD Johnston and Dr. Saija Kontulainen, for providing me with a supportive research environment and the opportunity to grow with such a motivated, team. Thank you for letting me explore as many opportunities as I could and for providing me with a place where I knew I was always welcome to return.

Thank you to my Advisory Committee: Dr. Allan Dolovich, Dr. David Hunter, Dr. Stephan Milosavljevic, and Dr. David Wilson; and to my External Examiner: Dr. Gregory Wohl.

Thank you to my co-authors: Christine McLennan, Diane Hazel, and Dr. Carl Talmo.

Thank you to Hanieh Arjmand for your dedication to our finite element work. Your willingness to teach me how they all came together made all the difference.

Thank you to my research group. It's been a pleasure to work with individuals with so many unique perspectives, in and out of research.

Thank you to my many research and teaching mentors: Dr. Emily McWalter, Dr. Steve Machtaler, Dr. David Cooper, Dr. Terry Fonstad, Dr. Brian Eames, Tracy Walker, Dr. Joyce McBeth, Dr. Joel Frey, Dr. Lisa Feldman, Dr. Joy Agnew, Dr. Jim Bugg, Dr. Sean Maw, Debbie Rolfes, Noreen Predicala, and Dr. Bruce Sparling.

Thanks to Liv Marken and the Writing Centre for providing me with opportunities leading to my growth as a writer.

Thanks to Victoria Martinez and the Outreach Team at CLS for sparking my love for science communication and knowledge translation.

Thanks to Meena, my sister-from-another-mister. We kept each other focused, and for that I am eternally grateful.

Thanks to Shaun, my Superman and my partner in conventions, concerts, and comics.

Thanks to my family: Mom, Dad, Wyatt, Chelsey, but especially to Porter and Weston. You kept me grounded when things got rough, and you were always there for support.

I would like to acknowledge funding from the Canadian Arthritis Network, the Division of Biomedical Engineering, the College of Engineering, Natural Sciences and Engineering Research Council of Canada, that Canadian Institutes for Health Research, the College of Graduate Studies and Research, and the Canadian Federation of University Women—Saskatoon Branch.

PREFACE

Sections of this thesis have been submitted as multi-authored papers in refereed journals or as chapters of books. Trained technicians carried out computed tomography imaging, and participating orthopaedic surgeons and clinicians performed clinical diagnoses. Dr. JD Johnston developed and modified depth-specific image processing technique, and Hanieh Arjmand and Dr. Majid Nazemi developed finite element modeling processes and material mapping programs, with input and guidance by myself. I performed data analysis and manuscript preparation, and co-authors contributed in statistical guidance and editing the manuscripts for submission to refereed journals and subsequent revisions.

Published Papers:

1. Burnett WD, Kontulainen SA, McLennan CE, Hazel D, Talmo C, Hunter DJ, Wilson DR, Johnston JD. Knee osteoarthritis patients with severe nocturnal pain have altered tibial subchondral bone mineral density. *Osteoarthritis & Cartilage*. 2015; 23(9): 1483-1490. Epub April 20, 2015.

   Authors' contribution: Dena Burnett carried out the image processing, contributed to statistical analysis and interpretation of data, and composed the draft manuscript. Dr. Saija Kontulainen contributed to statistical analysis and interpretation of data. Christine McLennan contributed to study design and acquisition of patient data. Diane Hazel contributed to coordination of the study and acquisition of patient data. Dr. Carl Talmo contributed to study design, participant recruitment and acquisition of patient data. Dr. David Hunter contributed to study design and coordination. Dr. David Wilson contributed to study design. Dr. JD Johnston conceived the study, assisted in image processing, and interpretation of data. This research is discussed in **Chapter 4** of this thesis.

   The results of this study were presented at local and international conferences:

   i. American Society of Bone and Mineral Research Annual Meeting. Houston, TX, September 12-15, 2014. Poster No. MO0204
   ii. Bone Imaging Group Research Day. Saskatoon, SK. January 24, 2014.

iii. University of Saskatchewan Life and Health Sciences Research Day. Saskatoon, SK. March 14, 2014. *Awarded First Place Poster – Imaging Group*

2. Burnett WD, Kontulainen SA, McLennan CE, Hazel D, Talmo C, Wilson DR, Hunter DJ, Johnston JD. Proximal tibial trabecular bone mineral density is related to pain in patients with osteoarthritis. *Arthritis Research & Therapy*. 2017; 19(1): 200. Available September 12, 2017.

   Authors' contribution: Dena Burnett contributed in conceiving the study, carried out the image processing, contributed to statistical analysis and interpretation of data, and composed the draft manuscript. Dr. Saija Kontulainen contributed to statistical analysis and interpretation of data. Christine McLennan contributed to study design and acquisition of patient data. Diane Hazel contributed to coordination of the study and acquisition of patient data. Dr. Carl Talmo contributed to study design, participant recruitment and acquisition of patient data. Dr. David Wilson contributed to study design. Dr. David Hunter contributed to study design and coordination. Dr. JD Johnston conceived the study, assisted in image processing, and interpretation of data. This research is discussed in **Chapter 5** of this thesis.

   The results of this study were presented at international conferences:

   i. ISMRM Workshop on Imaging Based Measures of Osteoarthritis. Monterey, CA. September 12, 2015. Podium Presentation. *Awarded Highest Ranked Trainee Abstract.*

3. Johnston JD, Burnett WD, Kontulainen SA. Subchondral bone features and mechanical properties as biomarkers of osteoarthritis. In: VR Preedy (ed.) *Biomarkers in Bone Disease. Biomarkers in Disease: Methods, Discoveries and Applications*. Springer: Dordrecht. 2016. Epub July 19, 2016.

   Authors' contribution: Dr. JD Johnston drafted the manuscript. Dena Burnett performed literature review and assisted in drafting the manuscript. Dr. Saija Kontulainen assisted in

literature review and drafting the manuscript. Portions of this literature review are discussed in **Chapter 2** of this thesis.

Submitted Papers

1. Burnett WD, Kontulainen SA, McLennan CE, Hazel D, Talmo C, Wilson DR, Hunter DJ, Johnston JD. Knee osteoarthritis patients with more subchondral cysts have altered tibial subchondral bone mineral density. *BMC Musculoskeletal Disorders.* Submitted December 1, 2017.

   Authors' contribution: Dena Burnett contributed in conceiving the study, carried out the image processing, contributed to statistical analysis and interpretation of data, and composed the draft manuscript. Dr. Saija Kontulainen contributed to statistical analysis and interpretation of data. Christine McLennan contributed to study design and acquisition of patient data. Diane Hazel contributed to coordination of the study and acquisition of patient data. Dr. Carl Talmo contributed to study design, participant recruitment and acquisition of patient data. Dr. David Wilson contributed to study design. Dr. David Hunter contributed to study design and coordination. Dr. JD Johnston assisted in study conception and image processing, and interpretation of data. This research is discussed in **Chapter 6** of this thesis.

   The results of this study were and will be presented at local and international conferences:
   i. Alberta Biomedical Conference. Banff, AB. November 10-12, 2017. Podium Presentation.
   ii. American Society of Bone and Mineral Research Annual Meeting. Montreal, QC September 28-30, 2018. Abstract submitted April 11, 2018.

2. Burnett WD, Arjmand HA, McLennan CE, Hazel D, Talmo C, Wilson DR, Hunter DJ, Kontulainen SA, Johnston JD. Mechanical stress and strain at the proximal tibia are related to pain in patients with knee osteoarthritis: A subject-specific finite element study. Plan to submit to *Scientific Reports*, August 2018.

Authors' contribution: Dena Burnett contributed in conceiving the study, carried out the finite element analysis, contributed to statistical analysis and interpretation of data, and composed the draft manuscript. Hanieh Arjmand developed finite element modeling techniques, contributed to interpretation of data, and assisted in composing the draft manuscript. Dena Burnett and Hanieh Arjmand share first-authorship of this paper. Christine McLennan contributed to study design and acquisition of patient data. Diane Hazel contributed to coordination of the study and acquisition of patient data. Dr. Carl Talmo contributed to study design, participant recruitment and acquisition of patient data. Dr. David Wilson contributed to study design. Dr. David Hunter contributed to study design and coordination. Dr. Saija Kontulainen contributed to statistical analysis and interpretation of data. Dr. JD Johnston assisted in study conception and finite element modeling techniques, and interpretation of data. This research is discussed in **Chapter 7** of this thesis.

The results of this study were and will be presented at local and international conferences:

i. Alberta Biomedical Conference. Banff, AB. October 21-23, 2016. Poster Presentation.
ii. International Workshop on Osteoarthritis Imaging. Menton, France. July 5-8, 2018. Abstract to be submitted May 10, 2018.

3. Burnett WD, Kontulainen SA, Johnston JD. Image-based bone features and mechanical properties as biomarkers of osteoarthritis-related knee pain. Plan to submit to *Journal of Musculoskeletal and Neuronal Interactions*, August 2018.

Authors' contribution: Dena Burnett contributed to literature review and composed the draft manuscript. Dr. Saija Kontulainen assisted in literature review and drafting the manuscript. Dr. JD Johnston assisted in literature review and drafting the manuscript. Portions of this literature review are discussed in **Chapter 2** of this thesis.

TABLE OF CONTENTS

LIST OF TABLES

page

LIST OF FIGURES

page

LIST OF ABBREVIATIONS AND SYMBOLS

Abbreviation	Definition
2D	Two-dimensional
3D	Three-dimensional
aBMD	Areal bone mineral density (mg/cm^2)
Avg. Cyst.V	Average cyst volume
BMD	Bone mineral density(mg/cm^3)
BMI	Body mass index
BML	Bone marrow lesion
BV/TV	Bone volume fraction
CI	Confidence interval
CT-TOMASD	Computed tomography topographical mapping of subchondral density
Cyst.N	Cyst number
Cyst.N/TV	Cyst number per total volume
Cyst.V/TV	Cyst volume per total volume
$CV\%_{RMS}$	Root mean square coefficient of variations
DOF	Degrees of freedom
DXA	Dual energy x-ray absorptiometry, also DEXA
E-BMD	Density-modulus equations
FE	Finite element
FSA	Fractal signature analysis
HMH	Half maximum height
HR-pQCT	High-resolution peripheral quantitative computed tomography
HU	Hounsfield units
ICC	Intra-class correlation coefficient
JSN	Joint space narrowing
K_2HPO_4	Dipotassium phosphate
KL	Kellgren-Lawrence
KOOS	Knee Osteoarthritis Outcome Scale
M:L	Medial to lateral ratio

MANCOVA	Multivariate analysis of covariance
Max.Cyst.V	Maximum cyst volume
micro-CT	Micro-computed tomography
Min.Cyst.V	Minimum cyst volume
MR	Magnetic resonance
MRI	Magnetic resonance imaging
NS	Not significant
OA	Osteoarthritis
OARSI Atlas	Osteoarthritis Research Society International Radiographic Atlas
OR	Odds ratio
PF	Patellofemoral
pQCT	Peripheral quantitative computed tomography
QCT	Quantitative computed tomography
ROI	Region of interest
SD	Standard deviation
SD.Cyst.V	Cyst volume standard deviation
SE	Standard Error
TF	Tibiofemoral
Tot.Cyst.V	Total cyst volume
TKR	Total knee replacement
VAS	Visual analog scale
vBMD	Volumetric bone mineral density, same as BMD
VIF	Variance inflation factor
WOMAC	Western Ontario and McMaster Universities Osteoarthritis Index
WORMS	Whole-Organ Magnetic Resonance Imaging Score
X-ray	Radiographic image, or x-ray image

Symbol	Definition
p	P-value, level of significance
r	Pearson's correlation coefficient
β	Beta coefficient, or regression coefficient
τ	Thompson tao
ρ	Spearman's rank coefficient
ρ_{app}	Apparent density
ρ_{ash}	Ash density
ρ_{real}	Real density
R^2	Coefficient of determination
d	Depth
d_{ss}	Subject-specific depth
Δ	Change in, e.g., ΔR^2 is a change in coefficient of determination
E	Young's modulus, elastic modulus

GLOSSARY

TERM	DEFINITION
Areal bone mineral density	Bone mineral mass per unit area (aBMD)
Anisotropic	Material with different physical properties (e.g., material stiffness) in different directions.
Anterior	Front plane of a body; referring to surface facing forward.
Attrition	Flattening of cortical bone near articular surface of a joint.
Axial	Oriented along the long axis of the body.
Bone mineral density	Bone mineral mass per unit volume (BMD)
Bone marrow lesion	Region of increased signal in bone marrow on fat-suppressed T2-weighted MIR images.
Coronal	Plane that divides the body into anterior and posterior sections.
Cortical bone	Bone tissue referring to bone of the cortex or outer shell of bone.
Distal	Pertaining to the end of an extremity situated furthest from the center of a body (e.g., the distal femur is located at the tibiofemoral joint).
Epiphyseal	Pertaining to the epiphysis
Epiphysis	Region of bone between subchondral bone and epiphyseal plate (or line).
Ex vivo	Experiment done on a tissue out of its natural environment.
In vitro	Experiment taking place outside a living organism.
In vivo	Latin term for “within the living”; experiment using an entire living organism.
Inferior	Bottom plane of a body; referring to the bottom surface of region.

Isotropic	Object with equal dimensions in all directions (e.g., isotropic voxel); a material with similar physical properties (e.g., material stiffness) in all directions.
Joint space narrowing	Reported change in joint space width on radiographs.
Lateral	Located at or extending to the side.
Medial	Located at or extending to the center.
Metaphyseal	Pertaining to the metaphysis.
Metaphysis	Narrow region of bone between the epiphysis and the diaphysis (shaft).
Osteophyte	Bony projection that forms along the periphery of joints.
Patellofemoral joint	Joint comprised of articulating surfaces of the patella and the femur.
Peripheral	Located at the edge of a surface.
Pixel	A picture element; two-dimensional unit of a digital image.
Posterior	Back plane of a body; referring to a surface facing rearward.
Proximal	Pertaining to the end of an extremity situated nearest to the center of a body (e.g., the proximal tibia is located at the tibiofemoral joint).
Sagittal	Plane that divides a body into left and right portions.
Sclerosis	Region of increased bone mineral density as apparent on radiographs; stiffening of hardening of a structure.
Structural stiffness	Describes bone's response to deflection; dependent upon both material stiffness properties and displacement.
Subchondral bone	Bone region below cartilage; pertaining to the region of bone immediately adjacent to articular cartilage.
Subchondral cyst	Spherical of ellipsoidal cavities within the subchondral bone region.
Superior	Top plane of a body; referring to the top surface or region.

Tibiofemoral joint	Joint comprised of articulating surfaces of the tibia and the femur.
Trabecular bone	Bone tissue referring to bone with vertical or horizontal trabeculae, creating a spongy, cellular-like tissue; less dense than cortical bone.
Transverse	Plane that divides the body into superior and inferior sections; also referred to as the axial plane.
Valgus	Outward angulation of the distal segment of a bone or joint; synonymous with “knock-kneed”; opposite of varus.
Varus	Inward angulation of the distal segment of a bone or joint; synonymous with “bow-legged”; opposite of valgus.
Voxel	A volume element; three-dimensional unit corresponding to a pixel for a given slice thickness in CT images.

1. INTRODUCTION

1.1. Overview

Osteoarthritis (OA) is a painful debilitating disease characterized by cartilage degeneration and changes to the underlying subchondral bone[1, 2]. OA affects approximately 37% of Canadians aged 20 or older; of these, 29% experience knee pain[3], which can lead to diminished quality of life[4, 5]. Pain is the dominant symptom of OA, which often initiates clinical intervention, and pain reduction as the primary focus of most treatment strategies[1]. Unfortunately, the source of OA-related knee pain is poorly understood.

Knee OA is commonly characterized by cartilage degeneration and subchondral bone changes including osteophytes, sclerosis, attrition, subchondral cysts, bone marrow lesions (BML), altered bone mineral density (BMD), and altered morphology or mechanical properties. Cartilage is aneural and insensate[6], but subchondral bone is densely innervated[7, 8] and a plausible site for OA-related pain initiation. Bone can also be viewed and assessed using various clinical imaging techniques, such as X-rays, quantitative computed tomography (QCT), magnetic resonance imaging (MRI), and dual-x-ray absorptiometry (DXA), each permitting *in vivo* evaluation of the associations between these bony features and OA-related pain.

Multiple studies have investigated the relationship between image-based bone features and OA-related pain. Although there are many reported associations between bony features and OA-related knee pain[9-12], there are few consistent relationships between pain severity and bony feature severity. Alterations in BMD and the relationships between BMD and pain may be promising metrics to evaluate as it is associated with many other bony features, such as sclerosis[13], BMLs[14, 15], attrition[16], and subchondral cysts[17, 18], and can be evaluated using multiple imaging modalities.

Recent work using QCT-based depth-specific image processing at the patella[19, 20] has reported that OA patients with more severe pain at rest have lower BMD in trabecular regions of the patella. As tibial BMD is associated with OA severity[21-23], similar associations may present in subchondral cortical or trabecular bone at the tibia. Additionally, as commonly overlooked epiphyseal and metaphyseal trabecular bone is associated with OA severity[24], BMD at these regions may also have a role in OA-related pain pathogenesis. These alterations in subchondral[14, 22] and trabecular[23] bone during OA, may also alter the mechanical environment of the proximal

tibia. This could have an effect various structural elements, such as mechanical properties[25], loading patterns[26-28], or localized bone remodeling[29], each potentially relating to pain.

Subject-specific finite element (FE) modeling is a promising non-invasive image-based tool that can be used to investigate the structural role of bone in OA. Recent work in developing subject-specific FE models of the proximal tibia has shown differences in stress distributions through the proximal tibia of healthy participants and participants with OA[30, 31]. These same techniques could also be used to evaluate the relationship between mechanical outcomes and pain in OA patients. This work would aid in determining the mechanical role of bone in OA-related pain.

The overall aim of this dissertation research was to explore relationships between knee pain in patients with OA with QCT-based BMD at various depths of the proximal tibia (subchondral BMD, epiphyseal BMD, metaphyseal BMD, cysts) as well as FE-based mechanical outcomes (stress, strain, stiffness). Findings from this *in vivo* research will help to determine how mechanics environment may influence pain in OA, and may provide insight into OA-related pain pathogenesis.

1.2. Scope

Chapter 2 provides a review of current literature evaluating relationships between image-based bony features and OA-related knee pain, the relationship between BMD and mechanical environment of the proximal tibia, and the rationale behind this research. Chapter 3 includes my research questions, and objectives. Chapter 4 presents our study evaluating tibial subchondral BMD in patients with and without nocturnal knee pain. Chapter 5 describes our study exploring associations between proximal tibial epiphyseal and metaphyseal BMD and WOMAC pain. Chapter 6 describes our study exploring associations between proximal tibial cyst parameters (number, size, etc.) and characteristics of OA, including pain, as well as regional BMD. Chapter 7 presents our study using FE techniques to determine differences in mechanical outcomes (stress, strain, stiffness) between OA patients with and without nocturnal pain. Chapter 8 presents the overall contribution of this research, strengths, limitations, study conclusions, and recommendations for future research.

2. LITERATURE REVIEW

2.1. Functional Anatomy and the Knee Joint

The human knee is a complex joint composed of three bones: the proximal tibia, the distal femur, and the patella, and two distinct articulating joints: the patellofemoral (PF) joint and the tibiofemoral (TF) joint (Figure 2-1). The TF joint, which can be divided into medial and lateral plateaus (Figure 2-2), provides flexing and extending motion of the leg, and is also the main load-bearing joint within the knee. Load-bearing tissues at the knee joint include meniscus, cartilage, and bone. The knee is a commonly affected site for osteoarthritis (OA) with approximately 40-85% of cases occurring at the TF joint[32, 33], with ~50% of cases occurring at the medial compartment [33].

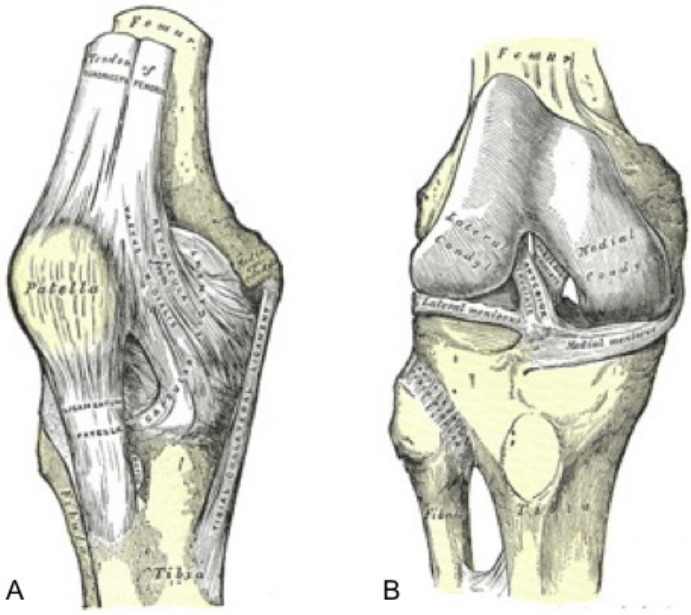

Figure 2-1 Anterior views of the bone of the knee joint, including the patella (A) and with the patella removed (B). Bones include the distal femur, proximal tibia, and proximal fibula. Modified from Grey's Anatomy[34].

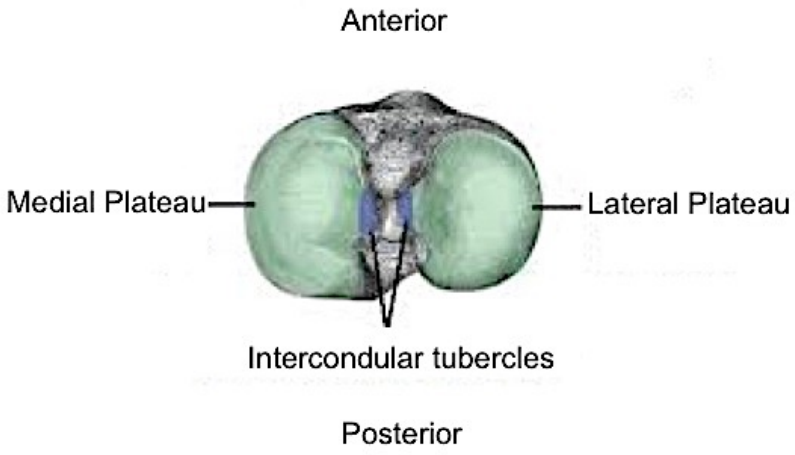

Figure 2-2. Anatomical features of the proximal tibia include the medial and lateral plateaus as well as the intercondylar tubercles (or tibial spine). Adapted from teachmeanatomy.com.

The meniscus is composed of two fibrous, C-shaped fibrocartilage wedges located between the articulating surfaces of the distal femur and proximal tibia (Figure 2-3). These structures are semi-rigidly attached to the medial and lateral proximal tibial surface and function to transfer and distribute load through the underlying articular cartilage during movement and loading[35, 36]. Approximately 50% of the load on the proximal tibia is distributed through the meniscus to articular cartilage[37, 38].

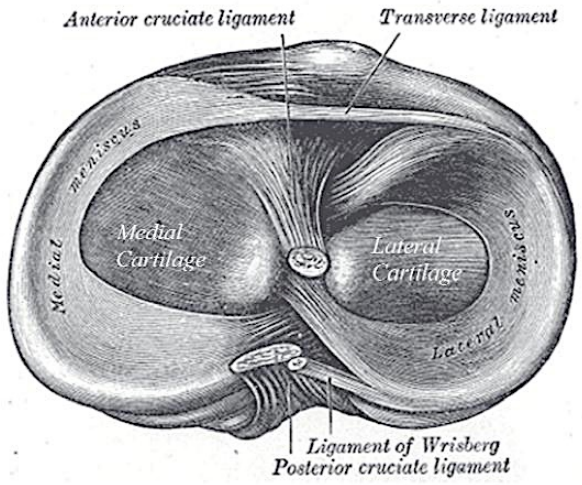

Figure 2-3. Axial view of the articulating surface of the proximal tibia, including medial and lateral menisci overlying articular cartilage. Modified from Grey's Anatomy[34]

The joint surfaces of the proximal tibia, distal femur, and patella are covered with articular cartilage: a viscoelastic, fibre-reinforced material serving as a low-friction surface bearing material able to transmit loads to the underlying subchondral bone. Cartilage is avascular[8] and aneural[7, 39], with consequently low levels of regeneration after damage or trauma.

Immediately adjacent to the articular cartilage at the proximal tibia, are various layers of bony tissues including[40]:

- the tidemark, a thin outer border of the articulating bone surface and the boundary between articular and calcified cartilage (Figure 2-4);
- calcified cartilage, a partially mineralized cartilage layer interconnected with subchondral bone (Figure 2-4);
- subchondral cortical bone (or subchondral plate or endplate), a thin layer of compact highly mineralized layer of bone (Figure 2-4, Figure 2-5);
- subchondral trabecular bone, a layer of cancellous (or trabecular) bone immediately adjacent to the subchondral cortical bone which supports the overlying cortical shell (Figure 2-4, Figure 2-5);
- epiphyseal trabecular bone, a layer of trabecular bone between the subchondral trabecular bone and the epiphyseal scar which forms the proximal tibial epiphysis (Figure 2-4, Figure 2-5);
- epiphyseal scar (or epiphyseal line), a faint to distinct line distinguishing the epiphyseal and metaphyseal regions of the proximal tibia as a remnant of the epiphyseal or childhood growth plate[41] (Figure 2-5); and
- metaphyseal trabecular bone, trabecular bone forming the proximal tibial metaphysis (Figure 2-5).

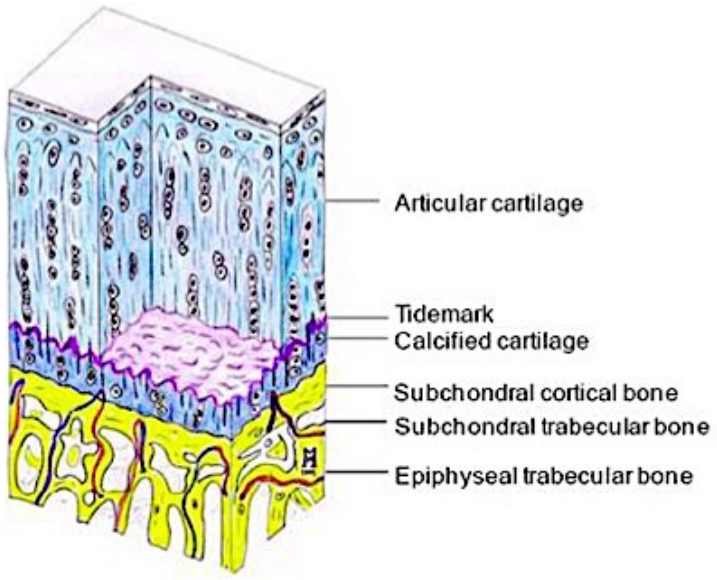

Figure 2-4. Representative diagram of the tissue layers of cartilage and subchondral bone regions, including articular cartilage, tidemark, calcified cartilage, subchondral cortical bone, subchondral trabecular bone, and epiphyseal trabecular bone. Adapted from Madry et al. (2010)[40].

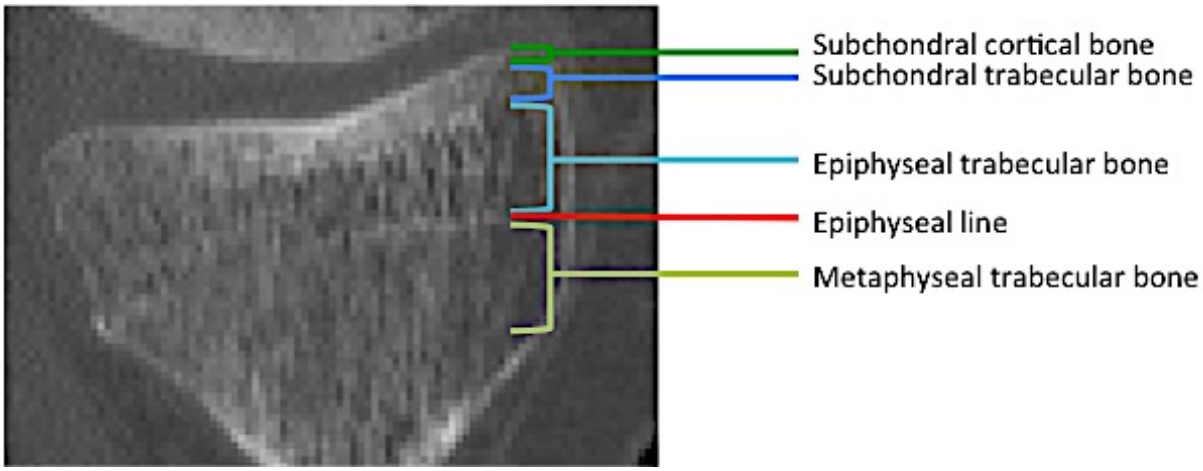

Figure 2-5. Computed tomography (CT) image in the sagittal plane of the proximal tibia including subchondral cortical bone, subchondral trabecular bone, epiphyseal line (epiphyseal scar)[41], epiphyseal trabecular bone, and metaphyseal trabecular bone.

"Subchondral bone" is a term used to describe the bony structure immediately adjacent to the articular cartilage, including both cortical and trabecular bone. This structure functions as the knee joint's primary supportive and energy-transferring structure[42]. Subchondral bone and cartilage both have a role in the development and pathogenesis of OA[42-45], but the distinct role and mechanical changes at various stages of disease severity still remains unknown. Additionally, bone at the epiphyseal and metaphyseal depths may be involved in OA development and progression[24], but their role or contribution are still unknown.

2.2. Osteoarthritis

Osteoarthritis (OA) is a degenerative joint disease affecting approximately 37% of Canadians over 20 years of age[3] and 85% of Canadians over 75 years of age[46]. OA is characterized by various clinical symptoms, such as joint pain, swelling, stiffness, and loss of function[45, 47-49], and morphological or physiological joint changes, such as cartilage degeneration, subchondral bone sclerosis, osteophyte presence, and changes in bone mineral density (BMD)[2, 47-50] (Figure 2-6). Pain is the dominant symptom of OA[51], but the source of OA-related pain is poorly understood. Unfortunately, OA is not typically detected or diagnosed until the patient begins to feel pain or joint discomfort, often after significant joint tissue damage.

OA is a complex disease involving many known and potential risk factors. Known risk factors can be systemic or biomechanical, and include: age, sex, hormonal status, bone metabolic biomarkers, joint mechanical environment, obesity, joint injury, and joint alignment[48]. As there is no known single risk factor, current disease management strategies focus on pain management, where treatments range along a spectrum from non-invasive pharmaceutical or physical interventions to invasive surgical joint replacements. It is very likely that OA onset and progression is a result of a combination of risk factors, therefore treatment strategies typically incorporate a variety of methods[1].

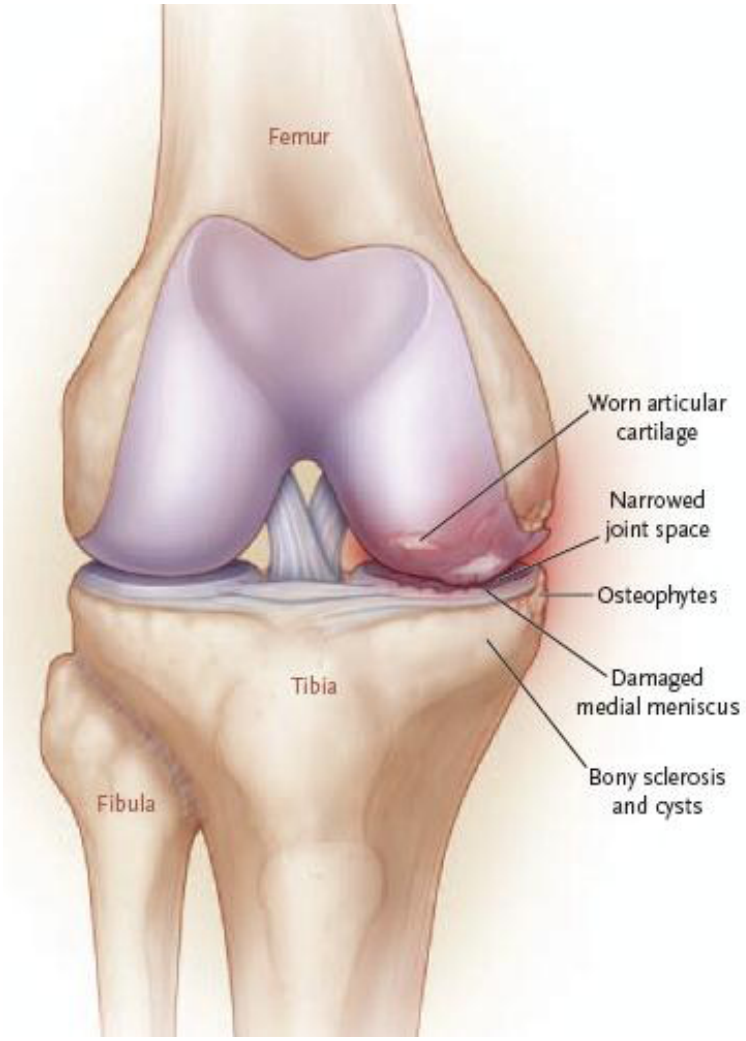

Figure 2-6. Characteristics of OA include cartilage wear, joint space narrowing, osteophytes, and sclerosis. Adapted from Felson 2006[1].

Disease characteristics include clinical symptoms, morphological changes, and biomechanical alterations to the joint environment. Symptoms can include a combination of pain, joint dysfunction, limited or reduced motion, swelling, or stiffness[1, 2]. Morphological changes to the joint environment may include articular cartilage loss, synovial inflammation, or subchondral bone alterations including sclerosis, osteophytes, attrition, cysts, or bone marrow lesions (BMLs)[10, 52-54]. Biomechanical changes include alterations in cartilage mechanical properties (lower compressive stiffness, lower shear stiffness, lower tensile stiffness)[55] and altered mechanical stiffness in subchondral bone[56] which could be the result of altered loading patterns[57, 58].

2.3. Clinical Classification and Diagnosis

OA is clinically assessed using semi-quantitative scales either focusing on radiographic (or structural) progression or symptomatic progression. Radiographic OA is commonly assessed using radiographic atlases, such as the Kellgren-Lawrence (KL) scale[59] or Osteoarthritis Research Society International Radiographic Atlas (OARSI Atlas)[60, 61], to evaluate and quantify evidence of visual radiographic changes, such as osteophyte presence, joint space narrowing, or sclerosis, within the knee joint. Symptoms of OA (e.g., pain, joint stiffness, inflammation, or loss of function) may or may not be present in all cases of radiographic OA[62]. For example, in a study of 6880 individuals, 14.6% reported knee pain but only 3.7% exhibited evidence of radiographic OA[62]. Of the individuals with radiographic OA, only 47% reported any symptoms; however, in those who reported symptoms, only 15% had radiographic evidence of OA. Severe radiographic OA may exist without pain or symptoms, and patients may experience painful symptoms of OA without radiographic evidence of severe OA[33, 62, 63]. The relationship between radiographic evidence of OA and related symptoms is unclear.

2.3.1. Imaging OA

Clinical imaging techniques currently used to assess OA and morphological OA-related characteristics include radiography or x-rays, dual-energy x-ray absorptiometry (DXA), magnetic resonance imaging (MRI), and computed tomography (CT).

2.3.1.1. Radiography and Radiographic OA

Radiographs are the most common and most accessible imaging tool to diagnose and measure OA severity. The most commonly used clinical radiographic OA scoring system is the KL scale[59] (Table 2-1). The KL system uses radiographic images to grade radiographic OA severity according to qualitative, subjective assessments of sclerosis, osteophyte presence and size, and joint space narrowing (JSN). A KL score of 0 indicates no OA, a score of 1-2 indicates mild OA, whereas a score of 3-4 indicates moderate to severe OA. A similar scoring tool is the OARSI Atlas[60, 61]. In addition to the overall joint score, the OARSI system can be used for scoring specific qualities, such as only osteophyte size or JSN, providing additional freedom to evaluate and isolate certain radiographic qualities associated with OA. Radiographic scoring techniques could also be applied to sequential or reformatted CT images[64]

Table 2-1. Kellgren-Lawrence (KL) scoring system for radiographic OA severity[59].

Grade	Qualifier	Radiographical features
0	None	Normal, no osteophytes, no evidence of OA
1	Doubtful	Possible osteophytic lipping
2	Minimal	Definite osteophytes, possible joint space narrowing, multiple of moderate osteophyte, definite joint space narrowing
3	Moderate	Evidence of sclerosis, possible deformity of bone ends, possible bony attrition
4	Severe	Large osteophytes, marked joint space narrowing, severe sclerosis, definite deformity of bone ends, definite bony attrition

2.3.1.2. Magnetic Resonance Imaging (MRI)

MRI offers non-ionizing three-dimensional (3D) imaging and also has the capability to observe changes in bone and surrounding soft tissues, thus providing an alternative to radiography to quantify OA severity. MRI is becoming more available, and can be used to evaluate joints with OA with severity scoring techniques, such as the Whole-Organ Magnetic Resonance Imaging Score (WORMS)[65]. This system evaluates 14 characteristics related to both bony and soft tissues: cartilage signal and morphology, subarticular bone marrow abnormalities, subarticular cysts, subarticular bone attrition, marginal osteophytes, medial and lateral meniscal integrity, anterior and posterior cruciate ligament integrity, medial and lateral collateral ligament integrity, synovitis, loose bodies, and periarticular cysts/bursae[65]. In addition to multiple tissue evaluation, the WORMS system also accommodates for regional analysis, dividing the knee joint into medial, lateral, posterior, central, and anterior regions. Each element is scored on individual scales, where bony feature scoring uses scales of 0 to 3 (subarticular bone marrow abnormalities, subarticular cysts, subarticular bone attrition) or 0 to 7 points (marginal osteophytes) (Table 2-2). Although the radiographic methods are the current "gold standard", the WORMS scale is widely used in MRI-based studies in patients with OA[9, 66-68].

Table 2-2. Whole-Organ Magnetic Resonance Imaging Score (WORMS) for scoring OA severity using MRI[65].

Articular feature	Severity scoring scale
Subarticular bone marrow abnormalities	0 = none, 1 = <25% of region, 2 = 25% to 50% of region, 3 = >50% of region
Subarticular cysts	0 = none, 1 = <25% of region, 2 = 25% to 50% of region, 3 = >50% of region
Subarticular bone attrition	0 = normal, 1 = mild, 2 = moderate, 3 = severe
Marginal osteophytes	0 = none, 1 = equivocal, 2 = small, 3 = small-moderate, 4 = moderate, 5 = moderate-large, 6 = large, 7 = very large

2.3.2 Symptomatic OA

Common symptoms of OA can include a combination of pain, stiffness, joint dysfunction, limited or reduced motion, or swelling. Pain is the dominant symptom of OA, with pain reduction as the primary focus of most treatment strategies[1]. Unfortunately, pain may not be apparent in early stages of OA[69, 70], making early diagnosis and detection difficult. In many cases, joint degeneration may already be present within the knee joint before the patient seeks treatment[71]. Of note to this work is nocturnal pain, or pain lying in bed at night. Nocturnal pain is of particular concern to patients and clinicians as it disturbs sleep quality, thus disturbing quality of life[5], and is most often unpredictable[4, 72]. Nocturnal pain is most likely to occur in late to final stages of OA progression[73], typically manifesting after pain going up or downstairs, walking, standing, or sitting. Also, nocturnal pain, or pain lying down in bed at night, is often a required criteria for surgical interventions[74].

The most common technique to assess and quantify OA-related symptoms at the knee is the Western Ontario and McMaster Universities Osteoarthritis Index (WOMAC)[75], which assesses OA-related pain, stiffness, and physical function (Table 2-3). The pain subsection assesses pain while going up/down stairs, walking, standing, sitting, and lying down in bed at night. Patient responses can either be based on a self-reported visual analog scale (VAS), where the patient marks their level of pain for each element on a scale from 0 to 100[75], or as a questionnaire where patients are posed a series of questions, which are scored on a 5-point Likert scale and summed for a total possible pain score of 20 points (Table 2-4)[75]. Pain, stiffness, and function subsections can be used independently or collectively. Although the WOMAC tool is

most often reported in clinical studies, the Knee Osteoarthritis Outcome Scale (KOOS)[76] or simply the presence or absence of pain[63] are also used.

Table 2-3. Western Ontario and McMaster Universities Osteoarthritis Index (WOMAC) questionnaire subsections with corresponding question elements[75].

Subsection	Question elements
Pain	Up/down stairs, Walking, Standing, Sitting, Lying in bed at night
Stiffness	Morning stiffness, Stiffness later in the day
Physical Function	Descending stairs, Ascending stairs, Rising from sitting, Standing, Bending to the floor, Walking on a flat surface, Getting in/out of car, Going shopping, Putting on socks or shoes, Taking off socks of shoes, Rising from bed, Lying in bed, Getting in/out of the bath, sitting, Getting on/off the toilet, Performing heavy domestic duties, Performing light domestic duties

Table 2-4. Western Ontario and McMaster Universities Osteoarthritis Index (WOMAC) 5-point Likert scale scoring values[75].

Response	Score
None	0
Mild	1
Moderate	2
Severe	3
Extreme	4

2.4 OA-related Pain

Evaluating and quantifying pain is challenging as pain is a subjective and patient-specific experience. As the knee is composed of many different tissues, with many different characteristics, the source of OA-related knee pain is poorly understood and could be the result of multiple factors or multiple tissues[71]. Interestingly, patients with OA-related pain show similar changes in brain structure as patients with other diseases with chronic pain (fibromyalgia and complex regional pain syndrome) illustrating that although pain may be joint-specific, there may be additional underlying factors to consider such as pain duration (in years) and prolonged pain intensity[77] . Also, within the knee joint, pain may be related to local changes in pain pathways, which could cause normal function and stimuli (which would otherwise be painless) to become painful[1].

The large majority of our current understanding of OA pain pathogenesis relies primary on studies focusing on articular cartilage[78]. Although there is evidence of relationships between cartilage degeneration and OA-related pain[79-82], cartilage is generally aneural and insensate[83], and may not be the source of pain generation within the joint. Bone, on the other hand, is densely innervated[7, 8] and may be a plausible site of pain initiation. Evidence from both human and animal studies suggest that subchondral bone may play a role in OA disease severity[21], initiation[45, 84], progression[43, 85], and OA-related pain[19].

OA-related pain may be attributed to abnormal joint biomechanics[45, 47]. One such theory suggests that a major element of OA initiation and progression is through adaptation and subchondral bone remodelling of the affected joint to compensate for biomechanical abnormalities[45] (Figure 2-7). If abnormal mechanics are successfully controlled, the joint self-stabilizes. If abnormal mechanics are not successfully controlled, then the joint will continue to adapt through bone remodelling in an attempt to alter joint shape, potentially further altering local joint mechanics in a positive feedback loop, resulting in more severe pain.

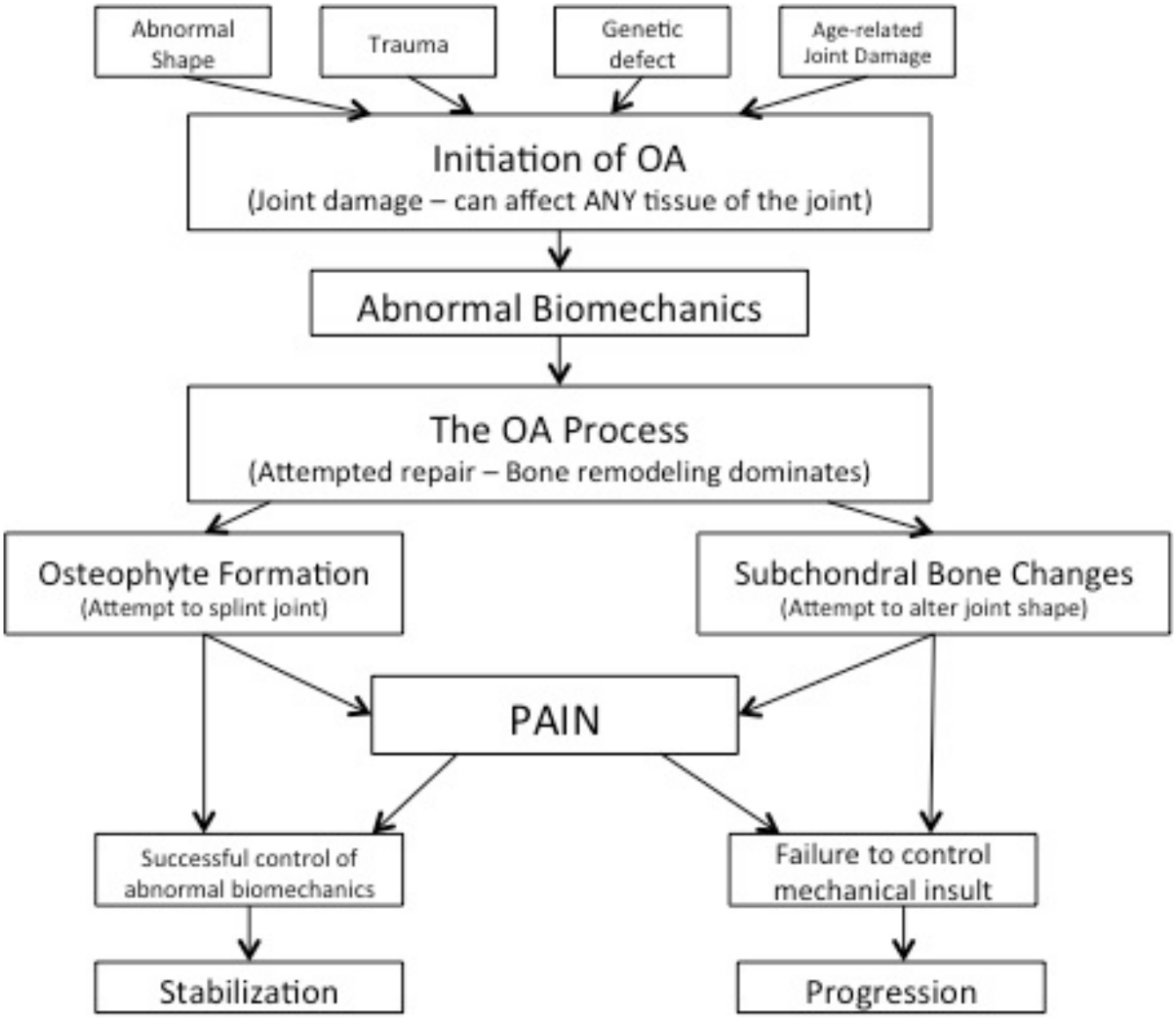

Figure 2-7. Schematic diagram of a hypothetical process of pain pathogenesis and joint remodelling, emphasizing that subchondral bone remodelling could be the primary source of OA-related pain. In this model, the joint attempts to regulate abnormal biomechanics through joint remodelling and subchondral bone changes. If abnormal biomechanics are successfully controlled, the joint self-stabilizes; if abnormal biomechanics are not successfully controlled, then the joint continues to proceed through bone remodelling, in an attempt to alter joint shape. Joint repair depends largely on the response and remodelling of subchondral bone; with increased bone turnover potentially increasing joint pain. Adapted from Dieppe 1999[45].

2.5. Image-based relationships between bone and pain

Clinical imaging (radiographs, DXA, MRI, and CT) can provide *in vivo* measurement techniques of bony structures in patients with OA. Commonly assessed structural bony features include alignment, osteophytes, sclerosis, attrition, subchondral cysts, BMLs, and BMD. As these are *in vivo* measurements, they also permit for non-invasive analysis of associations between bony features and OA-related pain.

2.5.1. Alignment

Alignment is not typically considered an imaged bony feature, but it is possible to measure (or estimate) knee alignment using radiographs, CT, or MRI. As previously mentioned, knee alignment is a commonly investigated risk factor for OA[49, 86]. In a neutrally aligned knee, the medial compartment supports from 60 to 80% of total joint load[87]. Minor alterations in alignment, either malalignment laterally (valgus), or medially (varus) (Figure 2-8), may result in abnormal load distribution across the tibial plateau[88]. Although malalignment is commonly associated with OA progression[89, 90], it may[91-93] or may not[94-96] be associated with OA-related pain. Malalignment may also contribute to other OA-related bony features such as osteophytes[97] or attrition[98].

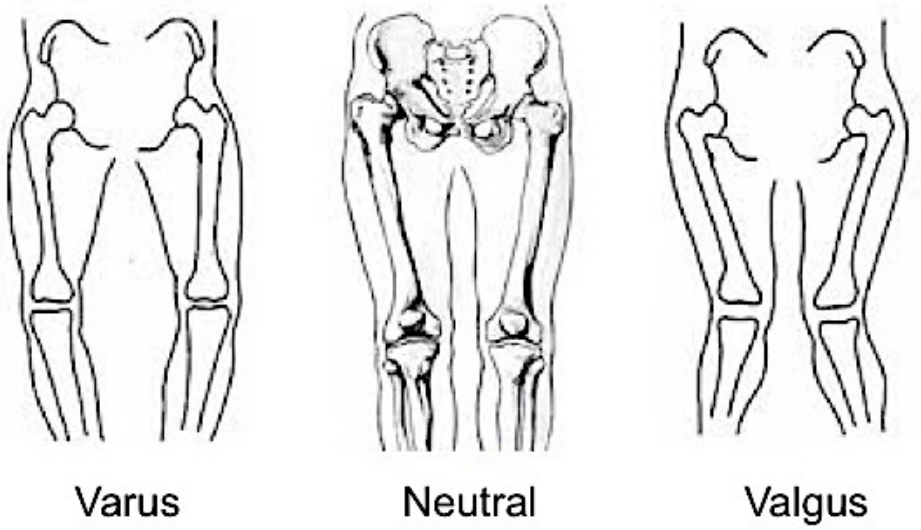

Figure 2-8. Tibial position in varus (left), neutral (middle), and valgus (right) alignment. Adapted from teachmeanatomy.com.

2.5.2. Osteophytes

Osteophytes, or bone spurs or outgrowths along the joint margin, are perhaps the defining bony feature most associated with OA[60, 61, 99] (Figure 2-9). Although the genesis or function of osteophytes within the knee joint is unclear, they may be assessed using radiographic (x-ray, DXA, or CT) or MR imaging tools, perhaps contributing to the volume of studies evaluating the association between osteophyte presence and OA-related knee pain. Osteophytes may[9, 10, 47, 63, 66, 69, 99-108], or may not be[92, 109-113] associated with OA-related knee pain (summarized in Table 2-5). Most often, more severe osteophytes were related to more severe pain[9, 63, 69, 107]. In addition, the relationship between osteophyte presence or size and pain may change with OA progression[105, 106].

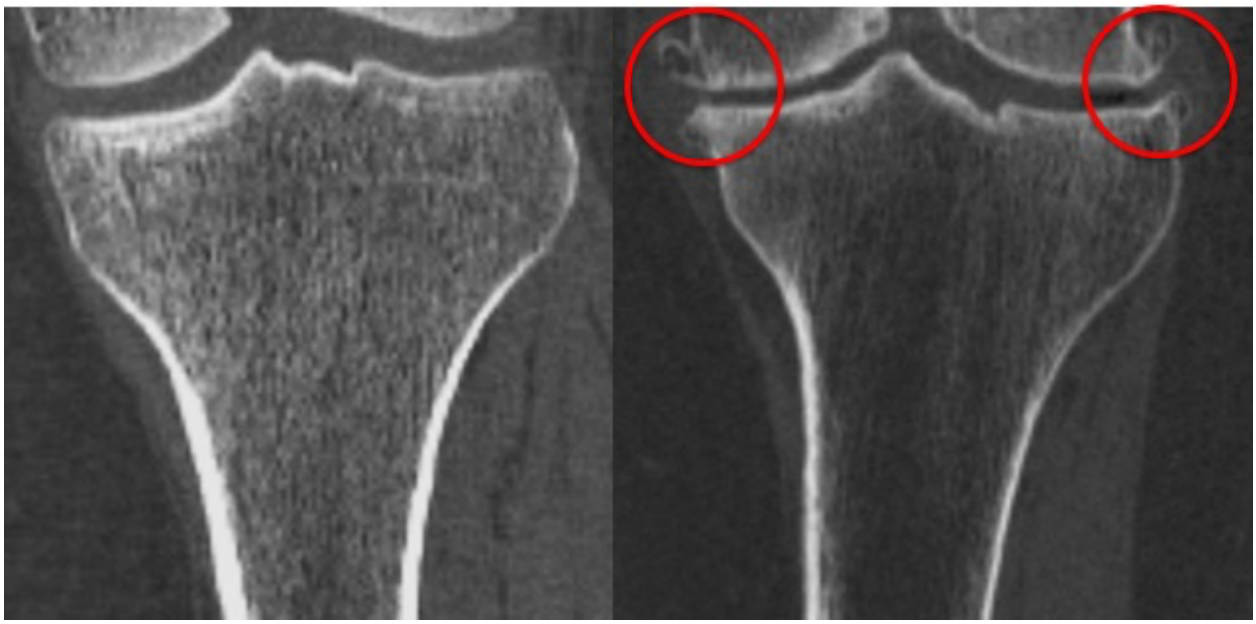

Figure 2-9. Sample CT images of knees with no osteophytes (left) and severe medial and lateral osteophytes on both the femur and tibia (right).

Table 2-5. Summary of image-based studies evaluating relationships between osteophytes and OA-related pain.

Author	Study design	Imaging modality	Pain measurement tool	Findings	Comments
Ai et al.[109]	Cross-sectional	MRI	3-pt verbal rating scale	No significant relationship with pain.	n=31 knees from 28 patients (16 male, 12 female) Osteophytes were either present or absent.
Boegård et al.[100]	Cross-sectional	X-ray	Presence/absence of pain	Presence at inferior patellar pole, $p<0.05$.	n=40, Only assessed PF joint. Osteophytes were either present or absent.
Boegård et al.[101]	Cross-sectional	X-ray	Presence/absence of pain	Presence at medial tibial plateau, $p<0.05$.	n=42, Only assessed TF joint, Osteophytes graded according to Altman[61] scale.
Chang et al.[111]	Cross-sectional	X-ray	WOMAC	OR=0.97 (95% CI: 0.14 to 6.65), NS (adjusted for: age, sex, height, body weight, BMI, TF angle).	n=151 knees from 107 patients (104 females, 3 males). Osteophytes graded using: absent (0), <1cm (0.5), >1cm (1).
Chang et al.[92]	Cross-sectional	X-ray	WOMAC	PF presence: β= -0.380 (SE=0.843), NS. Medial TF presence: β=0.877 (SE=0.952), NS. Lateral TF presence: β=0.301 (SE=1.037), NS. (All tests adjusted for: age, sex, BMI).	n=341 knees from 217 patients (208 females, 9 males). Osteophytes graded using: absent (0), <1cm (0.5), >1cm (1).
Cicuttini et al.[103]	Cross-sectional	X-ray	Presence/absence	PF osteophytes in skyline view: OR=7.66 (95% CI: 3.68 to 15.90), Chi statistic for trend = 40.30, $p<0.001$. PF osteophytes in lateral view: OR=1.83 (95% CI: 2.40 to 10.43), Chi statistic for trend = 1.34, $p=0.25$.	n=504 knees from 252 female patients. Osteophytes graded using a 4-point scale (0-3)[114] .
Cicuttini et al.[102]	Cross-sectional	X-ray	Presence/absence	Anteroposterior view: OR=5.00 (95% CI: 0.14 to 6.65), Chi statistic for trend: $p<0.001$ Lateral view: OR=2.87 (95% CI: 1.41 to 5.82), Chi statistic for trend: $p<0.001$. Skyline view: OR=7.56 (95% CI: 3.85 to 14.81), Chi statistic for trend: $p<0.001$.	n=500 knees from 200 female patients. Osteophytes graded using a 4-point scale (0-3)[114].
Dieppe et al.[110]	Longitudinal	X-ray	4-pt Likert scale and presence/absence of night pain	Medial presence and change in pain over 37 months: NS Lateral presence and change in pain over 37 months: NS	Total n=415 (135 males, 280 females), for osteophyte presence and pain n=101. Osteophytes graded as either absent (0), present (1), or severe (2).

Dieppe et al.[47]	Cross-sectional	X-ray	4-pt Likert scale and presence/absence of night pain	Global pain: r, Not mentioned, NS. Night pain: OR=0.7 (95% CI: 0.1 to 6.2), significant.	n=90 knees from 75 patients (33 males, 42 females). Osteophytes graded using a 4-point scale (0-3)[61].
Hayashi et al.[104]	Cross-sectional	X-ray, Tomosynthesis	WOMAC	Femur: X-ray, lateral: OR=5.0, p=0.004, X-ray, medial: OR=8.4, p=0.001, CT, lateral: OR=4.4, NS, CT, medial: OR=6.4, p=0.001. Tibia: X-ray, lateral: OR=5.9, p=0.002, X-ray, medial: OR=6.3, p=0.001, CT, lateral: OR=4.2, NS, CT, medial: OR=5.7, p=0.002.	n=80 knees from 40 patients (10 males, 30 female). Osteophytes were graded using a 4-point scale (0-3)[60].
Hayes et al.[63]	Cross-sectional	MRI	Presence/absence of pain	Positive association between pain and osteophyte severity, p<0.001.	n=117 females; no OA/no pain=30, OA/no pain=29, no OA/pain=30, OA/pain=28. Osteophytes assessed using: absent (0), <5mm (0.5), >5mm (1).
Javaid et al.[9]	Cross-sectional	X-ray	Presence/absence of pain and WOMAC	X-ray: Any: OR=1.94 (95% CI: 1.10 to 3.43), p=0.022, Severe: OR=4.20 (95% CI: 2.11 to 8.37), p<0.001. MRI: Any: OR=1.47 (95% CI: 0.83 to 2.63), NS, Severe: OR=2.67 (95% CI: 1.61 to 4.40), p<0.001.	Total n=636 (226 male, 410 female), with pain n=283 (112 male, 171 female), without pain n=353 (114 males, 239 female). Osteophytes graded on 8-point scale (0-7) on MR images[65], and 4-point scale (0-3) on x-rays[61].
Kinds et al.[105]	Longitudinal	X-ray	Presence/absence of pain and WOMAC	T_0: OR=1.43 (95% CI: 1.09 to 1.88), p=0.01. T_2: OR 1.42 (95% CI: 1.06 to 1.91), p=0.02. T_5: OR=1.47 (95% CI: 1.08 to 2.01), p=0.02.	n=1713 knees from 1004 patients assessed at baseline (T_0), 2 years (T_2), and 5 years (T_5). Osteophyte area (mm^2) included the sum of lateral and medial femur and tibia.
Kornaat et al.[106]	Cross-sectional	MRI	Presence/absence of pain	Any: OR=1.05 (95% CI:0.38 to 2.91), NS. Central presence: OR=1.65 (95% CI: 0.67 to 4.10), NS. PF presence: OR=2.25 (99% CI: 1.06 to 4.77), p=0.005. TF presence: OR=1.19 (95% CI: 0.46 to 3.09), NS.	n=205 (42 males, 163 females), n=97 with radiographic OA. Osteophytes assessed using: absent (0), minimal <3mm (1), moderate 3-5mm (2), severe >5mm (3).

Lanyon et al.[107]	Cross-sectional	X-ray	Presence/absence of pain	Maximum grade osteophyte over whole knee: >1: OR: 2.5 (95% CI 1.6 to 3.4), >2: OR: 5.2 (95% CI 2.9 to 9.3), >3: OR: 5.5 (95% CI 2.1 to 14.6).	n=452 (158 male, 294 female). Osteophytes graded on 4-point scale (0-3)[61].
Link et al.[112]	Cross-sectional	MRI	WOMAC	No significant relationship between pain and osteophytes at any location.	n=50 (20 male, 30 female). Osteophytes scored as either absent, mild (<0.5cm), or severe (>0.5cm) at 6 regions of the knee.
Neogi et al.[69]	Cross-sectional	X-ray	WOMAC	Pain frequency: p=0.007 for trend. Pain consistency: not significant for trend (adjusted for JSN).	n=1032 (346 male, 686 female). Osteophytes graded on 4-point scale (0-3)[115].
Sanghi et al.[113]	Cross-sectional	X-ray	WOMAC and VAS	VAS: r=0.10, NS. WOMAC: r=0.05, NS.	n=180 (57 male, 123 female). Osteophytes graded using a standardized[60].
Sowers et al.[10]	Cross-sectional	MRI	WOMAC	Medial: Positive association with pain, p<0.0001. Lateral: Positive association with pain, p<0.0001.	n=543 females. Osteophytes graded on a 4-point scale: absent (0), <5mm (1), 5-10mm (2), >10mm (3).
Spector et al.[99]	Cross-sectional	X-ray	Presence/absence of pain	Medial: OR=3.73 (95% CI: 2.60 to 5.35), significant. Lateral: OR=3.16 (95% CI: 2.25 to 4.43), significant.	n=1954 knees from 977 women. Osteophytes graded using a 3-point scale[116].
Szebenyi et al.[108]	Cross-sectional	X-ray	VAS	Presence at TF only, NS. Presence at PF only, NS. Presence at TF and PF, p<0.05.	n=167 (55 male, 112 female). Osteophytes graded using a standardized atlas[61].
Torres et al.[66]	Cross-sectional	MRI	VAS	Unstandardized β=0.50 (95% CI: 0.07 to 0.94), significant (Adjusted for age, BMI).	n=143 (31 male, 112 female). Osteophytes graded using an 8-point scale (0-7)[65].

BMI: Body mass index. CI: Confidence interval. JSN: joint space narrowing. MRI: magnetic resonance imaging. NS: Not significant. OR: Odds ratio, odds of having pain. PF: Patellofemoral joint. r: Spearman's or Pearson's correlation coefficient. SE: Standard error. TF: Tibiofemoral joint. VAS: Visual analog scale. WOMAC: Western Ontario and McMaster Scoring. X-ray: radiographs. β: regression coefficient.

2.5.3. Sclerosis

Subchondral sclerosis is another image-based defining feature of OA. Sclerosis is most commonly assessed using radiographic techniques, appearing as subchondral plate thickening and is likely the result of subchondral bone remodelling[50, 117, 118] (Figure 2-10). Although sclerotic regions may appear to have higher density, these regions may include trabecular thickening[119], poorly organized trabeculae[120], or poorly mineralized bone[54]. Like osteophytes, the association between OA-related pain and sclerosis is variable, with some studies reporting relationships between sclerosis and OA-related pain[9, 63, 105, 113] and others reporting no relationships[47, 92] (Table 2-6).

Figure 2-10. Sample radiographs of knees with no sclerosis (left) and severe medial tibial sclerosis (right). Adapted from Altman 2007[60].

Table 2-6. Summary of image-based studies evaluating relationships between sclerosis and OA-related pain.

Author	Study design	Imaging modality	Pain measurement tool	Findings	Comments
Chang et al.[92]	Cross-sectional	X-ray	WOMAC	Medial: β=-1.578 (SE=0.865), NS. Lateral: β=0.029 (SE=1.153), NS (Adjusted for age, sex, BMI).	n=341 knees from 217 patients (208 females, 9 males). Sclerosis was either absent (0) or present (0.5).
Dieppe et al.[47]	Longitudinal	X-ray	4-pt Likert scale and presence/absence of night pain	Medial: presence, NS. Lateral: presence, NS.	n=90 knees from 75 patients (33 males, 42 females). Sclerosis was either present or absent.
Hayes et al.[63]	Cross-sectional	MRI	Presence/absence of pain	Positive association between subchondral sclerosis and pain, $p<0.001$.	n=117 females; no OA/no pain=30, OA/no pain=29, no OA/pain=30, OA/pain=28. Sclerosis assessed using: absent (0), extending less than 5mm (1), extending greater than 5mm (2).
Javaid et al.[9]	Cross-sectional	X-ray	Presence/absence of pain (WOMAC)	Any: OR=2.50 (95% CI: 1.49 to 4.20), $p=0.001$. Severe: OR=4.44 (95% CI: 2.16 to 9.16), $p<0.001$.	Total n=636 (226 male, 410 female), with pain n=283 (112 male, 171 female), without pain n=353 (114 males, 239 female). Sclerosis was assessed using a standardized atlas[61].
Kinds et al.[105]	Longitudinal	X-ray	WOMAC and presence/absence	T_2: OR=1.14 (95% CI: 0.21 to 2.07), $p=0.02$.	n=1713 knees from 1004 patients assessed at baseline (T_0), 2 years (T_2), and 5 years (T_5). Sclerosis was measured as mmAl equivalents and included the sum of lateral and medial femur and tibia regions.
Sanghi et al.[113]	Cross-sectional	X-ray	WOMAC and VAS	VAS: NS. WOMAC: Positively associated with higher subchondral sclerosis, $p=0.04$.	n=180 (57 male, 123 female). Sclerosis scored using a standardized atlas[60].

BMI: Body mass index. CI: Confidence interval. MRI: magnetic resonance imaging. NS: Not significant. OR: Odds ratio, odds of having pain. PF: Patellofemoral joint. r: Spearman's or Pearson's correlation coefficient. SE: Standard error. TF: Tibiofemoral joint. VAS: Visual analog scale. WOMAC: Western Ontario and McMaster Scoring. X-ray: radiographs. β: regression coefficient.

2.5.4. Attrition

Subchondral attrition is the flattening or depression of the subchondral bone surface[121, 122](Figure 2-11). Using radiographs, attrition may also be considered as a loss of bone along the subchondral surface[47]. The initiation and progression of attrition is not yet understood, but it may be due to malalignment or mechanical overloading[123] and may be present in early OA[124]. Currently, there is no clear relationship between attrition and OA-related pain as studies have shown that attrition is[9, 66, 124] and is not[47, 92, 111, 125] associated with OA-related pain (Table 2-7). Subchondral attrition may also be associated with pain in patients without radiographic OA[125].

Figure 2-11. Sample radiographs of knees with no attrition (left) and severe attrition at the medial tibial plateau (right). Adapted from Altman et al.[61]

Table 2-7. Summary of image-based studies evaluating relationships between attrition and OA-related pain.

Author	Study design	Imaging modality	Pain measurement tool	Findings	Comments
Chang et al.[111]	Cross-sectional	X-ray	WOMAC	OR=0.71 (95% CI: 0.30 to 1.69), NS (Adjusted for age, sex, BMI, height, body weight, TF angle).	n=151 knees from 107 patients (104 females, 3 males). Attrition was either absent (0) or present (1).
Chang et al.[92]	Cross-sectional	X-ray	WOMAC	PF joint only: β =1.391 (SE=0.939), NS (age, sex, BMI).	n=341 knees from 217 patients (208 females, 9 males). PF attrition was either absent (0) or present (1).
Dieppe et al.[47]	Longitudinal	X-ray	4-pt Likert scale and presence/absence of night pain	Global pain: OR=0.1, (95% CI: -0.1 to 0.4), NS. Night pain: OR=4.2 (95% CI: 0.5 to 34.9), NS.	n=90 knees from 75 patients (33 males, 42 females). Attrition was scored on a 4-pt scale (0-3)[126].
Hernandez-Molina et al.[125]	Cross-sectional	MRI	Presence/absence of pain	Overall pain: OR=0.9 (95% CI: 0.6 to 1.4), NS (Adjusted for age, sex, OA severity, BMI, presence of BML, effusion). Night pain: OR=1.0 (95% CI: 0.5 to 2.1), NS (Adjusted for age, sex, OA severity, BMI, presence of BML, effusion).	n=1627 knees (662 males, 965 females) from 1273 patients. Attrition was scored from 0-3[65].
Javaid et al.[9]	Cross-sectional	X-ray, MRI	Presence/absence of pain (WOMAC)	X-Ray: Any: OR=7.25 (95% CI: 2.55 to 20.62), p<0.001. MRI: Any: OR=2.40 (95% CI: 1.51 to 3.83), p<0.001, Severe: OR=3.00 (95% CI: 1.67 to 5.38), p<0.001.	Total n=636 (226 male, 410 female), with pain n=283 (112 male, 171 female), without pain n=353 (114 males, 239 female). Attrition was graded on 4-point scale (0-3)[65] using MRI, and with a standardized atlas[61] on radiographs.
Reichenbach et al.[124]	Cross-sectional	X-ray, MRI	Presence/absence of pain	Day pain: OR=2.37 (95% CI: 1.48 to 3.80), p<0.001. Night pain: OR=0.94 (95% CI: 0.58 to 1.53), p<0.001 (All tests adjusted for age, sex, BMI, KL, effusion).	n=656 (266 male, 390 female). Attrition was graded on a 4-point scale: none (0), <5mm (1), 5-10mm (2), >10mm (3).
Torres et al.[66]	Cross-sectional	MRI	VAS	Unstandardized β= 1.91 (95% CI: 0.68 to 3.13), significant (Adjusted for age and BMI).	n=143 (31 male, 112 female). Attrition graded using a 4-point scale (0-3)[65].

BMI: Body mass index. CI: Confidence interval. KL: Kellgren-Lawrence scoring. MRI: magnetic resonance imaging. NS: Not significant. OR: Odds ratio, odds of having pain. PF: Patellofemoral joint. r: Spearman's or Pearson's correlation coefficient. SE: Standard error. TF: Tibiofemoral joint. VAS: Visual analog scale. WOMAC: Western Ontario and McMaster Scoring. X-ray: radiographs. β: regression coefficient.

2.5.5. Subchondral cysts

Subchondral cysts are voids within the subchondral bone, typically observable with MRI and CT but also identifiable in x-ray images (Figure 2-12). The genesis and development of cysts is not fully understood; however, there are two primary hypotheses: (1) the 'bony contusion theory'[127, 128], which proposes that excessive localized loading or trauma can induce trabecular micro fractures, necrotic bone, and localized bone resorption, eventually leading to cyst development; and (2) the 'synovial fluid intrusion theory'[129, 130], which proposes that the calcified barrier between cartilage and subchondral bone is damaged and breached, allowing fluid to seep into adjacent subchondral bone, creating a fluid-filled lesion. Cysts near the subchondral surface may change local stress distributions[131], which could potentially lead to pain or discomfort. There is evidence presenting that subchondral cyst presence is associated with OA-related pain[9, 63, 104], but there is also contradictory evidence presenting that subchondral cysts are not associated with OA-related pain[10, 66, 104, 106, 112] (Table 2-8). Discrepancies in these studies may due to differences in imaging modalities. As cysts are a 3D structure, it may be beneficial to evaluate the association between subchondral cysts and pain using 3D imaging modalities, such as QCT.

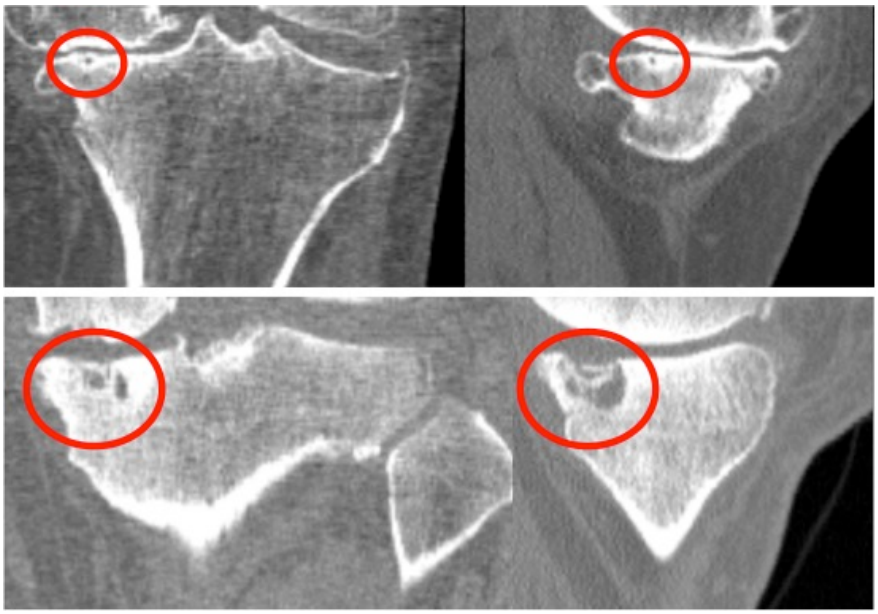

Figure 2-12. Sample CT images in coronal (left) and sagittal (right) views of OA patient with mild subchondral cysts (top row) and severe subchondral cysts (bottom row).

Table 2-8. Summary of image-based studies evaluating relationships between subchondral cysts and OA-related pain.

Author	Study design	Imaging modality	Pain measurement tool	Findings	Comments
Hayashi et al.[104]	Cross-sectional	X-ray, CT	WOMAC	Femur: X-ray, medial and lateral: NS, CT, lateral: OR=17.8, *p*=0.004, CT, medial: OR=4.3, NS. Tibia: X-ray, lateral: OR=2.6, NS, X-ray, medial: OR=3.8, NS, CT, lateral: OR=3.6, NS, CT, medial: OR=6.7, *p*=0.03.	n=80 knees from 40 patients (10 males, 30 female). Subchondral cysts were scored as either absent or present, using both x-ray and tomosynthesis.
Hayes et al.[63]	Cross-sectional	MRI	Presence/absence of pain	Positive, p<0.001.	n=117 females; no OA/no pain=30, OA/no pain=29, no OA/pain=30, OA/pain=28. Subchondral cysts assessed using: absent (0), <10mm (1), >10mm (2).
Javaid et al.[9]	Cross-sectional	MRI	Presence/absence of pain (WOMAC)	X-Ray: Any: OR=4.50 (95% CI: 1.84 to 0.68), *p*=0.001. MRI: Any: OR=1.61 (95% CI: 1.03 to 2.52), *p*=0.037, Severe: OR=1.90 (95% CI: 1.11 to 3.27), *p*<0.001.	Total n=636 (226 male, 410 female), with pain n=283 (112 male, 171 female), without pain n=353 (114 males, 239 female). Subchondral cysts graded on a 4-point scale (0-3) on MRI[65].
Kornaat et al.[106]	Cross-sectional	MRI	Presence/absence of pain	Presence: OR=1.71 (99% CI: 0.81 to 3.63), NS. PF: OR=1.83 (99% CI: 0.80 to 4.16), NS. TF: OR=1.14 (99% CI: 0.44 to 2.92), NS (All tests adjusted for age, sex, and BMI).	n=205 (42 males, 163 females), n=97 with radiographic OA. Subchondral cysts assessed using: absent (0), minimal <3mm (1), moderate 3-5mm (2), severe >5mm (3).
Link et al.[112]	Cross-sectional	MRI	WOMAC	NS.	n=50 (20 male, 30 female). Subchondral cysts were scored as either absent or present.
Sowers et al.[10]	Cross-sectional	MRI	WOMAC	NS.	n=543 females. Subchondral cysts were scored as absent, <1cm or >1cm.
Torres et al.[66]	Cross-sectional	MRI	VAS pain	Unstandardized β= 0.82 (95% CI: -0.50 to 2.14), NS (Adjusted for age and BMI).	n=143 (31 male, 112 female). Subchondral cysts graded on a 4-point scale (0-3)[65].

BMI: Body mass index. CI: Confidence interval. CT: Computed tomography. MRI: Magnetic resonance imaging. NS: Not significant. OR: Odds ratio, odds of having pain. PF: Patellofemoral joint. r: Spearman's or Pearson's correlation coefficient. SE: Standard error. TF: Tibiofemoral joint. VAS: Visual analog scale. WOMAC: Western Ontario and McMaster Scoring. X-ray: radiographs. β: regression coefficient.

2.5.6. Bone Marrow Lesions

Bone marrow lesions (BML) are indicated by regions of increased signal within the subchondral region on fat-suppressed T2-weighted MR images[29, 132] (Figure 2-13). BMLs are dynamic in nature and have been observed to change during OA progression[133], and may even be present in patients without radiographic OA[134]. Histologically, BMLs are comprised of necrotic tissue, trabecular abnormalities, and fibrosis[135], suggesting that BMLs may be regions of bone trauma or turnover[15, 136]. BMLs are the imaged feature most consistently associated with pain, found in 78% of patients with painful knee OA[136], 30% of patients with non-painful knee OA[136], and in 38% of patients with pre-radiographic OA[137]. BML presence may be consistently associated with pain, but relationships between BML size and pain tend to be less consistent, as some studies report that greater pain is associated with larger BMLs[78, 138], whereas others report that BML size is not associated with pain[133] (Table 2-9). Recent work has reported that regions adjacent to BMLs show localized higher BMD[15, 139], suggesting that BMD may also be associated with OA-related pain.

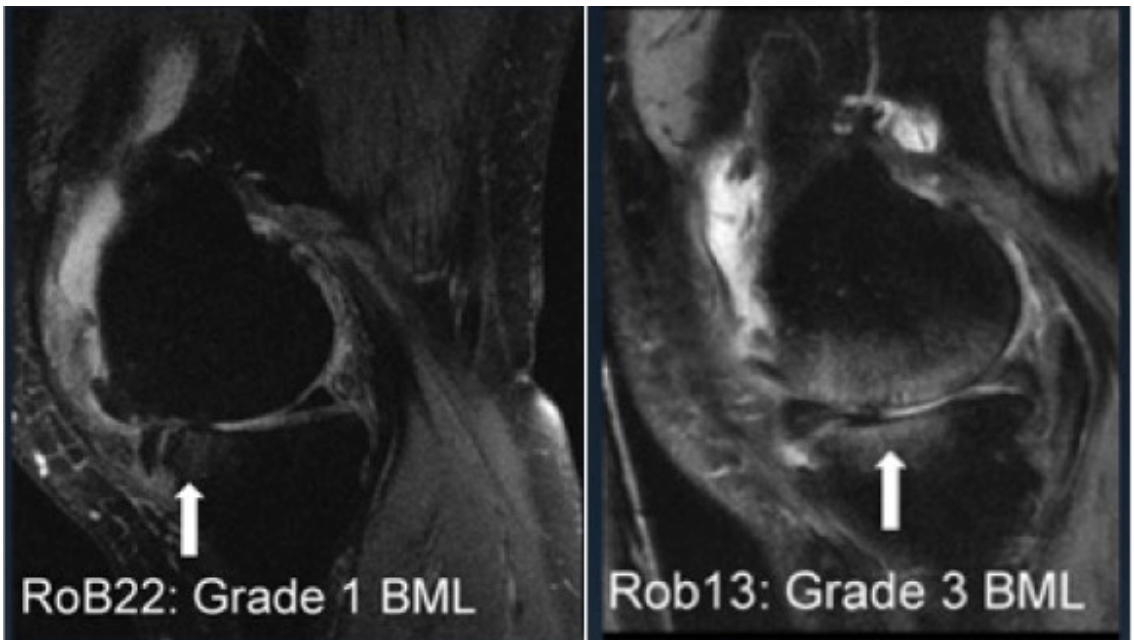

Figure 2-13. Sample MR image of OA patients with grade 1 BML (A) and grade 3 BML (B). Adapted from Seah 2012[140]

Table 2-9. Summary of image-based studies evaluating relationships between bone marrow lesions (BML) and OA-related pain.

Author	Study design	Imaging modality	Pain measurement tool	Findings	Comments
Ai et al.[109]	Cross-sectional	MRI	3-pt verbal rating scale	NS.	n=31 knees from 28 patients (12 male, 16 female). BML graded on a 4-point scale: absent (0), <1cm (1), 1-2cm (2), >2cm (3).
Baert et al.[141]	Cross-sectional	MRI	KOOS	NS.	n=87 female patients. BML scores summed over both PF and TF joint using semi-quantitative scoring (BLOKS)[142].
Bilgici et al.[143]	Cross-sectional	MRI	WOMAC	Pain is higher in patients with BML, $p<0.001$.	n=34 (10 male, 24 female). BML graded using 4-point scale (0-3) and summed over 14 regions of the knee (WORMS)[65].
Dore et al.[144]	Longitudinal	MRI	WOMAC	Change in pain vs. change in BML over 5 years, NS (All tests adjusted for age, sex, BMI, leg strength, baseline pain, and quality of life).	n=392 (192 male, 200 female). BML graded at baseline and follow-up (2.0 to 4.7 years) with a 4-point scale (0-3); largest BML was used for analysis.
Driban et al.[133]	Longitudinal	MRI	WOMAC	Baseline pain vs. total volume: $\beta=0.16$, $p=0.014$. Pain change vs. baseline total volume: $\beta=0.01$, NS. Pain change vs. volume change: $\beta=0.121$ $p=0.004$ (All tests adjusted for age, sex, weight and height).	n=404 (205 male, 199 female). BML volume was measured at baseline and follow-up (24months or 48 months).
Felson et al.[136]	Cross-sectional	MRI	WOMAC	BML presence and pain, $p<0.001$. Large BML and pain, $p<0.001$.	n=351 patients with knee pain (235 male, 116 female) and n=50 patients without knee pain (26 male, 24 female). BML graded using 4-point scale (0-3).

Felson et al.[145]	Longitudinal	MRI	WOMAC	Increase in BML with incident pain: OR=1.61 (95% CI: 1.24 to 2.09), significant Increase in pain and increase in BML size over 15 months, p=0.002 for trend (All tests adjusted for age, sex, race, BMI, CES-D, baseline quadriceps strength, KL, effusion, baseline BML, change in effusion, alignment).	Case: n=110 knees from 102 patients (31 male, 79 female); Control n=220 knees from 220 patients (88 male, 132 female). BML graded using 4-point scale (0-3) and summed over 9 regions of the tibia and patella[65].
Ip et al.[137]	Cross-sectional	MRI	WOMAC (VAS)	Total pain, NS. Walking pain, NS. Pain while climbing stairs: Maximal BML r=0.60 (95% CI 0.04 to 1.17), p<0.05 (All tests adjusted for age, sex, BMI, OA severity, effusion, and meniscal damage).	No OA: n=33 (14 male, 19 female); Pre-radiographic OA: n=124 (56 male, 68 female); Radiographic OA: n=98 (39 male, 59 female). BML graded using a 4-point scale and summed over 6 regions of the knee.
Javaid et al.[9]	Cross-sectional	MRI	Presence/absence of pain (WOMAC)	Any BML: OR=1.70 (95% CI: 1.08 to 2.67), p=0.021. Severe BML: OR=1.91 (95% CI: 1.24 to 2.92), p=0.003.	Total n=636 (226 male, 410 female), with pain n=283 (112 male, 171 female), without pain n=353 (114 males, 239 female). BML graded on 4-point scale (0-3) in 14 regions of the knee[65].
Kim et al.[67]	Cross-sectional	MRI	Presence/absence of pain and WOMAC	Any TF region: OR=2.61 (95% CI 1.32 to 5.16), *p*<0.001 for trend. Lateral TF: OR=1.54 (95% CI 0.84 to 2.82), *p*<0.001 for trend. Medial TF: OR=3.43 (95% CI 1.62 to 7.26), *P*<0.001 for trend. (All tests adjusted for age, sex, BMI, and OA severity).	n=358 (184 male, 174 female). BML graded on 4-point scale (0-3) and summed over 10 regions of the knee[65].
Kornaat et al.[146]	Longitudinal	MRI	WOMAC	NS (Adjusted for age, sex, BMI).	n=182 patients (25 male, 157 female) over 2 years. BML graded on 4-point scale (0-3): absent (0), <5mm (1), 5-20mm (2), >20mm (3), and summed over 9 regions of the knee.
Link et al.[112]	Cross-sectional	MRI	WOMAC	NS.	n=50 patients (20 male, 30 female). BML were classified as either absent, mild (<1cm), moderate (1-2cm), or severe (>2cm).

Lo et al.[78]	Cross-sectional	MRI	WOMAC (weight-bearing, non-weight-bearing)	Weight-bearing pain, p for trend <0.05 Non-weight-bearing pain, NS (All tests adjusted for age, sex, BMI, effusion, and synovitis).	n=160 patients (80 male, 80 female). BML graded on 4-point scale (0-3) and summed over 9 regions of the knee.
Ratzlaff et al.[147]	Cross-sectional	MRI	WOMAC (weight-bearing)	Total BML: positive, p<0.01. Femur BML: positive, p<0.01. Tibia BML: NS (All tests adjusted for age, sex, BMI, race, and minimum JSN).	n=115 patients (60 male, 55 female). BML were graded on 4-point scale (0-3)[65] and summed over 3 lateral or 3 medial tibial compartments.
Seah et al.[140]	Cross-sectional	MRI	WOMAC (nocturnal)	NS.	n=37 (16 male, 21 female). BML parameters include: contrast uptake rate, contrast uptake area, surface permeability, and washout rate.
Sowers et al.[10]	Cross-sectional	MRI	WOMAC	OR range from 1.75 to 14.93, 5 regions, all significant.	n=543 females. BML graded with 4-point scale (0-3) at 7 regions of the knee.
Stefanik et al.[148]	Cross-sectional	MRI	Presence/absence of pain, VAS pain	Any BML: OR=1.5 (95% CI: 1.1 to 2.0), OR=2.4 (95% CI: 1.7 to 3.5). Large BML: OR=1.2 (95% CI: 0.7 to 2.1), OR=1.4 (95% CI: 0.6 to 3.1), All significant (age, sex, BMI, depressive symptoms).	n=2017 patients (450 male, 1261 female). BML graded with 4-point scale (0-3)[65]. Considered any BML as score of 1-3, and large BML as score of 2-3.
Torres et al.[66]	Cross-sectional	MRI	VAS pain	Adjusted coefficient = 53.72 (95% CI: 1.76 to 5.68), significant (age, BMI).	n=143 (31 male, 112 female). BML graded on a 4-point scale (0-3)[65].
Wildi et al.[68]	Longitudinal	MRI	WOMAC	12-month follow-up: Global BML, r= -0.036, NS, PF BML, r= -0.239, p<0.01. 24-month follow-up: Global BML, r= -0.085, NS, PF BML, r= -0.154, NS.	n=161 (54 male, 107 female). BML graded on a 4-point scale (0-3)[65].

BMI: Body mass index. BML: bone marrow lesion. CI: Confidence interval. JSN: joint space narrowing. MRI: magnetic resonance imaging. NS: Not significant. OR: Odds ratio, odds of having pain. PF: Patellofemoral joint. r: Spearman's or Pearson's correlation coefficient. SE: Standard error. TF: Tibiofemoral joint. VAS: Visual analog scale. WOMAC: Western Ontario and McMaster Scoring. β: regression coefficient.

2.5.7. Bone Mineral Density

Imaged BMD is the amount of bone mineral mass within unit of volume (BMD or vBMD) or a unit of area (aBMD) depending on the imaging tool. BMD can be measured using computed tomography (CT) or MRI, whereas areal BMD (aBMD) is measured using dual-energy absorptiometry (DXA). Although each of these metrics provides a measurement of bone quantity, each differs slightly from one another, thus it is important to note that it is challenging to compare BMD values between studies using differing imaging modalities. Also, as the actual amount of bone differs between different depths from the subchondral surface, it is important to take note of the depth and the region of interest (ROI) used for each BMD measurement. Regions within the same subject at differing depths[19, 23], ROIs[149, 150], or using different image processing tools[21] may include different types of subchondral bone (subchondral cortical, subchondral trabecular, epiphyseal trabecular), which may be affected differently by OA[44], and have differing BMD values[20], and thus may have different associations with OA-related pain.

2.5.7.1. DXA and Areal Bone Mineral Density (aBMD)

The majority of studies evaluating the association of bone density and OA use DXA[14, 28, 149, 151-154]. DXA is a projection-based imaging tool used to measure the amount of bone within a specified two-dimensional (2D) area (mg/cm^2) expressed as areal BMD (aBMD), or amount of bone per unit area (Figure 2-14). Some of these studies have reported that patients with OA have higher aBMD[14, 28, 152], some have reported lower aBMD[152, 155], while others have reported no differences in aBMD[153, 156] when compared to asymptomatic controls. These discrepancies are most likely due to inherent limitations of DXA. Specifically, DXA images represent a 3D structure as a 2D projection image, thus are sensitive to patient size, positioning, and chosen ROI. Larger individuals will contain more bone material within a specified 2D area, potentially under-estimating aBMD, and vice versa for smaller individuals. Deviations in patient positioning, such as joint rotation, may also alter aBMD measurements within a fixed ROI[157]. The size and placement of ROI may also contribute to variation in aBMD measurements. For example, Dore et al.[149] evaluated aBMD using 6 ROIs at the proximal tibia, ranging in height from 10mm to 20mm, using different joint landmarks for placement (e.g., from the edge of the image to the highest point of the lateral or medial spine). The reproducibility (intra-class correlation coefficients, ICC) of each respective ROI was excellent, ranging from 0.98 to 1.00,

but aBMD values varied as some ROIs contained both subchondral cortical and subchondral trabecular bone. To date, only two studies have reported the association between aBMD and OA-related knee pain, reporting higher medial aBMD[158] and lower lateral aBMD[149] is associated with OA-related knee pain (Table 2-10).

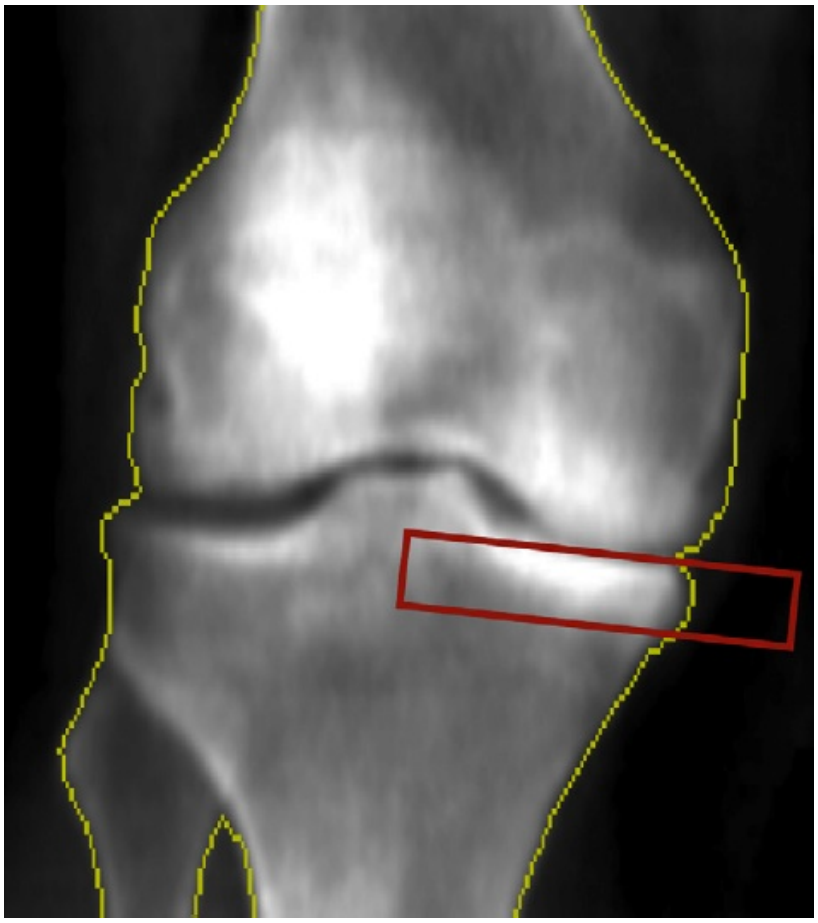

Figure 2-14. Representative ROI used in studies evaluating proximal tibial aBMD[159].

Table 2-10. Summary of image-based studies evaluating relationships between bone mineral density (BMD) and OA-related pain.

Author	Study Design	Imaging modality	Pain measurement tool	Findings	Comments
aBMD					
Akamatsu et al.[158]	Cross-sectional	DXA	VAS	Tibia, medial: β=0.372, p<0.001. Tibia, lateral: β=-0.058, NS. Tibia, M:L: β=0.388, p<0.001. Femur, medial: β=0.367, p<0.001. Femur, lateral: β=-0.038, NS. Femur, M:L: β=0.343, p<0.001 (All tests adjusted for age and BMI).	n=192 patients. aBMD was measured at the lateral and medial tibial plateaus and femoral condyles
Dore et al.[149]	Cross-sectional	DXA	WOMAC	Medial: r=0.07, NS. Lateral: r=-0.308, p=0.035 (All tests adjusted for age, sex, and BMI).	n=50 patients (27 male, 23 female). aBMD was measured at the lateral and medial tibial plateaus using six different ROIs.
BMD					
Burnett et al.[19]	Cross-sectional	QCT	WOMAC	Medial: 52mg/cm^3 (95%CI: -99 to -5, p=0.033) at 2.5-5mm and 58 mg/cm3 (95% CI -104 to -12, p=0.016) lower BMD in patients with moderate-to-severe pain at rest. Lateral 56mg/cm^3 (95% CI -110 to -3, p=0.041) at 0-2.5mm, 64 mg/cm^3 (95% CI -116 to -12, p=0.017) at 2.5-5mm, and 72 mg/cm^3 (95% CI -120 to -24, p=0.004) lower BMD in patients with moderate-to-severe pain at rest.	n=41 patients (17 male, 24 female), 19 with mild-to-no pain at rest and 22 with moderate-to-severe pain at rest. BMD was measured at 0-2.5mm, 2.5-5mm, and 5-7.5mm from the subchondral surface of the lateral and medial patellar facets.

aBMD: areal bone mineral density. BMI: Body mass index. CI: Confidence interval. DXA: dual x-ray absorptiometry. M:L: medial to lateral bone mineral density ratio. MRI: magnetic resonance imaging. NS: Not significant. OR: Odds ratio, odds of having pain. PF: Patellofemoral joint. QCT: quantitative computed tomography. r: Spearman's or Pearson's correlation coefficient. ROI: region of interest. SE: Standard error. TF: Tibiofemoral joint. VAS: Visual analog scale. BMD: (volumetric) bone mineral density. WOMAC: Western Ontario and McMaster Scoring. X-ray: radiographs. β: regression coefficient

2.5.7.2. Bone Mineral Density (BMD)

Quantitative CT (QCT) is a 3D imaging technique that uses a calibrated phantom to convert grayscale CT Hounsfield units (HU) to equivalent volumetric BMD (mg/cm^3), providing means to measure varying BMD throughout the proximal tibia at differing ROIs from the subchondral surface. CT, combined with custom image processing, has been used to measure depth-specific BMD at the acetabulum[160], proximal femur[161], proximal tibia[21, 22, 162], patella[19, 20], and distal tibia[163]. Concerning the relationship between BMD and knee OA severity or progression, few studies are available. This may be due to recent improvements in image slice thickness. Previously, image slice thicknesses were larger (1-4mm), hindering the ability to measure BMD adjacent to the subchondral surface and capture other bony features such as small osteophytes and subchondral cysts[164]. Newer scanners provide thinner slice thickness (0.3–0.625mm) allowing for more reliable imaged reconstructions with isotropic voxels, permitting analysis at any point within an imaged volume through using image-processing tools.

Studies evaluating the relationship between BMD and knee OA have been performed at both the proximal tibia[21-23] and the patella[19, 20]. At the proximal tibia, patients with OA have higher BMD at the subchondral trabecular region[21] (Figure 2-15), and lower BMD at the epiphyseal trabecular region[23], when compared to patients without OA. Similar results were reported at the patella, where participants with OA had lower BMD than healthy participants[20]. Prior to this work, a single study at the patella has reported associations between BMD and OA-related pain, where participants with moderate-to-severe pain at rest had 10% lower BMD in subchondral cortical regions, and 20% - 28% lower BMD in subchondral trabecular regions than participants with mild-to-no pain at rest[19] (Table 2-10, Figure 2-16).

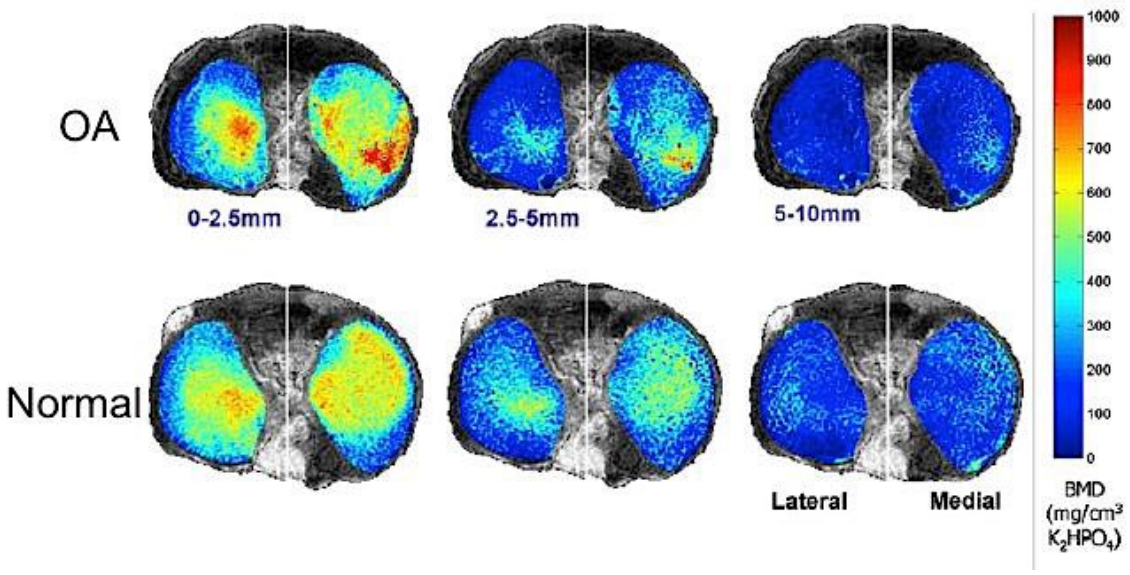

Figure 2-15. Tibial subchondral BMD measurements of patients with OA (top row) and healthy participants (bottom row) at three depths from the subchondral surface (0-2.5mm, 2.5-5mm, 5-10mm) using depth specific QCT imaging techniques.[22]

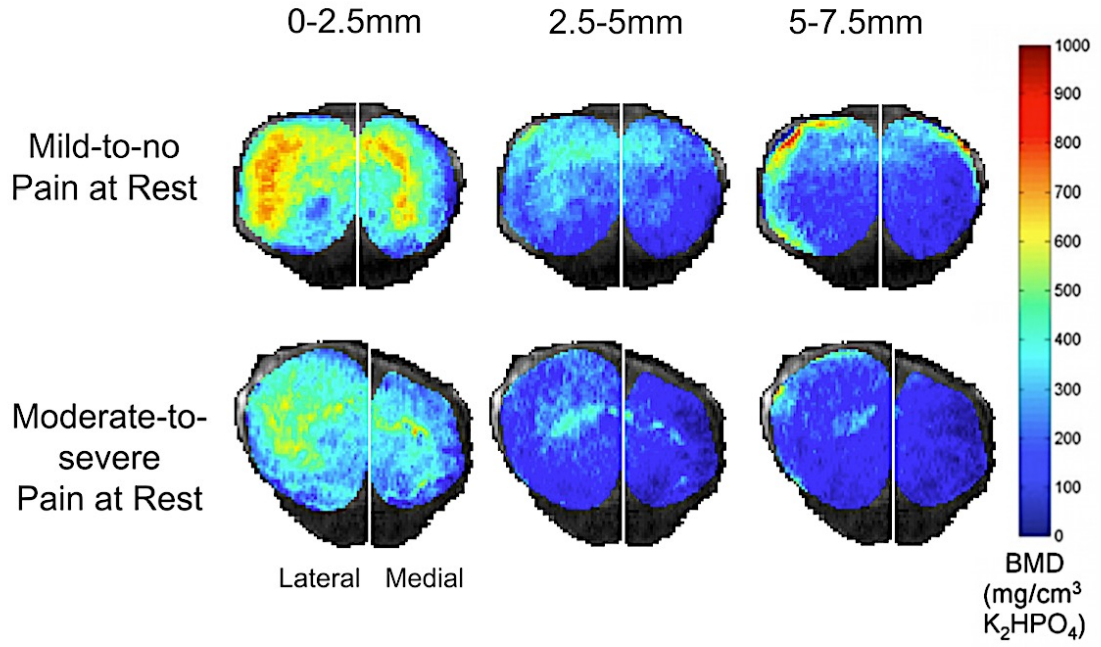

Figure 2-16. Patellar subchondral BMD measurements of OA patients with low pain at rest (top row) and high pain at rest (bottom row) at three depths from the subchondral surface (0-2.5mm, 2.5-5mm, 5-7.5mm) using depth-specific QCT imaging techniques. [19].

Although these findings suggest associations between BMD and OA severity and related pain, the underlying mechanisms of this association are unclear. Primary hypotheses infer that observed BMD alterations are associated with mechanical behaviour such as altered bone stiffness[165] or loading patterns[27, 45]. As BMD alterations may be a promising metric of OA-related knee pain, mechanical behaviour and loading patterns as interpreted through mechanical outcomes (such as stress, strain, and stiffness) may be worthwhile investigating as well, thereby providing additional understanding of the mechanical role of bone in OA.

2.6. Finite Element Modeling

2.6.1. Overview

Finite element (FE) modeling provides a non-invasive *in vivo* technique to study the structural role of bone in OA as well as the effect of OA-related alterations to overall mechanical behaviour of bone. This technique can allow the evaluation of complicated structures, such as the proximal tibia, under varying loading conditions. Simplified models can be generated using idealized geometry[166], which provide a conceptual and general evaluation, but they do not provide the ability measure inter-subject variability. To overcome this, imaged volumes (typically using QCT or high resolution QCT images) can be used to construct models which incorporate subject-specific geometry, material property distribution, and alignment[30, 31], as well as the possibility to link with clinical data such as OA progression or symptoms, such as pain.

2.6.2. Subject-specific FE models

Image-based subject-specific QCT FE techniques have been successfully used at the proximal tibia to determine how altered subchondral morphology[167], mechanical properties[168], cyst formation[131], and joint alignment[169] may impact stress and strain distributions, as well as structural stiffness. Briefly, segmented QCT images are converted to imaged volumes to create an FE model. As these model volumes are based on images from a specific individual, they are able to incorporate joint and bone geometry as well as mapped material property distribution throughout the model.

Imaged BMD is related to bone's elastic modulus, or Young's modulus (E), through experimentally derived equations[170, 171], then mapped to the FE mesh, providing subject-specific distribution of material properties. These density-modulus equations (commonly referred to as E-

BMD equations) are typically obtained through mechanical tests on bone specimens at different skeletal sites[170]. E-BMD relationships are site-specific, as well as dependent on various test-related factors such as: specimen size[172], specimen geometry[173], testing boundary conditions[174], and displacement measurement method[175]. It is crucial to ensure that appropriate E-BMD relationships are used for subject-specific FE models as they can affect the accuracy and precision of the FE model. Recent work by Nazemi et al.[176] compared nine different E-BMD relationships across 21 subject-specific QCT-based FE models of 13 medial and lateral proximal tibial plateaus with known localized structural stiffness values obtained through experimental testing. Material properties were mapped using: (1) only trabecular-specific E-BMD relationships[25, 173, 177-181], and (2) trabecular-specific E-BMD relationships combined with two cortical-specific E-BMD relationships (Snyder & Schneider[182], Rho et al. [180]). Authors report that a combination of E-BMD equations, using Goulet et al.[179] for trabecular bone and either Snyder & Schneider[182] or Rho et al.[180] for cortical bone provided the most appropriate E-BMD relationships for FE models at the proximal tibia, with R^2 of 0.75 to 0.77 between experimental stiffness values and FE predictions. Though, models using a single E-BMD equation (Goulet et al.[179]) explained similar variance in stiffness ($R^2 = 0.70$) as models including both trabecular and cortical bone (R^2 ranging from 0.56 to 0.77).

2.6.2. Subject-specific FE Analysis of OA Bone

There are limited studies reporting the use of *in vivo* subject-specific FE modeling techniques at the proximal tibia in patients with OA. Early work from McErlain et al.[131] evaluated the effect of simulated subchondral cysts on stress distributions at the proximal tibia in 20 patients with early OA. Authors report trends where maximum stress values often appeared in the region surrounding the simulated subchondral cysts and adjacent to the joint space. Additionally, an increase in cyst diameter contributed to an increase in stress values surrounding the simulated cyst region (r^2=0.372, p=0.004) (Figure 2-17).

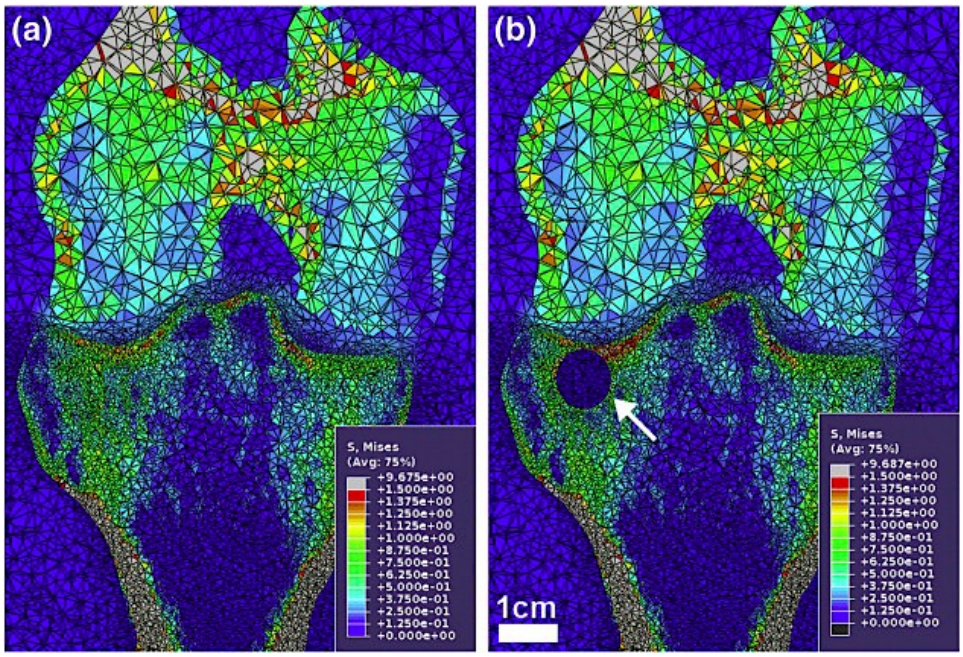

Figure 2-17. Comparison of von Mises stress distribution at the proximal tibia in participants with early OA with (right) and without (left) simulated subchondral cysts. Adapted from McErlain et al[131].

A recent precision study[30, 31] of *in vivo* subject-specific FE modeling at the proximal tibia reported differences in stress (von Mises and minimum compressive stress), in a small sample (n=7) of participants with OA compared to healthy participants (n=7). Differences in von Mises stress were greatest at medial cortical regions along the peripheral of the subchondral depth (101% greater in participants with OA) and along the outer epiphyseal depth (113% greater in participants with OA), and at lateral cortical regions along the peripheral of the subchondral region (31% greater in participants with OA) and along the outer epiphyseal depth (38% greater in participants with OA) (Figure 2-18). Participants with OA also had greater von Mises stress at medial trabecular regions at both the subchondral (37% greater) and epiphyseal (45% greater) depths. The difference in stress was up to 20 times the precision error, indicating that it may be possible to differentiate mechanical differences between healthy and OA tibiae using subject-specific QCT-based FE techniques. It may also be possible to differentiate pain in participants with OA using similar techniques. Given that both studies report higher stress distributions at the proximal tibia, either due to subchondral alterations related to OA progression[131] or OA presence[30], higher stress may also be related to OA-related knee pain.

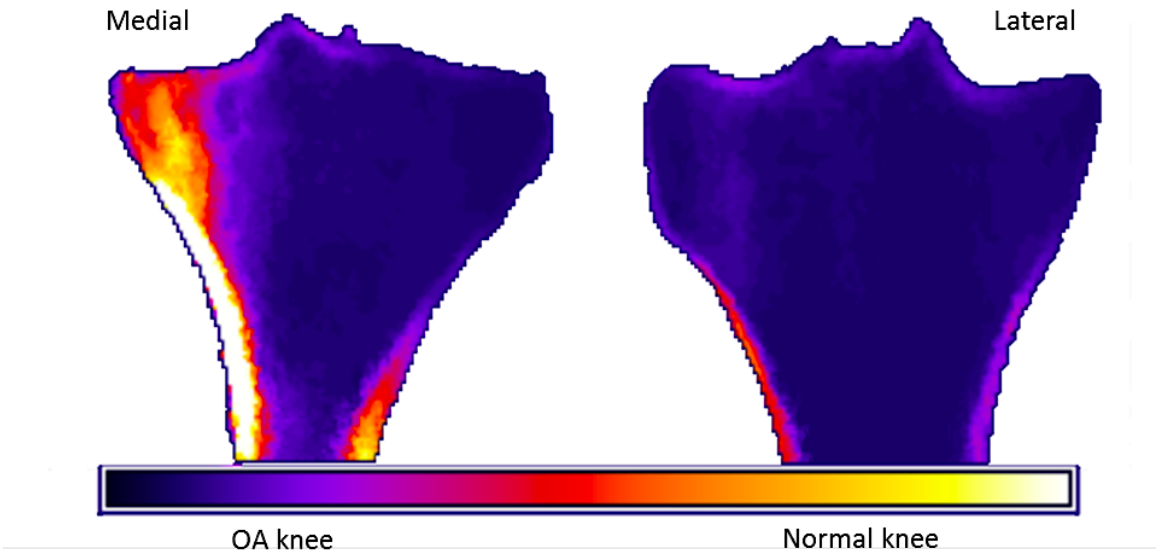

Figure 2-18. Representative von Mises stress distributions between OA and healthy participants at the proximal tibia. Yellow indicates high stress, while black indicates low stress[30, 31].

2.6.3. Subject-Specific FE and pain

To date, a single study[183] in patients with patellofemoral (PF) pain has used subject-specific FE modelling to determine relationships between mechanical outcomes and pain. This study used subject-specific FE models to evaluate hydrostatic pressure and octahedral shear stress in patellar and femoral cartilage in patients with and without PF pain. Compared to pain-free controls, individuals with PF pain exhibited greater peak hydrostatic pressure by 19% to 30% at the patella and by 25% to 29% at the femur. Mean octahedral shear stress was 10% to 50% greater at the patellar cartilage surface, and 20% to 33% greater at the femoral cartilage surface. Although this research evaluated mechanical behaviour of cartilage, it does support the hypothesis that mechanical changes within the knee joint may also be associated with OA-related pain.

2.7. Summary

1. OA is a debilitating and painful disease affecting a large portion of the Canadian population. Pain is the primary symptom of OA, but the joint tissues may already be mechanically compromised when the patient first feels pain.
2. Subchondral bone is heavily innervated and may be a likely location for pain initiation, as opposed to cartilage which is aneural and insensate.

3. Image-based bony features, such as joint alignment, osteophytes, sclerosis, attrition, subchondral cysts, and BMLs are often associated with OA-related pain, but relationships are inconsistent among various imaging modalities.
4. BMD, a surrogate measure of mechanical properties in bone, is associated with various image-based outcomes, and can be quantified *in vivo* using clinical QCT.
5. Lower trabecular BMD at the patella is related to pain at rest. Similar relationships may be present between OA-related pain and proximal tibial subchondral, epiphyseal, or metaphyseal BMD.
6. As BMD alterations may be a promising metric of OA-related knee pain, mechanical behaviour and loading patterns as interpreted through mechanical outcomes, such as stress, strain, and stiffness, may be worthwhile investigating.
7. Recent work using subject-specific FE modeling has shown differences in von Mises stress and minimum principal stress between healthy patients and patients with OA, and may be able to discriminate differences in mechanical outcomes between patients with differing levels of OA-related pain.

3. RESEARCH QUESTIONS AND OBJECTIVES

3.1. Research Questions

The fundamental question motivating my research is: What are the relationships between bone and OA-related knee pain? To help answer this question, the goal of my dissertation was to use and modify previously developed depth-specific QCT imaging techniques[22] and FE techniques[30] to evaluate relationships between OA-related pain and image-based CT and FE outcomes in a group of patients with OA. I aimed to answer the following research questions:

1. What are the relationships between tibial subchondral BMD and knee pain in patients with OA?
2. What are the relationships between tibial epiphyseal and metaphyseal BMD and knee pain in patients with OA?
3. What are the relationships between tibial subchondral cysts and knee pain in patients with OA?
4. What are the relationships between tibial FE-derived mechanical outcomes and knee pain in patients with OA?

3.2. Research Objectives:

To answer the questions posed in this study, the objectives were to:

1. Investigate if tibial regional subchondral BMD is associated with OA-related nocturnal knee pain using a depth-specific CT image processing tool,
2. Investigate if tibial epiphyseal and metaphyseal BMD is associated with OA-related knee pain using a modification of the previously used depth-specific CT image processing tool,
3. Modify our depth-specific imaging technique to measure subchondral cyst parameters and use this technique to determine if subchondral cyst characteristics are associated with OA-related knee pain,
4. Investigate if FE-derived mechanical outcomes at the proximal tibia are associated with OA-related pain.

4. SUBCHONDRAL BMD AND NOCTURNAL PAIN

4.1. Synopsis

This chapter outlines details of our study investigating relationships between proximal tibial subchondral BMD and nocturnal pain in patients with knee OA. In this study, we report that participants with severe nocturnal pain had higher lateral focal BMD than participants with no pain at subchondral trabecular depths of 2.5-5mm and 5-10mm from the subchondral surface. This study suggests that local subchondral BMD may have a role in OA-relates pain pathogenesis.

4.2. Introduction

Knee OA is a leading cause of chronic pain and disability in the elderly[184]. Pain is the dominant symptom of OA[2] and is often the first indication that patients may be afflicted with OA. OA-related pain is complex[47, 69, 70, 72, 78], as it is a combination of social, psychological, and biological factors, with no simple unitary concept linking symptoms with structural damage[71, 185]. Within the joint structure, pain could be due to the presence of various contributing factors (e.g., altered joint alignment, joint instability, osteophyte presence both peripherally and within the joint, inflammation, cyst presence, altered subchondral bone properties). Importantly, underlying sources of pain may be masked by specific structural factors, such as altered joint alignment, osteophyte presence, and inflammation, which would likely be present during dynamic weight-bearing activities such as climbing stairs or walking. To isolate potential underlying sources of pain, it is advantageous to study pain with non-weight bearing activities, such as lying in bed at night. Understanding potential sources of pain during non-weight bearing activities, such as nocturnal pain, is also relevant as it is related to sleeplessness and other disruptions to quality of life in OA patients[5].

Subchondral bone is one of the many tissues involved in OA pathogenesis and progression[1, 2, 84]. Importantly, it is densely innervated[8] and thus could be a factor in OA-related pain. Deeper tissues within the subchondral region, composed primarily of subchondral trabecular bone, have a greater concentration of nerve endings than the shallower, highly mineralized subchondral tissues (e.g., cortical bone)[186] and could be of particular importance for OA-related pain. Ex vivo studies have shown altered subchondral bone thickness[187], bone

volume fraction[188-190], and volumetric density[21, 24] with OA. These alterations may influence local innervation[191, 192] and/or the local mechanical behaviour of bone[193], possibly leading to pain.

Our current understanding of the relationship between pain and altered density, specifically subchondral BMD, relies on evidence from studies using 2D DXA[149, 158]. However, these studies provide8 conflicting results, reporting that both higher aBMD[158] and lower aBMD[149] are associated with OA-related pain. These conflicting results may be due to the inherent limitations of 2D projection techniques, such as patient size and positioning[157], unstandardized regions of interest[139, 149, 150], and the inability to evaluate distinct regions or depths[157, 194]. Three-dimensional CT-based depth-specific imaging techniques have the ability distinguish differences in subchondral volumetric BMD between normal and OA tibiae[21, 162], and may have the ability to identify regional BMD differences in patients with and without pain. Depth-specific imaging techniques also have the potential to determine approximate contrasts between subchondral cortical BMD and less dense trabecular BMD layers[195], which may have different roles in OA-related pain.

Using a depth-specific CT-based image processing tool, the objective of this study was to determine whether there are associations between proximal tibial subchondral BMD and OA-related nocturnal pain.

4.3. Methods

4.3.1. Study Participants

Fifty-two participants (23M: 29F; mean age 64, SD ± 9.4years) with OA were recruited prior to total knee replacement. Study exclusion criteria included: pregnant women, patients having a revision replacement instead of primary knee replacement, and patients with a prior history of bone pathology at the knee joint. CT images with excessive imaging artifacts, motion artifacts, or incomplete images were excluded, resulting in 42 study participants (17M: 25F; 64 ± 10 years). The Institutional Research Board of the New England Baptist Hospital approved the study. Informed consent was obtained from all study participants.

4.3.2. Patient Assessment

OA severity was classified using the KL grade[59] and OA-related pain severity was measured at the affected knee joint using a 5-point Likert scale (0 to 4) of the pain subsection of WOMAC[75]. Participants were asked to assess the level of pain in the affected knee joint within the past 24-hours while walking on a flat surface, going up or down stairs, nocturnal pain at night in bed, sitting or lying down, and standing upright. This study was focused on non-weight bearing nocturnal pain at night in bed.

4.3.3. CT Acquisition

We used a clinical single-energy QCT scanner (Lightspeed 4-slice, General Electric, Milwakee, WI, USA) with a solid QCT reference phantom (Model 3T, Mindways Software Inc., Austin, TX, USA) to collect CT data and convert grayscale CT HU to equivalent apparent BMD (mg/cm^3 K_2HPO_4). Participants were oriented supine within the CT gantry and both legs were simultaneously scanned. Scans included the distal femur, patella, proximal tibia, and the 66% tibial shaft site proximal to the distal tibial end-plate[196]. Only the proximal tibia and the 66% tibial shaft site were used in the current analysis.

CT scanning parameters included: 120kVp tube voltage, 150mA tube current, axial scanning plane, 0.625mm isotropic voxel size (0.625 slice thickness, 0.625mm x 0.625mm in-plane pixel size), ~250 slices, ~60s scan time, and 0.073mSv effective dosage. A standard bone kernel (BONE) was used for CT image post-processing. Effective radiation dosage was ~0.073mSv per scan, estimated using shareware software (CT-DOSE, National Board of Health, Herley, Denmark). For comparison, the average effective radiation dosage during a transatlantic flight from Europe to North America is about 0.05mSv[197].

4.3.4. CT Image Analysis

We used a validated depth-specific image processing technique (computed tomography topographical mapping of subchondral density, CT-TOMASD)[22, 162] to measure subchondral proximal tibial subchondral BMD . This method uses surface projection image processing to quantify volumetric subchondral bone density at user-defined depths from the subchondral bone surface. Briefly, equivalent volumetric BMD (mg/cm^3 K_2HPO_4) values were converted from grayscale HU using linear regression equations developed from known densities within the QCT phantom included in each image ($r^2>0.99$) (Matlab 2010b; MathWorks, Natick, MA, USA).

Subject-specific half maximum height thresholds[198, 199] were then determined to define the proximal tibial subchondral surface. Serial images were individually segmented using semi-automatic region growing and manual correction techniques using commercial software (Analyze10.0; Mayo Foundation, Rochester, MN, USA) and an interactive touch-screen tablet (Cintiq 21UX; Wacom, Krefeld, Germany), then grouped to build a 3D image volume. Medial and lateral plateau surfaces were then defined by manually selecting boundary points. Each plateau was then realigned and reconstructed relative to "best-fit" planes passing through the defined boundary points (Matlab 2010b) for surface projection analyses. Previously defined boundary points were then manually adjusted (using knot points and natural cubic splines), to ensure that the analysis region did not overlay high-density cortical edges, the tibial spine, or osteophytes[22, 162].

To allow for subject-to-subject comparisons, subject-specific depth was normalized based on user-defined depth, relative proximal tibia volume (volume superior to lateral inferior ridge of the proximal fibular head), and area (both lateral and medial plateaus) by using the following equation:

$$\frac{d_{ss} \cdot area_{ss}}{d \cdot area_{m}} = \frac{volume_{ss}}{volume_{m}}$$

where: $volume_{ss}/volume_{m}$ is a relative volume ratio defined by dividing each subject-specific proximal tibia volume by the mean proximal tibia volume of all specimens, $area_{ss}$ is the subject-specific (segmented) area of the medial and lateral plateaus, $area_{m}$ is mean area of all subjects, d is the desired user-defined normalized depth (i.e., 2.5 mm), and d_{ss} is the actual subject-specific depth corresponding to the user-defined normalized depth[162].

Regional analysis included total lateral and total medial plateau BMD, as well as average maximum BMD of a 10mm diameter core or 'focal spot' which searched each lateral and medial plateau for a maximum value[22] (Figure 4.1). We included focal analyses to locate small regions of high density bone possibly masked by whole compartment analyses. All analyses were performed at three normalized depths of 0-2.5mm, 2.5-5mm, and 5-10mm from the subchondral surface.

4.3.5. Internal Control

We compared cortical cross-sectional area and density of the tibia shaft (66% of tibia length, proximal from distal tibia plateau)[196] to assess possible between-group differences in local (e.g., mechanical loading) and systemic factors (e.g., nutrition, medication)[200].

4.3.6. Statistical Analysis

To examine associations between nocturnal pain at night in bed and proximal tibial subchondral BMD, we used Spearman's rank correlation. We report Spearman's rank correlation coefficients (ρ) for all associations.

We categorized participants into three groups based on their WOMAC score of pain at night in bed. Patients with a score of 0 or 1 were considered to have 'no pain', patients with a score of 2 were considered to have 'moderate pain', and patients with a score of 3 or greater were considered to have 'severe pain'[140]. To compare differences in proximal tibial subchondral BMD across patients with 'no pain' and patients experiencing either 'moderate pain' or 'severe pain' at night in bed, we used multivariate analysis of covariance (MANCOVA) and selected age, sex, and BMI as covariates[200]. We report the *F*-statistic for regions with significant between-group differences. We also performed pairwise comparisons with Bonferroni adjustment for multiple comparisons to determine individual group differences between pain ('severe pain' and 'moderate pain') and 'no pain' at each region. We report mean and standard deviation (SD), adjusted mean differences, and 95% confidence intervals. We also used MANCOVA to compare cortical cross-sectional area and density at the tibia shaft across pain groups, also adjusting for age, sex and BMI[200]. Statistical significance was defined as $p<0.05$, and statistical analyses were performed using SPSS 21.0 (IBM, Armonk, NY, USA).

4.4. Results

The characteristics of study participants are shown in Table 4-1. Patients had OA severity of KL grade ranging from 3 to 4. In the WOMAC assessment of non-weight bearing pain at night in bed, scores ranged from 0 (none) to 4 (extreme). Participants were divided into three groups based on pain at night in bed: 'no pain' (n=17), 'moderate pain' (n=16), and 'severe pain' (n=9).

Table 4-1. Background characteristics and clinical data for study participants and groups.

Characteristic	All Participants	'No Pain' (n=17)	'Moderate Pain' (n=16)	'Severe Pain' (n=9)
WOMAC (in bed at night)		0 or 1	2	3 or 4
Sex ratio (M:F)	17:25	7:10	7:9	3:6
Age (mean ± SD)	64.1 ± 10.1	67.5 ± 9.1	61.8 ± 11.0	61.8 ± 9.3
BMI ((mean ± SD)	28.7 ± 3.7	28.3 ± 4.1	29.1 ± 3.6	28.7 ± 3.0
Side (L:R)	18:24	7:10	6:10	5:4
OA Severity (KL)	3 to 4	3 to 4	3 to 4	3 to 4

Spearman's rank coefficients showed a significant association between pain at night in bed and lateral focal BMD at a depth of 2.5-5mm from the subchondral surface ($\rho = 0.388$, p=0.011). There were no other significant associations between pain scores and other BMD metrics (Table 4-2).

Table 4-2. Spearman rank correlation coefficients (ρ) for relationship between BMD measurements and WOMAC pain score while lying down. Bolded values indicate $p<0.05$.

Side	Region	Depth from subchondral surface		
		0-2.5mm	2.5-5mm	5-10mm
Medial	Total	-0.284 (p=0.069)	-0.244 (p=0.120)	-0.218 (p=0.165)
	Focal BMD	-0.211 (p=0.181)	-0.223 (p=0.157)	-0.248 (p=0.113)
Lateral	Total	0.290 (p=0.062)	0.301 (p=0.053)	0.203 (p=0.198)
	Focal BMD	-0.156 (p=0.323)	**0.388 (p=0.011)**	0.290 (p=0.063)

After adjusting for covariates, there was a significant between-group difference in lateral focal BMD at depths of 2.5-5mm (F (2,36) = 3.915, $p<0.05$) and 5-10mm (F (2,36) = 3.258, $p<0.05$) from the subchondral surface. Individual group differences showed that participants with 'severe pain' had higher lateral focal BMD than participants with 'no pain' at depths of 2.5-5mm (33% higher; adjusted mean difference: 114 mg/cm^3; 95% CI: 9.6 to 218 mg/cm^3; p=0.028) and 5-10mm (32% higher; adjusted mean difference: 60 mg/cm^3; 95% CI: 0.3 to 120 mg/cm^3; p=0.049) (Table 4-4). There were no significant differences in regional BMD between groups at depths of 0-2.5mm from the subchondral surface, or at the total lateral or medial plateaus (Figures 4-1. and 4-2, Tables 4-3 and 4-4). However, there was a statistically non-significant

trend for a lower BMD at the medial plateau (across all depths) across the groups with increasing pain (Figures 4-1 and 4-2, Tables 4-3 and 4-4).

At the tibial shaft, there were no significant differences in cortical cross-sectional area (F (2, 36)=0.208, $p > 0.05$) or density (F (2,36)=0.186, $p > 0.05$) between groups.

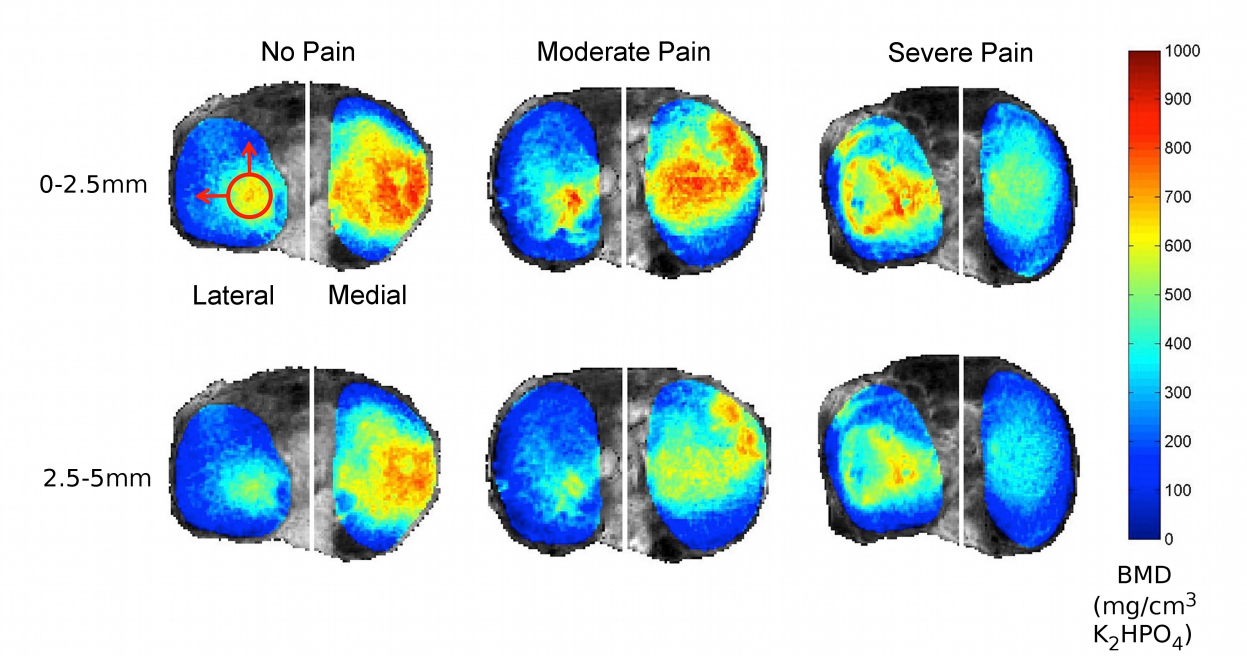

Figure 4-1. Representative topographical maps of tibial BMD at depths of 0-2.5mm (top row) and 2.5-5mm (bottom row) in one participant reporting 'no pain', 'moderate pain', and 'severe pain' while lying down. Regional analysis includes average BMD of the lateral and medial plateaus, and average maximum BMD of a 10mm diameter focal spot (shown in upper left-hand image) localized on the maximum value of each lateral and medial plateau.

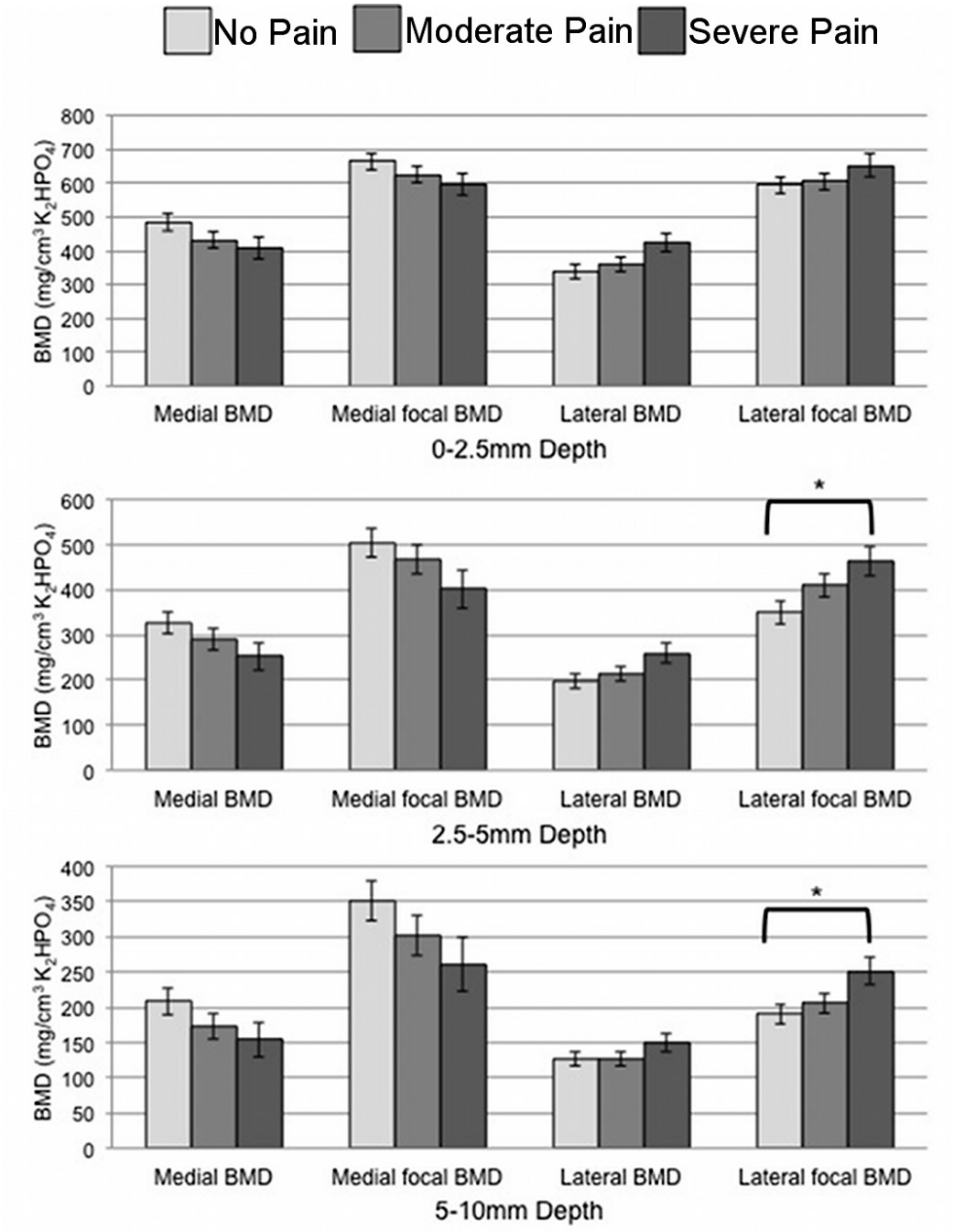

Figure 4-2. Adjusted mean regional BMD of each group ('no pain', 'moderate pain', and 'severe pain') at depths of 0-2.5mm, 2.5-5mm, and 5-10mm from the subchondral surface. Statistically significant differences ($p<0.05$) between groups are noted with brackets. Error bars represent 95% confidence intervals.

Table 4-3. Pair-wise comparison of tibial bone mineral density (BMD) measurements in patients with knee osteoarthritis with 'no pain' and 'moderate pain' while lying down, including mean ± standard deviation (SD), adjusted mean difference, percent difference from 'no pain', 95% confidence interval (CI), and *p*-value.

Region	Depth	BMD (mg/cm^3 K_2HPO_4)		Adjusted mean difference+ from No Pain (%)	95% Confidence Interval (mg/cm^3 K_2HPO_4)		*p*-value
		No Pain	Moderate Pain				
		Mean ± SD	Mean ± SD		Lower Limit	Upper Limit	
Medial Plateau							
Total	0-2.5 mm	480 ± 93	437 ± 116	-53 (-10.9%)	-146	41	0.50
	2.5-5 mm	322 ± 98	296 ± 91	-36 (-11.0%)	-122	49	0.90
	5-10 mm	203 ± 85	177 ± 61	-35 (-17.0%)	-102	31	0.57
Focal BMD	0-2.5 mm	658 ± 94	631 ± 108	-38 (-5.6%)	-127	51	0.88
	2.5-5 mm	499 ± 130	474 ± 123	-37 (-7.4%)	-152	77	1.00
	5-10 mm	347 ± 135	309 ± 94	-49 (-14.0%)	-152	54	0.71
Lateral Plateau							
Total	0-2.5 mm	339 ± 62	356 ± 112	19 (5.6%)	-58	96	1.00
	2.5-5 mm	198 ± 52	214 ± 80	17 (8.4%)	-44	77	1.00
	5-10 mm	127 ± 38	128 ± 45	0 (0%)	-38	38	1.00
Focal BMD	0-2.5 mm	596 ± 81	602 ± 124	11 (1.8%)	-79	100	1.00
	2.5-5 mm	352 ± 80	407 ± 120	61 (17.4%)	-28	150	0.29
	5-10 mm	193 ± 49	205 ± 60	15 (8.1%)	-36	66	1.00

+. Mean values adjusted for age (64.1), sex (1.6), and BMI (28.7).

Table 4-4. Pair-wise comparison of tibial bone mineral density (BMD) measurements in patients with knee osteoarthritis with 'no pain' and 'severe pain' while lying down, including mean ± standard deviation (SD), adjusted mean difference, percent difference from 'no pain', 95% confidence interval (CI), and *p*-value. Bolded values indicate $p<0.05$.

Region	Depth	BMD (mg/cm^3 K_2HPO_4)		Adjusted mean difference+ from No Pain (%)	95% Confidence Interval (mg/cm^3 K_2HPO_4)		*p*-value
		No Pain	Severe Pain				
		Mean ± SD	Mean ± SD		Lower Limit	Upper Limit	
Medial Plateau							
Total	0-2.5 mm	480 ± 93	406 ± 110	-76 (-15.8%)	-186	33	0.27
	2.5-5 mm	322 ± 98	251 ± 107	-74 (-22.7%)	-174	26	0.22
	5-10 mm	203 ± 85	154 ± 80	-54 (-25.8%)	-132	24	0.28
Focal BMD	0-2.5 mm	658 ± 94	595 ± 114	-66 (-9.9%)	-170	39	0.37
	2.5-5 mm	499 ± 130	399 ± 148	-102 (-20.3%)	-237	33	0.20
	5-10 mm	347 ± 135	258 ± 134	-90 (-25.7%)	-211	30	0.21
Lateral Plateau							
Total	0-2.5 mm	339 ± 62	427 ± 74	85 (25.1%)	-6	176	0.07
	2.5-5 mm	198 ± 52	261 ± 61	62 (31.2%)	-10	133	0.11
	5-10 mm	127 ± 38	150 ± 38	22 (17.5%)	-22	66	0.64
Focal BMD	0-2.5 mm	596 ± 81	652 ± 54	58 (9.7%)	-47	163	0.53
	2.5-5 mm	352 ± 80	461 ± 71	114 (32.7%)	-10	218	**0.028**
	5-10 mm	193 ± 49	249 ± 55	60 (31.6%)	0	120	**0.049**

+. Mean values adjusted for age (64.1), sex (1.6), and BMI (28.7).

4.5. Discussion

Our depth-specific imaging technique identified a positive association between lateral focal BMD at the 2.5-5mm depth and non-weight bearing pain at night in bed. Isolated comparisons identified higher lateral focal BMD at depths 2.5-5mm and 5-10mm from the proximal tibial subchondral surface in patients experiencing 'severe pain' than in patients experiencing 'no pain' at night in bed. This is the first study to assess the relationship between depth-specific proximal tibial subchondral BMD and symptomatic OA. These findings suggest that there may be previously overlooked characteristics in proximal tibial subchondral BMD, such as focal BMD at depths greater than 2.5mm from the subchondral surface, which may have a role in OA-related pain pathogenesis.

The results of this study give some insight into why the results from previous studies linking OA-related knee pain and proximal tibial subchondral bone density are conflicting. One study found an association between high aBMD and pain[158], where another found a relationship between low aBMD and pain[149]. The reasons for disagreement may be due to inherent limitations of DXA. For example, patient size and positioning sensitivities may affect aBMD measurements whereby larger and malpositioned patients have more bone in the projection direction, resulting in an overestimation of aBMD[157]. Also, there are no standardized regions of interest (ROI) with DXA to evaluate proximal tibial subchondral aBMD, with ROIs varying in size and placement from study to study[139, 149, 150, 201]. These ROIs most likely contain both subchondral cortical and trabecular bone. The results of this study suggest that sites distal to the subchondral surface (which contain primarily trabecular bone) appear to be most affected by OA. As such, aBMD measures containing both subchondral cortical and trabecular bone may not be sensitive enough to capture OA-effects on local bone density. Conversely, by evaluating BMD at specific depths from the subchondral surface, the depth-specific imaging technique used in this study was able to approximate individual effects of OA on regions composed of mostly mineralized subchondral cortical bone (0-2.5 mm layer) and trabecular bone (2.5-5 and 5-10 mm layers).

Another possible reason for disagreement between higher and lower aBMD and pain may be because previous studies reporting aBMD appear to have evaluated entire compartments of the proximal tibia[149, 158]. This study found no associations between pain severity and BMD at the total lateral or medial plateau. Instead, our findings suggest that pain may be related to localized

BMD differences[15], as indicated by the higher lateral focal 'spot' BMD in patients with 'severe pain' versus 'no pain' at depths of 2.5-5mm and 5-10mm from the subchondral surface. Further investigations, with depth-specific imaging techniques capable to measure localized regional BMD, are needed to clarify the possible role of local subchondral bone density in OA-related pain.

Our results show higher BMD at the lateral plateau and a tendency for lower BMD at the medial plateau and as pain severity intensifies. These observations may be due to cyst presence and associated knee alignment. First, cyst presence may have been indirectly captured as low BMD measures, especially in the medial plateau. In this study, 78% of the individuals with 'severe pain' had CT evidence of cysts of moderate size and number, focused predominately in the medial plateau. Conversely, only 12% of the individuals with 'no pain' had radiographic evidence of cysts of similar size and number. Interestingly, our regional BMD measures appeared to indirectly reflect cyst size and number. Second, patients with severe pain appear to have altered joint alignment. Of the 9 knees with severe pain, 44% had valgus alignment and 33% had evidence of joint laxity with medial shifting of the femur relative to the tibia. Conversely, of the 17 knees with no pain, most were in either varus (71%) or neutral alignment (24%), with only 1 knee in valgus. This malalignment could result in loading-induced adaptation and lower medial BMD and higher lateral BMD[28, 201, 202]. This malalignment may a consequence of advancing disease progression[203] or a consequence of self-adjusted joint alignment to help alleviate joint pain caused by other factors, such as medial cyst presence. Given that the lateral compartment has a smaller contact area then the medial compartment, and higher associated contact and interosseous stresses, it is possible that patients with valgus alignment are simply more susceptible to severe knee pain. It is possible that higher lateral BMD has influenced local innervation[191, 192], leading to pain. Though, as noted earlier, observed higher lateral BMD may be a secondary effect caused by medial cyst presence.

Cyst findings generate an interesting hypothesis to explain why individuals with 'severe pain' had a trend for lower medial bone density than individuals with 'no pain'. Severe pain may be partly due to greater bone resorption and necrotic cyst development, both manifesting as low BMD. The 'bony contusion theory' [127, 128] proposes that excessive loading or trauma causes trabecular micro fractures, necrotic bone and focal bone resorption, eventually resulting in cyst development near the subchondral bone surface. Inflammatory macrophages within the lining of

cysts are capable of forming into osteoclasts [204], which could promote further bone resorption and cyst expansion [205]. Bone surrounding cysts have been reported to be necrotic and lacking of blood vessels or normal marrow components[206], which could contribute to pain[207, 208]. Local subchondral bone cyst presence is also thought to increase intra-osseous stress distributions, leading to pain and disability[131]. Further research is needed to isolate cysts from surrounding subchondral bone to investigate this hypothesis further.

Strengths of this study include sample characteristics, the use of an internal control, normalization of our depth-specific measurements, and the use of a validated imaging technique. Our study sample was a homogeneous group of patients with similar OA severity and known covariates (age, sex, and BMI) between pain groups, possibly reducing the effect of possible confounding factors affecting BMD and pain. Also, we used tibial shaft cortical area and density measurements to account for possible between-group differences in systemic and/or local factors that may be associated with subchondral BMD. All BMD measurements were normalized according to mean proximal tibial volume and plateau surface area, and all imaged volumes were rotated and reoriented in similar 3D orientations relative to manually selected landmark boundary points and best-fit planes. This permitted reliable comparisons between groups. Lastly, we used a validated precise depth-specific image processing technique to assess plateau and local BMD[22]. The observed differences in local BMD between 'severe pain' and 'no pain' groups were ~7x greater than associated precision errors[22], and are therefore trustworthy.

This study has certain limitations. First, pain severity and assessment was based on the entire knee joint, including all joint surfaces (tibiofemoral and patellofemoral) and tissues (e.g., bone, menisci, synovium), and it is uncertain if pain originated at the proximal tibial surface, other tissues, or a combination of surfaces and tissues. Second, although OA severity was homogeneous throughout study participants, all were in late stages of OA and it may not be possible to apply our findings to patients with less severe OA. Larger longitudinal studies, with participants at varying stages of OA, should be completed to confirm our findings and clarify the relationship between BMD and OA-related pain, particularly nocturnal pain.

4.6. Conclusion

Depth-specific imaging techniques demonstrated higher lateral maximum focal BMD in patients with "severe pain', compared to patients with 'no pain' at night in bed, at depths of 2.5-5mm,

and 5-10mm from the proximal tibial subchondral surface. This study suggests that deep subchondral bone layers, as opposed to the bone immediately adjacent to the subchondral surface, may have a role in OA-related pain pathogenesis.

5. EPIPHYSEAL AND METAPHYSEAL BMD AND PAIN

5.1. Synopsis

This chapter outlines details of our study investigating relationships between proximal tibial epiphyseal and metaphyseal BMD and WOMAC pain in patients with knee OA. In this study, we report that higher total WOMAC pain is associated with lower total metaphyseal and epiphyseal BMD, as well as lower medial epiphyseal BMD. This study suggests that lower proximal tibial trabecular BMD may have a role in OA-relates pain pathogenesis.

5.2. Introduction

Knee OA is a debilitating and painful disease characterized by changes in cartilage and subchondral bone. Pain is a complex combination of social, psychological and biological factors[72]; and is often the primary sign that a patient may be afflicted with OA[2]. Unfortunately, the local biological pain pathogenesis within the knee joint is poorly understood[185] as it could be related to many structural factors (e.g., altered joint alignment[91], BMLs[78], cyst presence[106]). Knee OA is commonly characterized by altered subchondral properties, including altered subchondral bone thickness[187], bone volume fraction[188], and BMD[24]. Importantly, altered BMD may disrupt local innervation[192] and/or the local mechanical behaviour of bone[193], and thus may be a factor in OA-related knee pain.

To date, research investigating associations between OA-related knee pain and bone has focused primarily on bone near the subchondral surface (e.g., subchondral cortical and subchondral trabecular bone)[158, 209]. Adjacent trabecular bone (e.g., epiphyseal bone, metaphyseal bone) is also affected by OA[24], with observations of thinner trabeculae, lower bone volume fraction, and lower density with progressing OA severity[23, 190, 210]. To date, there are no studies reporting relationships between epiphyseal or metaphyseal trabecular BMD and pain. A recent FE study conducted by Amini et al.[166] has suggested that low epiphyseal trabecular bone density in OA[23, 190, 210] , which is directly linked to the elastic modulus of epiphyseal bone[211], may explain OA proximal tibiae being less stiff than normal[166]. Importantly, a less stiff proximal tibia would result in higher bone deformation potentially explaining (at least to some degree) OA-related knee pain.

A clear understanding of pain pathogenesis is crucial for rational therapeutic targeting[122]. Further, as pain is the reason patients seek medical care, rational treatment targeting requires specific understanding of which structures contribute to pain[122]. With the aim of furthering our understanding of potential factors that my influence knee pain, the objective of this study was to investigate relationships between proximal tibial epiphyseal and metaphyseal trabecular BMD and OA-related knee pain.

5.3. Methods

5.3.1. Study Participants

Forty-two participants (17M: 25F; mean age 64, SD ± 10.1 years; mean BMI 28.7 ± 3.7; 18L: 24R) with OA were recruited prior to TKR[209]. Study exclusion criteria included: pregnant women, patients having a revision replacement instead of primary knee replacement, and patients with a prior history of bone pathology at the knee joint. The Institutional Research Board of the New England Baptist Hospital approved the study. Informed consent was obtained from all study participants.

5.3.2. Participant Assessment

OA severity was classified using KL scoring[59]; participants ranged in severity from scores of 2 to 4. Pain severity was measured at the affected knee joint using the pain subsection of WOMAC[75]. Participants were asked to assess the level of pain in the affected knee joint within the past 24-hours while walking on a flat surface, going up or down stairs, nocturnal pain at night in bed, sitting or lying down, and standing upright using a 5-point Likert scale (0 to 4). Individual element pain scores were then summed for a possible WOMAC pain score of 20. Summed pain scores ranged from 4 to 16. We also used the Self-Administered Comorbidity Questionnaire[212] to assess participants for any potential confounding comorbidities (e.g., diabetes, heart disease).

5.3.3. CT Acquisition

We used a single energy clinical CT scanner (Lightspeed 4-slice, General Electric, Milwakee, WI, USA) for bone imaging. A solid QCT reference phantom of known bone mineral densities (Model 3T, Mindways Software Inc., Austin, TX, USA) was placed under the participants and included in all CT scans. Participants were oriented supine within the CT gantry and both legs were simultaneously scanned. Scans included the distal femur, patella, proximal tibia, and the

66% tibial shaft site proximal to the distal tibial end-plate[196]. Only the proximal tibia and the 66% tibial shaft site were used in the current analysis.

CT scanning parameters included: 120kVp tube voltage, 150mAs tube current-time product, axial scanning plane, 0.625mm isotropic voxel size (0.625 slice thickness, 0.625mm x 0.625mm in-plane pixel size), ~250 slices, ~60s scan time. A standard bone kernel (BONE) was used for CT image post-processing. Effective radiation dose was ~0.073mSv per scan, estimated using shareware software (CT-DOSE, National Board of Health, Herley, Denmark). For comparison, the average effective radiation dose during a transatlantic flight from Europe to North America is about 0.05mSv[197].

5.3.4. CT Image Analysis

We used a custom algorithm, developed specifically for this study, (Matlab 2010b; MathWorks, Natick, MA, USA) combined with manual segmentation to determine epiphyseal and metaphyseal trabecular BMD. We considered the epiphyseal region (subarticular region) as the proximal tibial volume between the subchondral surface and the epiphyseal line[41]. A single user (WDB) performed all segmentations and analyses. As this algorithm was developed specifically for this study, we assessed repeatability in a precision study performed on an independent sample of healthy participants and participants with OA[22] using recommended methods[213]. In summary, 14 participants were scanned 3 times with repositioning between each scan (42 scans, 28 degrees of freedom (DOF)). The repeatability expressed as precision error, of each BMD measurement was assessed using root mean square coefficients of variation (CV%) and ranged from 0.7% to 3.6%.

To derive BMD, grayscale HU were converted to equivalent volumetric BMD (mg/cm^3 K_2HPO_4) using subject-specific linear regression equations developed from known densities ranging from -50 to 375 mg/cm^3 K_2HPO_4 within the QCT phantom included in each individual axial image (r^2>0.99)[162] and interpolation to determine equivalent volumetric BMD values. Higher density values were linearly extrapolated. (Figure 5-1A). Subject-specific half maximum height thresholds[199] were then determined to define the proximal tibial subchondral and cortical surfaces. Two 3D image volumes were built, one including the entire proximal tibia as previously described[162, 209] and another by segmenting individual serial images using semi-automatic region growing and manual correction at the epiphyseal line (Figure 5-1B). Both sets

of imaged volumes were segmented using commercial software (Analyze10.0; Mayo Foundation, Rochester, MN, USA) and an interactive touch-screen tablet (Cintiq 21UX; Wacom, Krefeld, Germany). Imaged volumes were reoriented to a neutral position where medial and lateral plateaus were approximately parallel. We then divided the imaged volumes into medial and lateral compartments, measured by using 40% of the maximum medial-lateral axis of each respective side[23] (Figure 5-1C).

To ensure that trabecular BMD measures did not include cysts (which would lead to arbitrarily low measures of BMD)[209, 214] or peripheral high density cortical bone, the most proximal 7.5 mm region (relative to the subchondral surface) was removed from the segmentations (Figure 5-1D), as was 2.5 mm of peripheral cortical bone (Figure 5-1D). The 7.5 mm depth was based upon observed cyst locations from our earlier work[209, 214] and work by Chiba et al.[18], which limited depth analyses to 5 mm from the subchondral surface. In extreme cases, large cysts extended from the subchondral cortical region (0-2.5mm) through the subchondral trabecular region (2.5-5mm) and occasionally into depths greater than 5mm from the subchondral surface. By using a conservative 7.5mm depth from the subchondral surface, we ensured the exclusion of large cysts from our analysis. Following material removal, we measured epiphyseal trabecular BMD from the 7.5mm depth to the epiphyseal line (Figure 5-1E), which was located approximately 15 mm from the subchondral surface. Metaphyseal trabecular BMD was measured 10mm distal to the epiphyseal line (Figure 5-1E).

We included cortical BMD of the tibia shaft (66% of tibia length, proximal from distal tibia plateau)[196] to assess whether associations with pain were systemic or joint-specific. More specifically, if similar associations between pain and BMD were observed at the proximal tibia and tibial shaft, this would indicate systemic effects with low BMD being a plausible secondary effect of other factors, such as mechanical loading, nutrition or medication[200]. Tibial shaft cortical BMD was segmented using subject-specific half-maximum-height thresholds, and measured using commercial software (Analyze10.0; Mayo Foundation, Rochester, MN, USA).

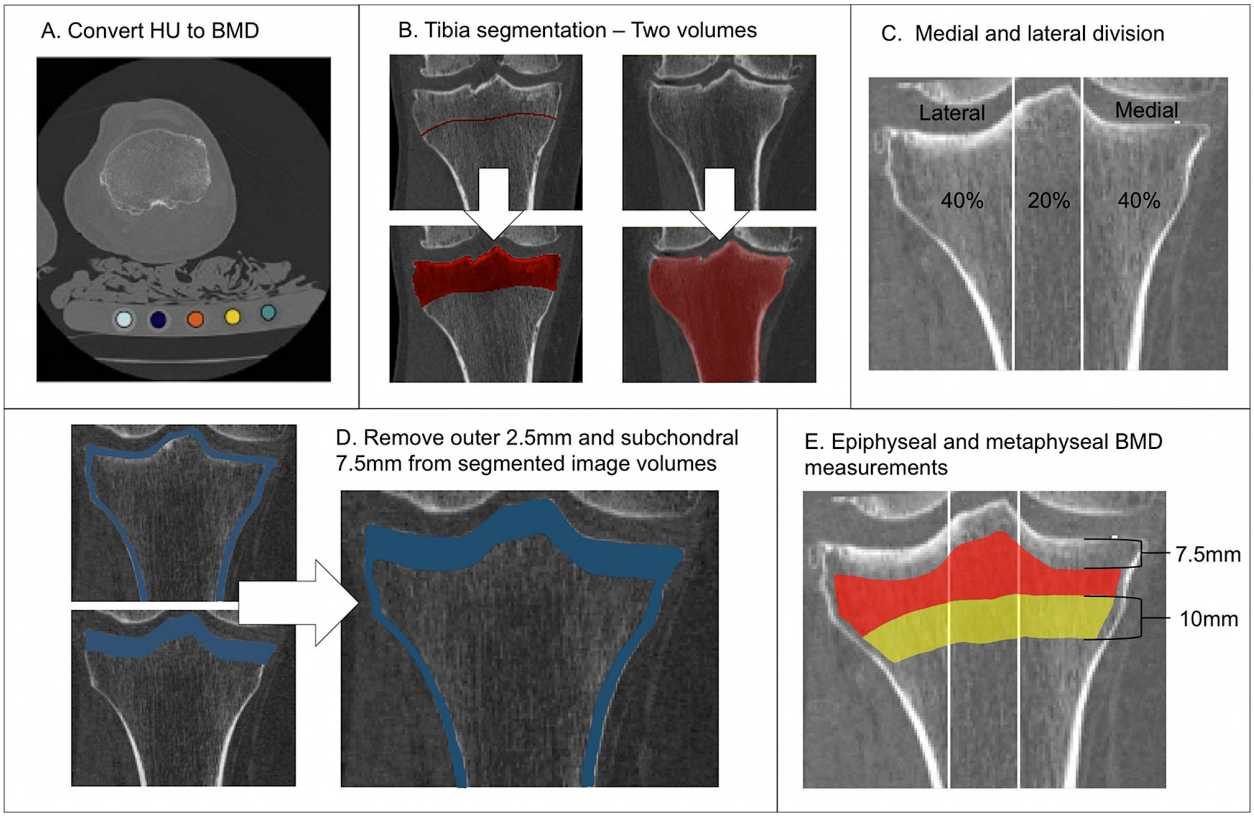

Figure 5-1. Methodological process consists of converting CT grayscale intensities to BMD using a QCT reference phantom (A), followed by building two imaged volumes for each tibia, one with manual correction at the epiphyseal line and one using the full tibia (B). Imaged volumes were divided into lateral and medial regions (C), then the outer 2.5mm and subchondral 7.5mm depth were removed from each imaged volume (D). BMD measurements included epiphyseal BMD between the epiphyseal line and 7.5mm from the subchondral surface and metaphyseal BMD 10mm distal from the epiphyseal line (E).

5.3.5. Statistical Analysis

We first checked all underlying assumptions for multiple linear regression (assumptions of linear relationships, homoscedasticity, independency and normality of residuals) using standardized residual scatter plots, P-P plots, and histograms[215]. We identified any outliers using modified Thompson tau (τ) test[216].

We illustrated univariate associations between pain and BMD using scatter plots and reporting coefficients of determination (R^2) for linear regression. We used hierarchical multiple regression analyses to explain the variance in total WOMAC pain. We selected age, sex, and BMI as covariates for our base model based on observed correlation in univariate analysis (age) and literature (age, sex, and BMI) evaluating relationships between BMD and pain[149, 158]. All

BMD measurements (total and regional epiphyseal BMD, total metaphyseal BMD, and tibial shaft cortical BMD) were individually added to our base model. We assessed multicollinearity between all independent variables in each model using variance inflation factor (VIF), setting the maximum tolerance value as 10. We report adjusted R^2, change in R^2 from the base model (Δ), standardized beta (β)-coefficients, and *p*-values. Statistical significance was defined as $p<0.05$, and analyses were performed using SPSS 21.0 (IBM, Armonk, NY, USA).

5.4. Results

Characteristics of all study participants, including age, sex, BMI, KL grades, joint space narrowing score (JSN), non-weight-bearing alignment scores, and BMD measures are shown in Table 5-1. Unadjusted relationships between total WOMAC pain and total or regional epiphyseal or metaphyseal BMD measurements are presented in Figure 5-2. As per the modified Thompson τ test[216], we identified a single outlier based on total WOMAC pain score with a τ-value outside of the sample's rejection zone ($\tau > 5.56$), and removed it from the analysis. All underlying assumptions for linear regression were appropriately met. There was no evidence of multicollinearity between independent variables in any of our models.

Regression models predicting variance in pain are presented in Table 5-2. After adding total epiphyseal BMD to the base model, (of age, sex, and BMI) the coefficient of determination (R^2) in total pain improved ($\Delta R^2=0.13$). Our models improved when medial epiphyseal BMD ($\Delta R^2=0.14$) and metaphyseal BMD ($\Delta R^2=0.13$) were independently added to our base model. There was no association between cortical BMD at the 66% tibial site and pain.

Table 5-1. Descriptive statistics for background characteristics of study participants.

Characteristic	Without outlier (n=41)
Age (mean ± SD)	64.1 ± 10.2
Sex (M:F)	17:24
BMI (mean ± SD)	28.6 ± 3.7
Side (L:R)	17:24
OA Severity (KL) (0/1/2/3/4)	0/0/2/19/18
WOMAC Score	9.7 ± 2.8
Medial Joint Space Narrowing (0/1/2/3/4)	0/6/9/24*
Lateral Joint Space Narrowing (0/1/2/3/4)	30/5/0/4*
Non-weight-bearing alignment	27 varus, 6 neutral, 8 valgus
Total epiphyseal BMD, mg/cm^3 K_2HPO_4 (mean ± SD)	106 ± 37
Lateral epiphyseal BMD, mg/cm^3 K_2HPO_4 (mean ± SD)	106 ± 34
Medial epiphyseal BMD, mg/cm^3 K_2HPO_4 (mean ± SD)	141 ± 68
Total metaphyseal BMD, mg/cm^3 K_2HPO_4 (mean ± SD)	90 ± 36

*JSN scores not available for 2 participants.

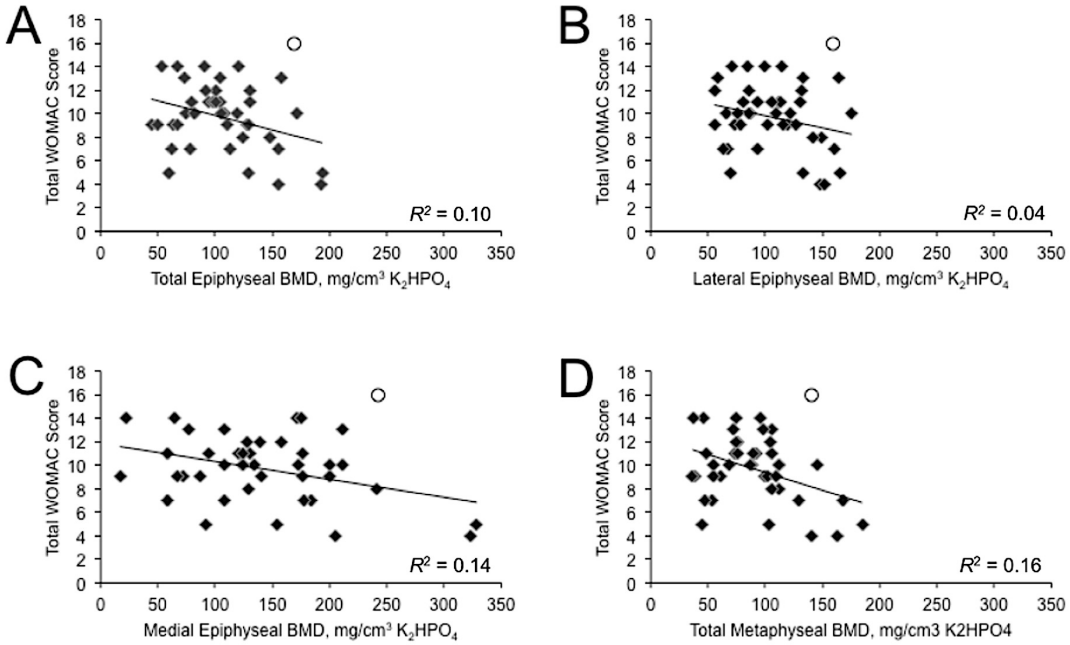

Figure 5-2. Scatter plots and coefficients of determination (R^2) of the relationships between total WOMAC score and A) total epiphyseal BMD (p=0.040), B) lateral epiphyseal BMD(p=0.187), C) medial epiphyseal BMD (p=0.015), and D) total metaphyseal BMD (p<0.009). The single outlier is noted as a circle, and was not included in the bivariate analysis.

Table 5-2. Adjusted coefficients of determination (R^2), standardized beta coefficients (β), and level of significance (p) of the base model (age, sex, and BMI) and change in base model R^2 (Δ) when including bone mineral density (BMD) at the total and regional proximal tibia to predict variance in total WOMAC pain. Significant R^2, Δ, and β are bolded.

		Total WOMAC		
		R^2	β	p-value
Base Model		**0.16**		**0.023**
	Age		**-0.41**	**0.011**
	Sex		0.19	0.206
	BMI		0.12	0.448
Total epiphyseal		**0.27**		**0.004**
	Δ	0.12		**0.017**
	Age		**-0.41**	**0.006**
	Sex		0.08	0.572
	BMI		0.18	0.242
	BMD		**-0.37**	**0.017**
Lateral epiphyseal		**0.19**		**0.020**
	Δ	0.05		0.140
	Age		**-0.40**	**0.011**
	Sex		0.145	0.338
	BMI		0.16	0.308
	BMD		-0.23	0.140
Medial epiphyseal		**0.30**		**0.002**
	Δ	0.15		**0.006**
	Age		**-0.39**	**0.008**
	Sex		0.12	0.388
	BMI		0.19	0.186
	BMD		**-0.40**	**0.006**
Total metaphyseal		**0.27**		**0.004**
	Δ	0.12		**0.017**
	Age		**-0.35**	**0.019**
	Sex		0.12	0.416
	BMI		0.15	0.302
	BMD		**-0.35**	**0.017**

5.5. Discussion

Our regression models suggested that tibial epiphyseal and metaphyseal BMD independently explained variance in total pain in OA patients prior to TKR, where patients with lower epiphyseal and metaphyseal BMD tended to have higher levels of pain. Regionally, our models indicated that medial epiphyseal BMD was a significant predictor of total OA-related pain, again where lower BMD was associated with higher levels of pain. This is the first study to assess the relationship between tibial epiphyseal and metaphyseal BMD and pain in a sample of patients with clinically assessed OA using clinical QCT. These findings suggest that there may be potentially overlooked characteristics in proximal tibial BMD, such as trabecular BMD, which may have a role in OA-related pain pathogenesis.

Study findings support our previous work (using the same cohort), which investigated links between OA-related nocturnal pain and subchondral cortical and subchondral trabecular bone near the subchondral surface (0-10mm from the surface). This previous study found a (nonsignificant) trend for low medial BMD[209] in patients with severe nocturnal pain, which is in agreement with study findings of low medial epiphyseal, total epiphyseal and metaphyseal BMD in patients with high levels of pain. We[209], and others[214], however questioned whether our previously observed trend for low medial BMD was due to cyst presence or diminished bone architecture and/or mineralization. Subsequent follow-up analyses indicated that both cyst presence and BMD were independently associated with pain[217]. The novelty of this study was that we focused our analyses in epiphyseal and metaphyseal trabecular regions largely void of cysts to determine any potential independent associations between BMD and pain.

Of note, study findings both support and contrast with the previous study which also identified high lateral focal BMD in the subchondral trabecular region (2.5-10mm below surface) of patients with severe nocturnal pain[209]. High lateral focal BMD may be explained by BML presence, chondroprotection, or altered loading. First, prior research with this cohort identified a positive association between nocturnal pain and bone marrow lesion (BML) presence[140]. Given that BMLs have higher local BMD than surrounding bone tissue[15], a positive association between nocturnal pain and BMD is foreseeable. Future research needs to evaluate whether high focal BMD measures exactly overlay BML locations. Second, high lateral focal BMD may be a consequence of chondroprotection developed via low trabecular bone density. To explain, recent finite element (FE) simulations indicated that reduced proximal tibial trabecular bone density

results in lower subchondral bone stiffness[166] and lower cartilage stresses[167], the latter presumably due to improved congruence between articulations[218]. As many of the study participants had evidence of medial OA, low trabecular BMD may be a physiologic response to lower medial cartilage stresses. At the same time, this chondroprotective process would also naturally transfer more load to the lateral compartment since the two compartments function in parallel. This altered loading should result in loading-induced adaptation; specifically, higher lateral BMD near the subchondral surface to meet the mechanical demands of higher load transmission. Third, many of the study participants with evidence of medial OA may be self-altering their knee kinematics and stance to off-load the medial compartment, with the aim of alleviating joint pain. This altered loading could result in loading-induced adaptation with higher lateral BMD and lower medial BMD[28]. Fourth, as higher BMD appears to be focused in subchondral regions (<10mm from the tibial surface)[209], joint load may be primarily transferred through the subchondral cortical endplate and subchondral trabecular bone to the peripheral cortex, off-loading epiphyseal and metaphyseal trabecular bone, thus explaining lower BMD found in these regions. However, this explanation warrants further research given that we did not find associations between pain and alignment[217]. Studies using subject-specific FE modeling are needed to investigate load transmission as well as subchondral bone stiffness at different stages of pain severity and disease progression.

By removing adjacent cortical bone and isolating trabecular BMD, we were able to focus on the potential mechanical relationship between low epiphyseal trabecular BMD and high OA-related pain. As noted earlier, a recent FE study[166] suggested that low epiphyseal trabecular bone density observed in OA[23, 190, 210] results in lower stiffness of OA proximal tibiae[166]. Less stiff trabecular bone could be subject to higher strain, deformation, and flexibility. Pain may result from potential micro-fractures or through a more flexible structure which may disturb local innervation[192]. These results suggest that epiphyseal trabecular bone may be just as important in OA-related pain pathogenesis as the more commonly examined subchondral bone.

This study has various strengths to consider. First, our study sample comprised of a homogeneous group of OA patients of similar age and BMI, as well as similar OA status, possibly reducing possible confounding factors affecting BMD and pain. Second, we used clinical QCT imaging to measure relationships between tibial epiphyseal BMD and OA-related pain. Our 0.625mm isotropic voxel size and the ability to build an imaged volume of the entire

proximal tibia allows for 3D measurements of larger regions previously not available using other imaging modalities such as pQCT or fractal signature analysis (FSA). Third, even with manual correction along the epiphyseal line, all precision errors associated with our segmentation and image-processing techniques were all under 5%.

This study has certain limitations. First, pain severity and assessment was based on the entire knee joint, including all joint surfaces (tibiofemoral and patellofemoral) and tissues (e.g., bone, menisci, synovium), and it is uncertain if pain originated within the proximal tibial bony structure, other tissues, or a combination of tissues. Second, although OA severity was homogeneous throughout study participants, all were in late stages of OA and it may not be possible to apply our findings to patients in early stages of OA. Third, our study sample size was small (n=41). Further analysis with larger samples including healthy participants and participants with various stages of OA severity and pain, are needed to verify these preliminary study findings. Of note, our sample was comprised of participants with severe OA (primarily with KL scores of 3 to 4). This limited range constrained our ability to include it in the statistical model. Also, with a basic rule of a minimum of 10 events (or samples) per predictor[219], we were limited to four predictors (independent variables) in each model: one independent variable (BMD) and three covariates (age, sex, BMI), and thus could not add additional known predictors of pain to our statistical analysis (e.g., smoking/alcohol history, activity level, mental health status, specific medications). Of note, we attempted to account for possible differences in physical activity (mechanical loading/unloading) through usage of cortical BMD measures at the 66% tibial shaft site. Previous works have noted differences in tibial shaft cortical BMD between highly active individuals (e.g., sprinters, endurance runners, triple- and high-jumpers, hurdlers) and less active controls[220]. However, in this study, we did not note any associations between pain and tibia shaft cortical BMD, potentially indicating, at least to some degree, similar levels of activity and mechanical loading amongst study participants. Fourth, in our interpretation of the effect of mechanical stiffness on OA-related knee pain, we have presumed that low epiphyseal and metaphyseal BMD is indicative of low proximal tibial bone stiffness. This presumption is based on a recent FE simulation study[166] and established relationships between bone density and elastic modulus[211]. Further research is needed using subject-specific FE modeling to directly investigate potential links between knee pain and proximal tibial mechanical behaviour (e.g., stiffness, stress/strain distribution). Fifth, our 0.625mm isotropic voxel size prevented assessment of

trabecular microarchitecture and limited us measures of volumetric BMD. Accordingly, it is unclear if low BMD is due to trabecular thinning or wide trabecular spacing. For future research, it would be advantageous to investigate links between pain and trabecular micro-architecture with advanced texture analysis and smaller voxel sizes[188].

It is worthwhile noting that we present statistically significant relationships as opposed to clinically significant relationships. As a statistically significant relationship does not measure the clinical effect of a result[221], it is important to consider the clinical effect that changes in epiphyseal or metaphyseal BMD may have on OA-related knee pain. According to Angst et al.[222], the minimal clinically important difference for OA-related pain is a change in WOMAC score greater than 6% of its maximum value (which is 20 for WOMAC). In other words, a change in pain will not be perceived unless the WOMAC score changes by 1.2 points. With this in mind, we can identify the BMD change that will correspond with a 1.2-point pain change. Based on our model, a 44 g/cm^3 reduction in epiphyseal or metaphyseal BMD will be marked by a perceived change in pain status. Assuming an average BMD of 100 g/cm^3 for epiphyseal and metaphyseal bone, this would equate with ~50% change in density. Accordingly, a rational therapeutic approach would be to monitor bone while simultaneously striving to maintain bone and limit bone loss. Density changes in these regions could be monitored using QCT, dual energy-absorptiometry (DXA) or x-ray. With regards to maintaining bone, potentially, this could be achieved through exercise interventions or pharmacological therapies. Our preliminary findings may also be clinically important for TKR preparation and planning. Patients with low pre-operative BMD have been shown to be at higher risk of implant failure by loosening or migration[223], higher risk for revision surgery[224], and risk of failure following revision procedures[224]. Current tibial implant design components typically include a single central post, which is inserted through the tibial epiphysis and extends into the tibial shaft. Based on our findings, there may be low quantities of bone stock in individuals with higher levels of OA-related pain, potentially placing them at risk for inadequate osseointegration and implant fixation[225] and possibly implant loosening[226]. As there is an expected normal decrease in tibial BMD during healing[227], reduced amounts of tibial epiphyseal bony support structure prior to TKR could compromise implant fixation and success in early stages, potentially compromising long-term implant success. It may be beneficial to use imaging and complementary image-processing techniques to evaluate pre-operative bone density, especially in the commonly

overlooked tibial epiphyseal and metaphyseal regions, to compliment customized surgical approaches in patients with higher levels of pain.

5.6. Conclusion

In our study, low tibial epiphyseal and metaphyseal BMD, as well as low medial epiphyseal BMD, was associated with OA-related pain in patients prior to TKR. This study suggests that there may be overlooked characteristics within trabecular bone that may be related to OA-related pain pathogenesis. These preliminary findings from current and previous studies[209] may be valuable in guiding outcome selection in OA studies addressing subchondral bone and pain, particularly in determining regions of interest of the proximal tibia for potential epidemiological studies.

6. SUBCHONDRAL CYSTS AND PAIN

6.1. Synopsis

This chapter outlines details of our study investigating relationships between proximal tibial cysts parameters and clinical characteristics of OA (alignment, joint space narrowing, OA severity, WOMAC pain) and subchondral BMD in patients with knee OA. In this study, we report that at the lateral region, greater cyst number and greater cyst volume are associated with higher subchondral BMD, valgus alignment, and lateral joint space narrowing. We also report that pain and OA severity were not associated with any evaluated cyst parameters. This study suggests that there may be disease-associated changes in tibial loading distribution leading to cyst development and further joint deterioration in patients with painful severe OA.

6.2. Introduction

Knee OA is a painful and debilitating disease characterized by cartilage deterioration and altered subchondral bone. Recently, there has been increasing interest in the role of subchondral bone cysts in OA progression; in particular how subchondral bone cysts may influence pain[9, 209, 217], or how subchondral bone cysts influence subchondral bone mechanical behaviour[131].

Subchondral cysts are typically spherical or ellipsoidal cavities within the subchondral bone region and are related to both altered subchondral bone and cartilage degeneration in patients with OA[17, 18, 228]. Recent studies have indicated associations between subchondral bone cysts and pain[9] as well as BMLs in patients with knee OA[228], though, evidence of relationships between cysts and other patient characteristics (e.g., disease severity, joint space narrowing, alignment) is limited. A clear understanding of disease pathogenesis is crucial for rational therapeutic targeting[122], particularly understanding of which structures contribute to pain[122]. As subchondral cysts are related to many elements in the progression of OA[206, 229], it is meaningful to investigate and improve our understanding OA subchondral bone cysts in patients with knee OA using clinical imaging tools and to determine if cyst parameters, specifically number and size are related to disease severity and pain.

It is believed that subchondral cyst presence promotes higher localized stress[131], which could stimulate bone remodelling or bone alterations. *Ex vivo* studies at both the hip using HR-QCT[18], and the tibia using micro-CT[17] report changes in BMD, especially in regions adjacent to cysts. These *ex vivo* studies are able to evaluate cyst number and size, but are not able to

correlate cyst properties with important clinical symptoms such as pain. Clinical techniques, such as MRI and QCT have the potential to offer 3D characterizations of cyst structure. Using MRI techniques, cysts can be distinguished from other bony features, such as BMLs[106, 230], but it is difficult to reliably quantify BMD. Clinical QCT has potential to characterize cysts *in vivo*, to explore relationships with clinical OA symptoms (such as pain), to determine tibial BMD, and could potentially be used to evaluate 3D cyst development throughout disease progression to determine the role of cysts in OA. However, it is unclear which specific cyst parameters (e.g., number, size) are associated with clinical symptoms, and which parameters are associated with BMD.

The objective of this study was to use QCT and image-processing techniques to determine relationships between subchondral cyst parameters and subchondral BMD as well as clinical characteristics of OA (OA severity, OA-related pain, alignment, joint space narrowing) in patients with knee OA.

6.3. Methods

6.3.1. Study Participants

Forty-two participants (17M: 25F; mean age 64, SD ± 10.2 years; mean BMI 28.6 ± 3.7; 18L:24R) with OA were recruited before total knee replacement. Study exclusion criteria included: pregnant women, patients having a revision replacement instead of primary knee replacement, and patients with a prior history of bone pathology at the knee joint. The Institutional Research Board of the New England Baptist Hospital approved the study. Informed written consent was obtained from all study participants.

6.3.2. Participant Assessment

OA severity was classified using KL scoring[59] on standardized radiographs. Participants ranged in severity from scores of 2 to 4. We included medial and lateral joint space narrowing (JSN), as a surrogate measure of lateral or medial cartilage degradation, and CT-measured knee alignment in our analysis. Knee alignment was categorized as varus, neutral, or valgus and measured using coronal and sagittal CT reconstructions to determine an estimate of mechanical alignment[217]. In brief, medial and lateral joint space widths were evaluated at equal distances from the tibial spine

permitting an estimation of alignment between the femoral and tibial axes. Neutral alignment was defined as 176 to 180°, and malalignment of ± 2° from the neutral position was considered as either varus (-2°) or valgus (+2°)[217]. For this analysis, alignment was treated as a categorical variable, where participants exhibited either varus (-1), neutral (0), or valgus (1) alignment. Pain severity was measured at the affected knee joint using the pain subsection of the WOMAC[75]. Participants were asked to assess the level of pain in the affected knee joint within the past 24-hours while walking on a flat surface, going up or down stairs, lying down in bed at night, sitting or lying down, and standing upright using a 5-point Likert scale (0 to 4). Individual element pain scores were then summed for a possible total WOMAC pain score of 20, with scores ranging from 4 to 14. We also included pain lying down in bed at night (nocturnal pain), scored from 0 (none) to 4 (extreme) as a patient characteristic to correspond with our earlier work evaluating pain and subchondral BMD[209] We used the Self-Administered Comorbidity Questionnaire[212] to assess participants for any potential confounding comorbidities (e.g., diabetes, heart disease).

6.3.3. QCT Acquisition

We used a single energy clinical CT scanner (Lightspeed 4-slice, General Electric, Milwaukee, WI, USA) for bone imaging. A solid QCT spine reference phantom of known bone mineral densities (Model 3T, Mindways Software Inc., Austin, TX, USA) was included in all CT scans. Participants were oriented supine within the CT gantry and both legs were simultaneously scanned. Scans included the distal femur, patella, proximal tibia, but only the proximal tibia was analyzed with this study.

CT scanning parameters included: 120 kVp tube voltage, 150 mAs tube current-time product, axial scanning plane, 0.625 mm isotropic voxel size (0.625 mm slice thickness, 0.625 mm x 0.625 mm in-plane pixel size), ~250 slices, ~60 second scan time. A standard bone kernel (BONE) was used for CT image post-processing. Effective radiation dose was ~0.073 mSv per scan, estimated using shareware software (CT-DOSE, National Board of Health, Herley, Denmark). For comparison, the average effective radiation dose during a transatlantic flight from Europe to North America is about 0.05 mSv[231].

Equivalent volumetric BMD (mg/cm^3 K_2HPO_4) values were obtained by converting grayscale Hounsfield units (HU) to BMD using subject-specific linear regression equations

developed from known densities within the QCT phantom included in each axial image (r^2>0.99)[162].

6.3.4. CT Image Analysis

6.3.4.1. Isolate Subchondral Region

We used a custom algorithm (Matlab 2016a, MathWorks, Natick, MA, USA) to isolate the subchondral region of the proximal tibia, by measuring a depth of 7.5mm from the subchondral surface (Figure 6-1A), using 3D imaged volumes of the proximal tibia from our previous work[232].

6.3.4.2. Cysts

Cysts were identified and manually segmented using commercial software (Analyze 10.0; Mayo Foundation, Rochester, MN, USA) and an interactive touch-screen tablet (Cintiq 21UX; Wacom, Krefeld, Germany). A single user (WDB) performed all segmentations. Cysts were considered as an elliptical or spherical volume of lower BMD (lower greyscale) surrounded entirely by an area of higher BMD (higher greyscale). Based Chiba et al.[18] and our previous studies evaluating cortical and trabecular subchondral bone[209] and the epiphyseal region of tibia[232], we only considered cysts within the subchondral region at a depth of 7.5mm from the subchondral surface (Figure 6-1B). All identified cysts were segmented using semi-automatic region growing guided by subject-specific and cyst-specific threshold values defining the 50% midpoint intensity values between cyst interior and adjacent bone, similar to the half maximum height threshold (HMH) technique[199]. Smaller cysts were manually segmented (Figure 6-1C). Any cyst volumes smaller than 8 voxels (1.95 mm^3) were not included in this analysis to mitigate any errors due to noise.

We used a custom algorithm (Matlab 2016a) to measure the following cyst parameters[18]: number of cysts, cyst number per total volume of the 0-7.5 mm depth region (number/cm^3), cyst volume per total volume (%), total cyst volume (mm^3), maximum cyst volume (mm^3), average cyst volume (mm^3), minimum cyst volume (mm^3), and standard deviation of cyst volume (mm^3) as a metric of cyst volume variability. To assess the repeatability of the cyst outcomes, a precision study was performed using recommended techniques (14 subjects scanned 3 times

each)[213]. Precision errors (root mean square coefficients of variation, $CV\%_{RMS}$) ranged from 0.7% to 3.6%.

6.3.4.3. BMD

We also determined relationships between cyst parameters and regional proximal tibial BMD. Segmented cyst volumes were subtracted from the previously defined subchondral volume of the proximal tibia (Figure 6-1D), to determine mean proximal tibial BMD excluding cysts. To assess the repeatability of BMD outcomes, a precision study was performed using recommended techniques (14 subjects scanned 3 times each)[213]. Precision errors (root mean square coefficients of variation, $CV\%_{RMS}$) ranged from 0.9% to 2.4%.

6.3.5. Regional Analysis

Proximal tibia imaged volumes were reoriented to a neutral position where medial and lateral plateaus were approximately parallel and divided into medial, central and lateral compartments, measured by using 40% of the maximum medial-lateral axis of each respective side (Figure 6-1D). We evaluated BMD and cyst parameters over the medial and lateral proximal tibial regions.

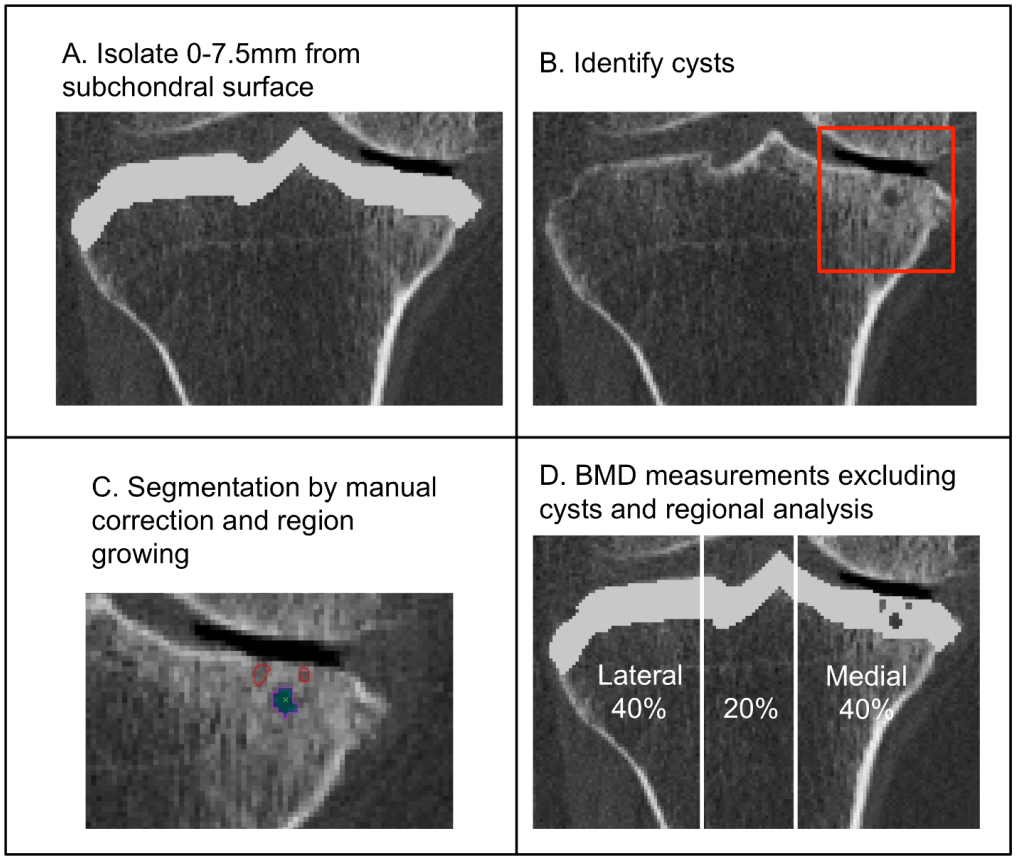

Figure 6-1. Process for identifying, isolating, and measuring cysts included isolating the subchondral region of 7.5mm from the subchondral surface (A), cyst identification on CT images (B), and segmenting individual cysts using semi-automatic region growing for larger cysts manual segmentation for smaller cysts (C). Segmented image volumes were then used to measure cyst parameters, and regional BMD excluding cysts which included total, lateral, and medial regions (D).

6.3.6. Statistical Analysis

We determined associations between cyst parameters and participant characteristics (age, sex, BMI) and clinical characteristics of OA (medial and lateral JSN, alignment, OA severity, total WOMAC pain, nocturnal pain, BMD) using Pearson's correlation coefficients for continuous variables and Spearman's rank correlation for categorical or ordinal variables. Due to the exploratory nature of this study with multiple correlations, we report the level of significance for both $p<0.01$ and $p<0.05$.

6.4. Results

Patient characteristics are found in Table 6-1. Total cyst number varied from none (0) to up to 30 over the total proximal tibia and up to 29 in the medial compartment (Table 6-2). Cysts were present in 88% of participants. Of these participants with subchondral cysts, 32% had cysts both medially and laterally, 14% had cysts only laterally, and 54% had cysts only medially. The ratio of cyst volume to tibial volume ranged from 0% to up to 14.8% over the total proximal tibia, and up to 13.7% in the medial region. For many cyst volume parameters, the standard deviation was similar to or greater than mean volume, indicating a large distribution in cyst volume within this sample (Table 6-2).

Table 6-1. Descriptive statistics for characteristics of study participants

Characteristic	Parameters
Age, years (mean ± SD)	64.1 ± 10.1
Sex (M:F)	17:25
BMI, kg/m^2 (mean ± SD)	28.7 ± 3.7
Side (L:R)	18:24
OA Severity (KL) (0/1/2/3/4)	0/0/2/21/19
WOMAC Score (score range: 0 to 20)	9.8 ± 2.9
Medial Joint Space Narrowing (JSN) (0/1/2/3/4)	10/6/10/14*
Lateral Joint Space Narrowing (JSN) (0/1/2/3/4)	30/5/1/4*
Non-weight-bearing alignment	28 varus, 6 neutral, 8 valgus
Total BMD, mg/cm^3 K_2HPO_4 (mean ± SD)	279 ± 51
Lateral BMD, mg/cm^3 K_2HPO_4 (mean ± SD)	240 ± 58
Medial BMD, mg/cm^3 K_2HPO_4 (mean ± SD)	311 ± 88

*Data missing for 2 participants

Table 6-2. Cyst parameters, mean ± SD (range).

	Total	Lateral	Medial
Cyst Number (Cyst.N)	7.0 ± 6.7 (0-30)	1.9 ± 3.0 (0-11)	3.9 ± 5.7 (0-29)
Cyst #/vol (Cyst.N/TV) (cm^3)	0.27 ± 0.26 (0-1.3)	0.2 ± 0.3 (0-1.3)	0.4 ± 0.6 (0-2.6)
Cyst vol/vol (Cyst.V/TV) (%)	1.3 ± 2.7 (0-14.8)	0.2 ± 0.5 (0-2.9)	1 ± 2.5 (0-13.7)
Total cyst volume (Tot.Cyst.V) (mm^3)	133.5 ± 245.8 (0-1253)	16.5 ± 44.1 (0-241.0)	98.6 ± 232.3 (0-1156)
Maximum cyst volume (Max.Cyst.V)(mm^3)	70.4 ± 140.6 (0-685.8)	9.5 ±32.5 (0-201.9)	58.0 ± 141.5 (0-685.8)
Average cyst volume (Avg.Cyst.V) (mm^3)	16.7 ± 25.8 (0-139.2)	2.6 ± 4.5 (0-21.9)	21.9 ± 49.9 (0-289.1)
Minimum cyst volume (Min.Cyst.V) (mm^3)	3.5 ± 5.9 (0-34.4)	1.0 ± 1.3 (0-4.2)	6.9 ± 19.2 (0-120.4)
Cyst volume SD (SD.Cyst.V)(mm^3)	28.4 ± 51.5 (0-252.1)	9.3 ± 16.2 (0.2-59.7)	40.8 ± 80.2 (0-338.8)

There were no significant associations between cyst parameters and age, OA severity (KL grade), total WOMAC pain, or nocturnal pain (Tables 6-3, 6-4 and 6-5). Over the total proximal tibia, we found significant positive relationships a) between alignment and total cyst number and b) between alignment and cyst number per tibial volume (Table 6-3). At the medial region, there were no significant associations between any cyst parameters and any participant characteristics (Table 6-4). At the lateral region (Table 6-5), valgus alignment was associated with most cyst parameters, including cyst number and volume. Similarly, greater JSN was associated with greater cyst number and volume. There were significant positive relationships between lateral BMD and cyst number as well as volume (Figure 6-2).

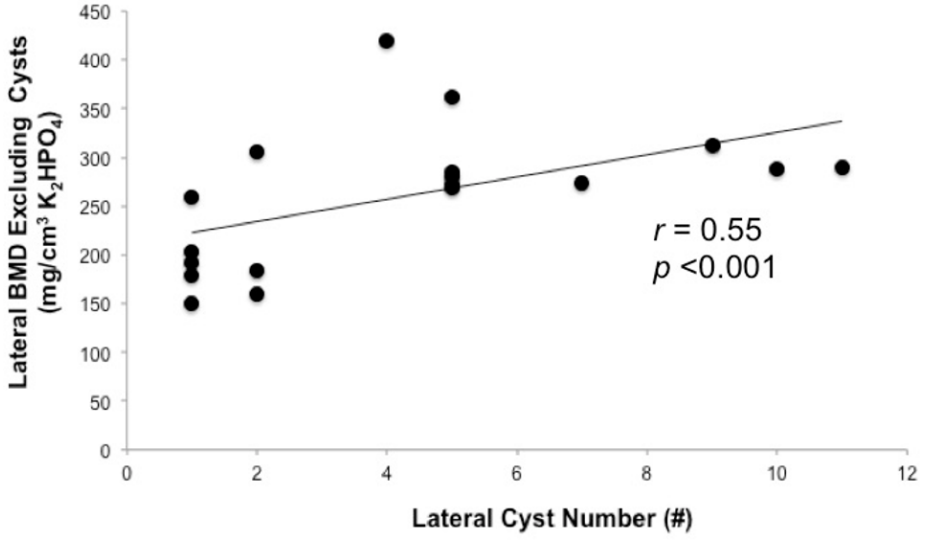

Figure 6-2. Scatterplot and Pearson's correlation coefficient (*r*) of the relationship between lateral BMD and lateral cyst number (Cyst.N), suggesting that more numerous cysts in the lateral region contributed to higher lateral BMD surrounding cysts.

Table 6-3. Correlation coefficients between cyst parameters and patient and clinical OA characteristics over the total proximal tibia. Pearson's correlation coefficient was used for all continuous variables. Spearman's correlation coefficient (*italics*) was used for all categorical variables where noted. Significant associations are marked.

	Cyst.N	Cyst.N/TV	Cyst.V/TV	Tot.Cyst.V	Max.Cyst.V	Avg.Cyst.V	Min.Cyst.V	SD.Cyst.V
Age	0.20	0.17	0.09	0.14	0.16	0.05	0.01	0.06
Sex	0.25	0.37	0.18	0.11	0.04	-0.03	-0.06	-0.11
BMI	-0.22	-0.27	-0.20	-0.18	-0.18	-0.08	0.04	-0.15
Alignment	0.33*	0.38*	0.19	0.16	0.09	0.02	0.01	-0.16
KL	0.30	-0.07	-0.08	0.37	0.32	0.31	0.11	0.17
Total WOMAC Pain	0.09	0.11	-0.03	-0.09	-0.11	-0.03	0.01	-0.11
Nocturnal Pain	0.26	0.25	0.07	0.09	-0.01	-0.09	-0.11	-0.12
Total BMD	0.05	0.02	-0.02	0.02	-0.003	-0.05	-0.04	-0.06

* $p<0.05$ ** $p<0.001$

Table 6-4. Correlation coefficients between cyst parameters and patient and clinical OA characteristics at the medial region**.** Pearson's correlation coefficient was used for all continuous variables. Spearman's correlation coefficient (*italics*) was used for all categorical variables. Significant associations are marked.

	Cyst.N	Medial Cyst.N/TV	Medial Cyst.V/TV	Medial Tot.Cyst.V	Medial Max.Cyst.V	Medial Avg.Cyst.V	Medial Min.Cyst. V	Medial SD.Cyst.V
Age	0.16	0.12	0.08	0.13	0.15	-0.04	-0.15	0.07
Sex	-0.05	0.06	-0.02	-0.05	-0.03	0.01	0.09	0.05
BMI	-0.07	-0.11	-0.12	-0.11	-0.10	-0.05	0.20	-0.17
Alignment	-0.10	-0.09	-0.14	-0.14	-0.14	0.00	-0.04	-0.41
Medial JSN	0.08	0.06	0.13	0.13	0.12	0.02	0.08	0.16
KL	-0.12	-0.13	-0.02	-0.02	0.03	0.05	0.04	0.19
Total WOMAC Pain	-0.06	-0.04	-0.04	-0.10	-0.08	0.06	0.06	-0.02
Nocturnal Pain	-0.09	-0.12	-0.11	-0.08	-0.08	-0.002	0.04	-0.003
Medial BMD	0.27	0.25	0.14	0.18	0.12	0.03	0.08	-0.02

* $p<0.05$ ** $p<0.001$

Table 6-5. Correlation coefficients between cyst parameters and patient and clinical OA characteristics at the lateral region. Pearson's correlation coefficient was used for all continuous variables. Spearman's correlation coefficient (*italics*) was used for all categorical variables. Significant associations are marked.

	Lateral Cyst.N	Lateral Cyst.N/TV	Lateral Cyst.V/TV	Lateral Tot.Cyst.V	Lateral Max.Cyst.V	Lateral Avg.Cyst.V	Lateral Min.Cyst.V	Lateral SD.Cyst.V
Age	0.16	0.15	0.12	0.14	0.09	0.19	0.21	-0.03
Sex	0.62**	0.62**	0.62**	0.62**	0.62**	0.64**	0.61**	-
BMI	-0.30	-0.31*	-0.35*	-0.34*	-0.34*	-0.36*	-0.26	-0.37
Alignment	0.60**	0.60**	0.61**	0.61**	0.62**	0.62**	0.44**	0.41
Lateral JSN	0.66**	0.66**	0.68**	0.67**	0.68**	0.68**	0.52**	0.40
KL	-0.13	-0.13	-0.11	-0.11	-0.10	-0.07	-0.08	0.22
Total WOMAC Pain	0.14	0.14	-0.10	-0.10	-0.14	-0.05	0.18	-0.46
Nocturnal Pain	0.24	0.25	0.23	0.23	0.22	0.20	0.17	-0.45
Lateral BMD	0.55**	0.52**	0.34*	0.36*	0.26	0.39*	0.17	0.07

* $p<0.05$ ** $p<0.001$

6.5. Discussion

In this exploratory study using 3D *in vivo* QCT for analysis of proximal tibial subchondral cysts, we report cyst characteristics as well as associations between total, medial, and lateral cyst parameters and patient characteristics. The results showed that lateral cyst number and volume was related to BMD, as well as alignment and JSN. We found no relationships between cyst parameters and total WOMAC pain, nocturnal pain, or OA severity. This is the first *in vivo* study to use clinical QCT imaging at the knee to evaluate associations between cyst parameters and WOMAC pain, OA severity, and volumetric subchondral BMD.

Our findings are consistent with prior research exploring *ex vivo* cyst characteristics at the hip[18] and at the tibia[17], where high cyst number per volume was also associated with high BV/TV (analogous to BMD)[18] and high trabecular thickness[17]. Our findings were especially pronounced in the lateral region, where high lateral cyst number and volume were associated with higher lateral BMD. Cysts, which present as voids in bone, create stress concentrations predisposing to localized high BMD, especially in the lateral region[131]. High BMD is likely a response to higher stress, with the response being multiple cyst formation may be related to regions with higher BMD or sclerotic bone formation[131], potentially as a result of local bone remodelling and altered bone structure near the subchondral surface[17, 233]. High subchondral BMD, resulting from bone remodelling, may counterbalance structural instability due to cyst presence and higher stress.

Although the mechanism of cyst formation in patients with knee OA is still unknown, there are two primary hypotheses: the "bony contusion theory"[127, 128]—which proposes that excessive loading or trauma can lead to trabecular microfractures, necrotic bone, and focal bone resorption, eventually resulting in cyst development—and the "synovial fluid intrusion theory"[129, 130]—which proposes that the calcified barrier between cartilage and subchondral bone is damaged, allowing for fluid to seep into the subchondral bone, creating a fluid-filled cyst lesion.

In this work, there may be indications of each of these mechanisms in cyst formation, either independently or in combination. Over the total tibial region, the strongest associations were observed between cyst number and alignment, while at the lateral region similar associations were observed between cyst parameters and alignment as well as lateral JSN. These

results suggest that cartilage degeneration may be associated with proportionally larger and more numerous cysts. Chen et al.[17] report similar findings, where subchondral cyst presence was associated with JSN and cartilage degeneration. Most likely, cyst development is a response to altered loading resulting in potential changes to bone congruence, contact forces, potentially changing load distribution through the proximal tibia[218, 234], possibly through JSN with disease progression or knee alignment. Although alignment was measured based on imaged reconstructions[217], it may be worthwhile hypothesizing why total cyst number and most lateral cyst parameters were associated with valgus alignment. As the lateral compartment is predisposed to higher tibial loads in patients with valgus alignment[235, 236], patients with valgus alignment may be predisposed to higher cyst numbers and volume, even before clinical signs of OA, such as pain. Based on this finding, it would be expected that varus alignment would be associated with medial cyst number and volume, but this relationship was not significant in our study. Previous works have reported that patients with valgus alignment also tend to have higher medial tibial loads[237], thus may also be more susceptible to lateral cyst development. We recommend further studies evaluating the effect of alignment on cyst characteristics and development in participants with OA.

As these patients are all in late-stage OA with severe to extreme pain, excessive lateral loading could also be the result of patients' efforts to actively unload the medial compartment in efforts to relieve initial knee pain[58], thus shifting load to the lateral plateau. Unloading the medial compartment may lead to lower BMD, as observed in our previous study of this sample[209], and reduced medial stiffness. To determine if this may be contributing to our observations, we performed *post hoc* analysis of relationships between medial BMD and lateral cyst number and cyst number per volume, both of which showed significant relationships between lower medial BMD and more numerous cysts. Medial plateau unloading, combined with lower medial BMD and reduced stiffness, may compress the medial plateau. During disease progression, medial plateau compression could lead to in an increase in lateral contact loads, creating a precursor to lateral cyst formation and propagation. Current studies using finite element (FE) modelling with simulated cysts propose that cyst presence alters load distribution within the subchondral region[131]. It would be worthwhile to monitor cyst development throughout the OA process, using both imaging and modelling methods to determine if this effect is unique to this sample, or if it is more widespread through the OA population.

Although our previous work evaluating relationships between BMD and pain in this sample reported an association with high lateral focal BMD and pain[209], we found no relationships between cyst parameters and WOMAC pain. In patients with late-stage OA, cyst presence or size may not be related to pain in later stages of cyst development where bone remodelling levels may be reduced, or the internal cyst surface is well formed and resistant to the effects of high stress. We recommend further work with patients with varying stages of OA and degrees of pain to evaluate associations between cysts, BMD and pain during disease progression.

The findings of this study present various potential clinical impacts. Using clinical QCT we were able to measure relationships between cyst parameters (number, size, volume) and participant characteristics in vivo as had previously only been done *ex vivo* using non-clinical imaging tools such as micro-CT[17] and HR-QCT[18]. This presents a promising clinical QCT-based technique for monitoring similar cyst parameters and regional BMD in a clinical sample and the ability to incorporate clinical symptoms such as pain. Clinical studies using MRI-based techniques present that cyst presence may[9, 63] or may not[10, 66, 106] be related to pain in patients with OA. Although these studies show that it is possible distinguish cysts and cyst-like lesions using MR, resolution limitations inhibit the ability to distinguish and measure smaller subchondral cysts. QCT provides higher resolution, as well as the ability to easily quantify cyst-adjacent BMD. This work further demonstrates the complexities of cyst presence in relation to pain in patients with OA, especially in late-stage OA, but may provide a comprehensive technique able to distinguish cysts, as well as regional or localized BMD *in vivo*.

This study has certain limitations to consider. First, our measurements use a larger voxel size than *ex vivo* approaches such as micro-CT and may ignore smaller cysts. It was difficult to reliably quantify any cysts smaller than 8 voxels (2x2x2 voxels or 1.95mm^3). It was also challenging to differentiate between small cysts and surrounding bone. Second, it was challenging to determine individual cysts with adjacent large cysts that would sometimes connect with one another in some participants. In these cases, these were counted as a single large cyst, but could also be regarded as multiple smaller cysts, which could have merged into a large cyst-like void. This could account for multiple large cysts within our study. Third, our alignment measurement was a custom in-house approach using CT reconstructions and relative joint space widths to approximate mechanical alignment. Although this technique has not been validated

against full-limb radiographs, in these patients with late OA malalignment was evident with values ranging from -18° to 8° from neutral position[217]. Fourth, as this was an *in vivo* study, we did not include biochemical or histological analysis, and are thus uncertain of cyst genesis or development. Fifth, our sample has various limitations including participants at late stage of OA severity and pain measurement. Our sample represented patients at late stages of OA and findings may not be applicable to patients with early OA. WOMAC pain severity and assessment was based on the entire knee joint, including all joint surfaces (tibiofemoral and patellofemoral) and tissues (e.g., bone, menisci, synovium), and it is uncertain if pain originated within the proximal tibial bony structure, other tissues, or a combination of tissues. Further prospective evidence from participants at varying initial stages of OA and OA-related pain could complement these preliminary findings and clarify the relationship between cyst parameters and patient characteristics, as well as the role of subchondral cysts in knee OA and OA-related pain.

6.6. Conclusion

In this exploratory study, we used clinical QCT to analyze subchondral cysts at the proximal tibia of OA patients to determine relationships between subchondral cyst parameters and clinical characteristics of OA. There was a large range in cyst number and volume in our sample, suggesting that cyst development and progression may vary from patient to patient. At the lateral region, cyst number and volume were strongly associated with several patient characteristics including joint alignment, JSN, and BMD, suggesting that there may be disease-associated changes in tibial loading distribution leading to cyst development and further joint deterioration. We found no associations between cyst number or cyst volume with OA-related knee pain in patients with late-stage OA. As such, it may be further worthwhile to explore other bone-related outcomes (e.g., BMLs, BMD), when investigating which structures contribute to pain

7. MECHANICAL FE OUTCOMES AND NOCTURNAL PAIN

7.1. Synopsis

This chapter outlines details of our study investigating relationships between finite element derived mechanical outcomes (stress, strain, stiffness) at the proximal tibia and nocturnal pain in patients with knee OA. In this study, we report that participants with severe nocturnal pain had higher lateral minimum principal stress than participants with no pain at all depths including trabecular bone (subchondral, epiphyseal, and metaphyseal) and most depths including cortical bone (subchondral, peripheral, and epiphyseal). This study suggests that pain in patients with knee OA may be associated with FE-based mechanical outcomes, especially minimum principal stress, which may have a role in OA-related pain pathogenesis.

7.2. Introduction

Knee osteoarthritis (OA) is a painful debilitating joint disease, and a leading cause of pain and disability in the elderly[184]. Pain is the dominant symptom of OA[2], and is often the primary motivation for treatment. Unfortunately, pain pathogenesis is poorly understood as it could be related to many contributing factors (e.g., altered subchondral bone properties, inflammation, bone marrow lesions, psychosocial factors). Of importance is nocturnal pain, or pain while lying in bed at night, as it is related to sleeplessness which disrupts quality of life[5], and is a common indicator for surgical intervention[74]. Pain in bed at night is also one of the final activities where patients will experience pain in conjunction with OA progression[73], and may be associated with underlying structural damage or remodelling[238] within the bone tissue.

Nocturnal pain is associated with various bone-related structural elements such as higher lateral focal subchondral bone mineral density (BMD)[209]. Additionally, BMD alterations are associated with many other bony features, such as sclerosis[13], BMLs[14, 15], attrition[16], and subchondral cysts[17, 18]. These individual image-based bone metrics may be interrelated at the structural level, thus incorporating a whole-joint approach including alignment, geometry, and material properties is important.

In subject-specific finite element (FE) modelling, QCT image volumes are used to generate computational models to measure the mechanical behaviour of joint tissues. This non-invasive image-based technique able to incorporate regional variations in bone material properties and geometry as well as accounting for limb alignment. To date, FE analyses of OA

limbs have indicated that bone may have a structural role in OA initiation and development[131]. Subject-specific FE models have been used to identify differences in mechanical outcomes (stress, strain, stiffness) between knees with and without OA[30]; however, it is uncertain if these same metrics are associated with OA-related pain. Additionally, as pain may be related to localized bone remodelling[238], which is partially driven by mechanical stimuli[57], it is advantageous to explore relationships between mechanical quantities and pain in patients with painful knee OA.

The primary objective of this study was to first determine relationships between FE-derived mechanical quantities (stress, strain, stiffness) and clinical characteristics of OA (OA severity, OA-related pain, alignment) in patients with knee OA. The secondary objective of this study was to then contrast FE-derived mechanical quantities across patients with differing levels of OA-related nocturnal knee pain when compared to those reporting no knee pain. To date, an FE analysis has not yet been conducted on a sample of participants with clinically diagnosed OA using subject-specific techniques. The results of this study provide further insight into how loading and the mechanical behaviour of bone may be related to pain in OA.

7.3. Methods

7.3.1. Study Participants

We recruited 42 participants with OA (23M: 29F; mean age 64, SD ± 9.4 years; mean BMI 28.7 ± 3.7; 18L:24R) prior to total knee replacement (TKR). Exclusion criteria included: pregnant women, patients having a revision replacement instead of primary knee replacement, and patients with a prior history of bone pathology at the knee joint. The Institutional Research Board of the New England Baptist Hospital approved the study. We obtained informed consent from all study participants.

7.3.2. Participant Assessment

OA severity was classified using Kellgren-Lawrence scoring[59] and standardized radiographs. We also included knee alignment, as it may also affect medial or lateral loading at the proximal tibia[27, 239], which was categorized as varus, neutral, or valgus and measured using coronal and sagittal CT reconstructions to determine an estimate of mechanical alignment[217]. In brief, medial and lateral joint space widths were evaluated at equal distances from the tibial spine permitting

an estimation of alignment between the femoral and tibial axes. Neutral alignment was defined as 176° to 180°, and malalignment of ± 2° from the neutral position (178°) was considered as either varus (-2°) or valgus (+2°) [217]. Of note, the 2° offset (from 180°) pertains to inherent differences in medial: lateral cartilage thickness, with lateral cartilage being thicker than medial cartilage[240]. For this analysis, alignment was treated as a categorical variable, where participants exhibited either varus, neutral, or valgus alignment.

Pain severity was measured using the pain subscale of the Western Ontario McMasters Osteoarthritis Index (WOMAC)[75]. Participants were asked to assess the level of pain in the affected knee joint within the past 24-hours while walking on a flat surface, going up or down stairs, lying down in bed at night, sitting or lying down, and standing upright using a 5-point Likert scale (0 to 4). Individual element scores were then summed for a possible score out of 20, with 20 being the highest amount of pain. As this sample consisted of late-stage OA patients immediately prior to total knee replacement (TKR) surgery, all had very similar pain scores for weight-bearing activities (going up/down stairs, walking, standing) and pain while sitting. Pain at night in bed is one of the final activities where OA patients experience pain[73], thus we used pain while lying down in bed at night (nocturnal pain) to categorize patients into differing pain groupings. Participants with a nocturnal pain score of 0 or 1 were considered to have 'no nocturnal pain', participants with a score of 2 were considered to have 'moderate nocturnal pain', and participants with a score of 3 or 4 were considered as 'severe nocturnal pain' as based on out previous study evaluating subchondral BMD in this same sample[209]. We also used the Self-Administered Comorbidity Questionnaire[212] to assess participants for any potential confounding comorbidities (e.g., diabetes, heart disease).

7.3.3. CT Acquisition

We used a single energy clinical CT scanner (Lightspeed 4-slice, General Electric, Milwakee, WI, USA) for bone imaging. Participants were oriented supine within the CT gantry and both legs were simultaneously scanned for bone imaging. A solid quantitative CT (QCT) reference phantom of known bone mineral densities (Model 3T, Mindways Software Inc., Austin, TX, USA) was placed under each participant and included in all CT scans (Figure 1A). Scans included the distal femur, patella, proximal tibia, proximal fibula, and the 66% tibial shaft site

proximal to the distal tibial end-plate[196]. Image volumes were cropped to exclude the patella in this analysis (Figure 1B).

CT scanning parameters included: 120kVp tube voltage, 150mAs tube current-time product, axial scanning plane, 0.625mm isotropic voxel size (0.625 slice thickness, 0.625mm x 0.625mm in-plane pixel size), ~250 slices, ~60s scan time. A standard bone reconstruction kernel (BONE) was used for CT image post-processing. The effective radiation dose was ~0.073mSv per scan, estimated using shareware software (CT-DOSE, National Board of Health, Herley, Denmark). For comparison, the average effective radiation dose during a transatlantic flight from Europe to North America is about 0.05mSv[231].

7.3.4. CT Image Analysis

Equivalent volumetric BMD (mg/cm^3 K_2HPO_4) values were converted from grayscale Hounsfield units (HU) using subject-specific linear regression equations developed from known densities within the QCT phantom included in each individual axial image (r^2>0.99) (Figure 7-1A)[162]. All bones were semi-automatically segmented using commercial segmentation software (Analyze 10; Mayo Foundation, Rochester, MN, USA) and an interactive touch-screen tablet (Cintiq 21UX; Wacom, Krefeld, Germany) (Figure 7-1B & 7-1C).

7.3.5. FE Analysis

We used an earlier developed finite element (FE) analysis technique[30] to measure mechanical quantities, specifically principal compressive stress and strain (minimum principal stress and strain) as well as stiffness. For the purpose of comparing our results with prior studies, we also measured von Mises stress and strain[30, 131, 241] (included in Supplemental Tables). A precision study[30] was performed on an independent sample using recommended techniques[213]. Precision errors ranged from 3.7% to 10.5% for principal compressive stress, 3.2% to 7.6% for principal compressive strain, with similar errors for von-Mises stress and strain[30].

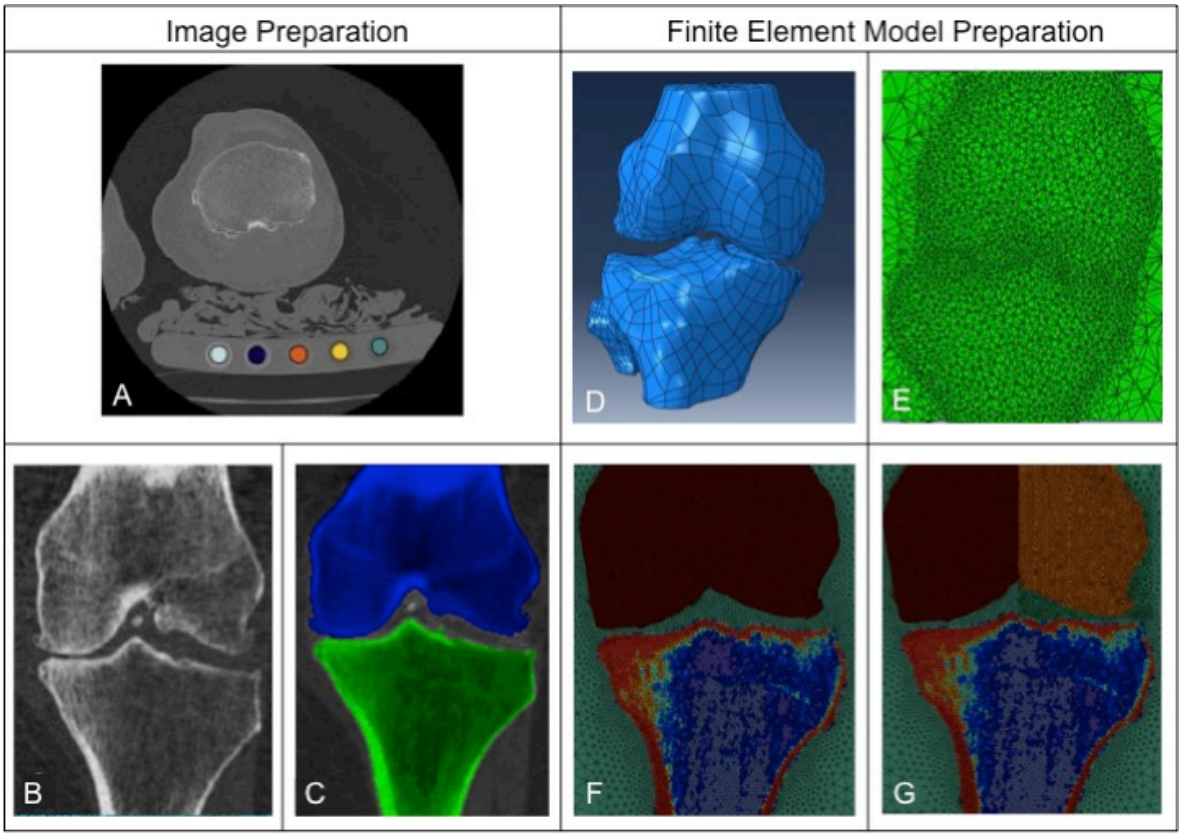

Figure 7-1. Process for developing subject-specific FE models. Grayscale Hounsfield units from CT images were converted to bone mineral density (BMD) values (A), serial images (B) were segmented (C) – coronal view of femur in blue and tibia in green – to create imaged volumes for each included bone. Imaged volumes were rendered and smoothed to create three-dimensional geometries (D), which were meshed with 10-node tetrahedral elements (E). All meshed models included the femur, tibia, and fibula (not pictured) within a cylinder representing surrounding soft tissue. BMD-based material properties were assigned and mapped to each model (F). To calculate lateral stiffness, the medial side was isolated from the model by assigning soft tissue material properties to the medial distal femur (G).

In brief, supine CT image volumes were reoriented to neutral standing alignment to model a single-leg stance (MATLAB, MathWorks, Natick, MA, USA)[30]. These re-aligned image volumes were used to develop our FE models. Polygonal surface meshes were created from the segmented tibia, femur and fibula (Analyze10, Mayo Foundation, Rochester, MN, USA). We then used reverse engineering software (Geomagic Studio 12, Systems, Rock Hill, SC, USA) to smooth 3D surface meshes and ensure the bone geometries were topologically valid without holes or rough edges (Figure 7-1D). The maximum smoothing distance was less than one voxel (0.625mm) to maintain geometric complexity. Smoothed 3D volumes were then imported into FE software (Abaqus, Providence, RI, USA) and encapsulated within a cylinder simulating soft

tissue (e.g., cartilage, meniscus, etc.). The FE models were meshed using 10-node quadratic tetrahedral elements with a maximum 2mm mesh edge size throughout the bones, and a 20mm maximum mesh edge length around the edge of the encapsulating cylinder representing soft tissue (Figure 7-1E). A bonded contact interface was assumed between bone and soft tissue. Mesh convergence was performed on seven knees, and the results did not change more than 1% when element size was changed from 2mm to 1.8mm.

We used a custom algorithm[176] to map image-based BMD values to element-based elastic moduli using the E-BMD relationship from Goulet et al[179] for the proximal tibia and fibula (Appendix A, Table A-1), as recommended for subject-specific FE models of the proximal tibia[176, 242]. Elastic moduli ranged from 1 MPa to ~25 GPa for elements of the proximal tibia and fibula. As our analyses was focused on the proximal tibia, we modeled the femur as a rigid body[243, 244] by assigning a high elastic modulus (500 GPa). All bone elements had isotropic linear material properties with a Poisson's ratio of 0.3[131]. We modeled all soft tissue (e.g., cartilage, meniscus, etc.) as a minimally compressive homogeneous material (E=10MPa, Poisson's ratio=0.495)[131] (Figure 7-1F). The most distal sections of the fibula and tibia were constrained in all directions. The proximal femur was also constrained in all directions except for a uniform displacement (1mm) along the longitudinal axis of the femur.

To calculate medial and lateral stiffness, we modified femur mechanical properties and developed two additional models for each sample. To study medial stiffness, we assigned a low elastic modulus (E=10MPa) to all of the elements in the lateral compartment of the distal femur (Figure 7-1G), ensuring that total load was transferred to the medial compartment of the proximal tibia through the medial condyle of the distal femur[30]. The opposite was done for studying lateral stiffness. Stiffness of each of the medial and lateral compartments was calculated as the applied vertical load (obtained at the top surface of the distal femur from each model) divided by the average vertical displacement of the nodes in the respective compartment.

We acquired FE-based principal compressive stress and strain as well as von Mises stress and strain across the proximal tibia. Stress and strain results were normalized according to participant body weight and subject-specific reaction force. We obtained the vertical reaction force at the top surface of the femur for each subject-specific model and multiplied all stress and strain outcomes by the ratio of participant body weight to reaction force (Body weight/Reaction force). We evaluated FE outcomes across various regions of the proximal tibia using a custom

algorithm (Matlab), including cortical and trabecular bone at subchondral, epiphyseal, and metaphyseal depths (Figure 7-2). According to previous precision analysis[30], we considered the following depths medially and laterally:

1. subchondral cortical, 0-2.5mm from the tibial plateau surface,
2. subchondral trabecular, 2.5-5mm from the tibial plateau surface,
3. epiphyseal trabecular, 5-15mm from the tibial plateau surface, and
4. metaphyseal trabecular, 15-35mm from the tibial plateau surface.

In the central region, we considered the following depths:

1. subchondral, 0-5mm depth from the top of the tibial spine,
2. epiphyseal, 5-15mm from the top of the tibial spine, and
3. metaphyseal, 15-35mm from the top of the tibial spine.

Along the outer cortical region, we considered the following depths both medially and laterally:

1. peripheral, 0-5mm depth from the tibial plateau surface,
2. epiphyseal, 5-15mm from the tibial plateau surface, and
3. metaphyseal, 15-35mm from the tibial plateau surface.

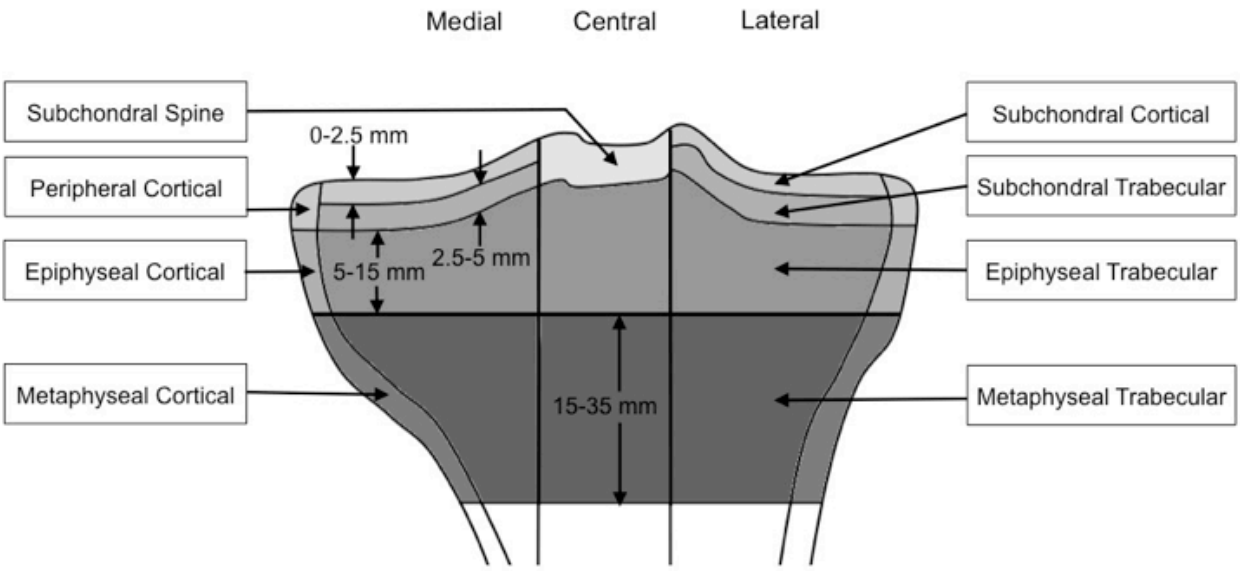

Figure 7-2. Analysis at the proximal tibia included cortical and trabecular bone at subchondral, epiphyseal, and metaphyseal depths in medial, central, and lateral regions.

7.3.6. Statistical Analysis

We used Shapiro-Wilk test and Q-Q plots to assess normal distribution of FE-derived mechanical quantities. For our primary objective, we assessed associations between FE outcomes (stress, strain) and clinical characteristics of OA (OA severity, total WOMAC pain, nocturnal pain, alignment) using Spearman's rank correlation coefficients.

For our secondary objective, we categorized participants into three groups based on their WOMAC score for pain while lying in bed at night (nocturnal pain)[140, 209]. As described above, participants were grouped as 'no nocturnal pain' (nocturnal pain score of 0 or 1), 'moderate nocturnal pain' (nocturnal pain score of 2), or 'severe nocturnal pain' (nocturnal pain score of 3 or 4). We used multivariate analysis of covariance (MANCOVA) with Bonferroni adjustment for multiple comparisons to contrast differences in mechanical quantities across pain groups to the no nocturnal pain group, selecting age and sex as covariates based on observed correlation with WOMAC pain in our initial bivariate analyses[232]. We focused on contrasting participants with differing levels of nocturnal pain directly to participants with no nocturnal pain as differences already existing in our previous study evaluating subchondral BMD[209] suggested that BMD in participants with severe nocturnal pain differed from BMD in participants with no nocturnal pain. We report mean and standard deviation (SD), absolute mean differences, and 95% confidence intervals. As this study is exploratory in nature, statistical significance was defined as $p<0.05$, and statistical analyses were performed using SPSS 23.0 (IBM, Armonk, NY, USA).

7.4. Results

7.4.1. Participant Characteristics

The characteristics of all participants, including BMI, side, OA severity, and alignment are shown in Table 7-1. OA severity ranged from 2 to 4. Pain at night lying in bed ranged from 0 (none) to 4 (extreme), and participants were divided into three groups: 'no nocturnal pain' (n=17), 'moderate nocturnal pain' (n=16), and 'severe nocturnal pain' (n=9).

Table 7-1. Background characteristics and clinical data for study participants and groups.

Characteristic	All Participants	No pain (n = 17)	Moderate pain (n = 16)	Severe pain (n = 9)
WOMAC (pain in bed at night)		0 or 1	2	3 or 4
Sex Ratio (M:F)	14:22	7:10	7:9	3:6
Age (mean ± SD)	64.7 ± 10.2	67.5 ± 9.1	61.8 ± 11.0	61.8 ± 9.3
BMI (mean ± SD)	28.8 ± 3.7	28.3 ± 4.1	29.1 ± 3.6	28.7 ± 3.0
Side (L:R)	14:22	7:10	6:10	5:4
Kellgren-Lawrence score (0/1/2/3/4)	0/0/3/17/14*	0/0/2/8/6*	0/0/1/6/9	0/0/0/5/3*
Alignment (varus/neutral/valgus)	28/6/8	12/4/1	12/1/3	4/1/4

* Data not available for 2 participants

7.4.2. Associations Between Mechanical Quantities and Clinical Characteristics

Spearman's rank coefficients showed various significant associations between mechanical quantities and clinical characteristics of OA. Principal compressive stress was associated with OA severity at the medial epiphyseal cortical region ($\rho = 0.34$, p=0.031), total WOMAC pain at the lateral peripheral cortical ($\rho = 0.45$, p=0.003) and lateral epiphyseal cortical ($\rho = 0.47$, p=0.002) regions, and nocturnal pain at all lateral regions except the lateral metaphyseal cortical region (ρ ranged from 0.33 to 0.50, p<0.05). Higher lateral principal compressive stress was also related to valgus alignment (ρ ranged from 0.56 to 0.65, p<0.05), while higher medial principal compressive stress was associated with varus alignment (ρ ranged from -0.53 to -0.65, p<0.05), (Table 7-2). Principal compressive strain was associated with nocturnal pain at the central metaphyseal region ($\rho = 0.32$, p=0.040), and higher principal compressive strain was associated with valgus alignment at all medial and central regions (ρ ranged from 0.34 to 0.56, p<0.05), and lateral regions at epiphyseal and metaphyseal depths (ρ ranged from 0.48 to 0.67, p<0.05) (Table 7-3). Similar associations were observed with von Mises stress and strain (Appendix A, Tables A-2 and A-3). Lower medial stiffness was associated with varus alignment ($\rho = -0.46$, p=0.002) (Table 7-4).

Table 7-2. Spearman's rank correlation coefficients (ρ) for relationships between regional principal compressive stress and OA characteristics (OA severity, total WOMAC pain, nocturnal pain, and alignment). For alignment, positive relationships represent associations with valgus alignment, and negative relationships represent associations with varus alignment. Bolded values indicate $p<0.05$.

Region	OA severity (KL grade)		Total WOMAC pain		Nocturnal pain		Alignment	
	ρ	*p*-value	ρ	*p*-value	ρ	*p*-value	ρ	*p*-value
Medial peripheral cortical	0.29	0.072	0.02	0.900	-0.19	0.233	**-0.59**	**<0.001**
Medial epiphyseal cortical	**0.34**	**0.031**	0.18	0.259	-0.05	0.771	**-0.53**	**<0.001**
Medial metaphyseal cortical	0.15	0.373	0.13	0.415	-0.16	0.314	**-0.61**	**<0.001**
Medial subchondral cortical	-0.03	0.860	-0.03	0.845	-0.23	0.143	**-0.60**	**<0.001**
Medial subchondral trabecular	0.01	0.943	-0.003	0.984	-0.20	0.196	**-0.65**	**<0.001**
Medial epiphyseal trabecular	0.03	0.857	0.01	0.935	-0.24	0.131	**-0.65**	**<0.001**
Medial metaphyseal trabecular	0.08	0.618	-0.07	0.661	-0.22	0.157	**-0.64**	**<0.001**
Subchondral spine	0.07	0.657	0.19	0.233	0.20	0.209	**0.31**	**0.050**
Epiphyseal central	-0.17	0.296	0.14	0.376	0.21	0.182	0.30	0.057
Metaphyseal central	-0.26	0.105	-0.07	0.659	0.10	0.518	0.15	0.334
Lateral subchondral cortical	0.08	0.636	0.21	0.175	**0.40**	**0.008**	**0.62**	**<0.001**
Lateral subchondral trabecular	0.03	0.865	0.23	0.150	**0.39**	**0.011**	**0.56**	**<0.001**
Lateral epiphyseal trabecular	0.05	0.758	0.17	0.284	**0.33**	**0.034**	**0.60**	**<0.001**
Lateral metaphyseal trabecular	-0.02	0.918	0.18	0.245	**0.33**	**0.033**	**0.65**	**<0.001**
Lateral peripheral cortical	0.06	0.726	**0.45**	**0.003**	**0.50**	**0.001**	**0.59**	**<0.001**
Lateral epiphyseal cortical	0.13	0.411	**0.47**	**0.002**	**0.41**	**0.007**	**0.55**	**<0.001**
Lateral metaphyseal cortical	0.28	0.084	0.20	0.208	0.26	0.093	**0.60**	**<0.001**

Table 7-3. Spearman's rank correlation coefficients (ρ) for relationships between regional principal compressive strain and OA characteristics (OA severity, total WOMAC pain, nocturnal pain, and alignment). For alignment, positive relationships represent associations with valgus alignment, and negative relationships represent associations with varus alignment. Bolded values indicate $p < 0.05$.

Region	OA severity (KL grade)		Total WOMAC pain		Nocturnal pain		Alignment	
	ρ	*p*-value	ρ	*p*-value	ρ	*p*-value	ρ	*p*-value
Medial peripheral cortical	-0.14	0.408	0.23	0.149	0.25	0.118	**0.55**	**<0.001**
Medial epiphyseal cortical	-0.002	0.988	0.17	0.283	0.21	0.179	**0.48**	**<0.001**
Medial metaphyseal cortical	0.25	0.119	0.16	0.307	0.21	0.173	**0.37**	**0.016**
Medial subchondral cortical	-0.24	0.144	0.14	0.384	0.09	0.568	**0.53**	**<0.001**
Medial subchondral trabecular	-0.06	0.719	0.20	0.214	0.16	0.302	**0.56**	**<0.001**
Medial epiphyseal trabecular	0.02	0.891	0.19	0.229	0.20	0.215	**0.52**	**<0.001**
Medial metaphyseal trabecular	0.21	0.199	0.19	0.224	0.28	0.071	**0.47**	**<0.001**
Subchondral spine	-0.20	0.217	0.09	0.564	0.15	0.354	**0.34**	**0.026**
Epiphyseal central	0.001	0.996	0.20	0.211	0.1	0.261	**0.51**	**<0.001**
Metaphyseal central	0.12	0.461	0.26	0.098	**0.32**	**0.040**	**0.54**	**<0.001**
Lateral subchondral cortical	0.02	0.890	0.08	0.623	-0.02	0.918	-0.13	0.421
Lateral subchondral trabecular	0.002	0.992	0.10	0.521	-0.08	0.636	-0.05	0.735
Lateral epiphyseal trabecular	0.03	0.869	0.25	0.111	0.17	0.281	**0.48**	**0.001**
Lateral metaphyseal trabecular	0.02	0.925	0.29	0.059	0.28	0.069	**0.51**	**0.001**
Lateral peripheral cortical	-0.02	0.891	0.17	0.272	-0.01	0.964	0.10	0.518
Lateral epiphyseal cortical	-0.06	0.693	0.29	0.062	0.21	0.179	**0.50**	**0.001**
Lateral metaphyseal cortical	-0.01	0.936	0.21	0.188	0.26	0.099	**0.67**	**<0.001**

Table 7-4. Spearman's rank correlation coefficients (ρ) for relationships between medial and lateral stiffness and OA characteristics (OA severity, total WOMAC pain, nocturnal pain, and alignment). For alignment, positive relationships represent associations with valgus alignment, and negative relationships represent associations with varus alignment. Bolded values indicate $p < 0.05$.

Region	OA severity (KL grade)		Total WOMAC pain		Nocturnal pain		Alignment	
	ρ	*p*-value	ρ	*p*-value	ρ	*p*-value	ρ	*p*-value
Medial stiffness	0.16	0.316	-0.25	0.111	-0.23	0.144	**-0.46**	**0.002**
Lateral stiffness	0.16	0.334	-0.11	0.510	0.06	0.707	-0.23	0.149

7.4.3. Differences Across Pain Groups

Overall, principal compressive stress was higher in participants with moderate pain and severe pain through the lateral trabecular region, as well as distal cortical regions of both lateral and medial sides (Figure 7-3). Compared to participants with no nocturnal pain, participants with severe nocturnal pain had between 47% to 65% higher stress throughout lateral regions at subchondral, epiphyseal, and metaphyseal depths (Table 7-6, Figures 7-3 & 7-4). There were no differences between participants with no nocturnal pain and moderate nocturnal pain. Similar differences were observed for von Mises stress (Appendix A, Tables A-4 & A-5). There were no statistically significant differences across groups in principal compressive strain (Tables 7-7 & 7-8), von Mises strain (Appendix A, Tables A-6 & A-7), or stiffness (Table 7-9).

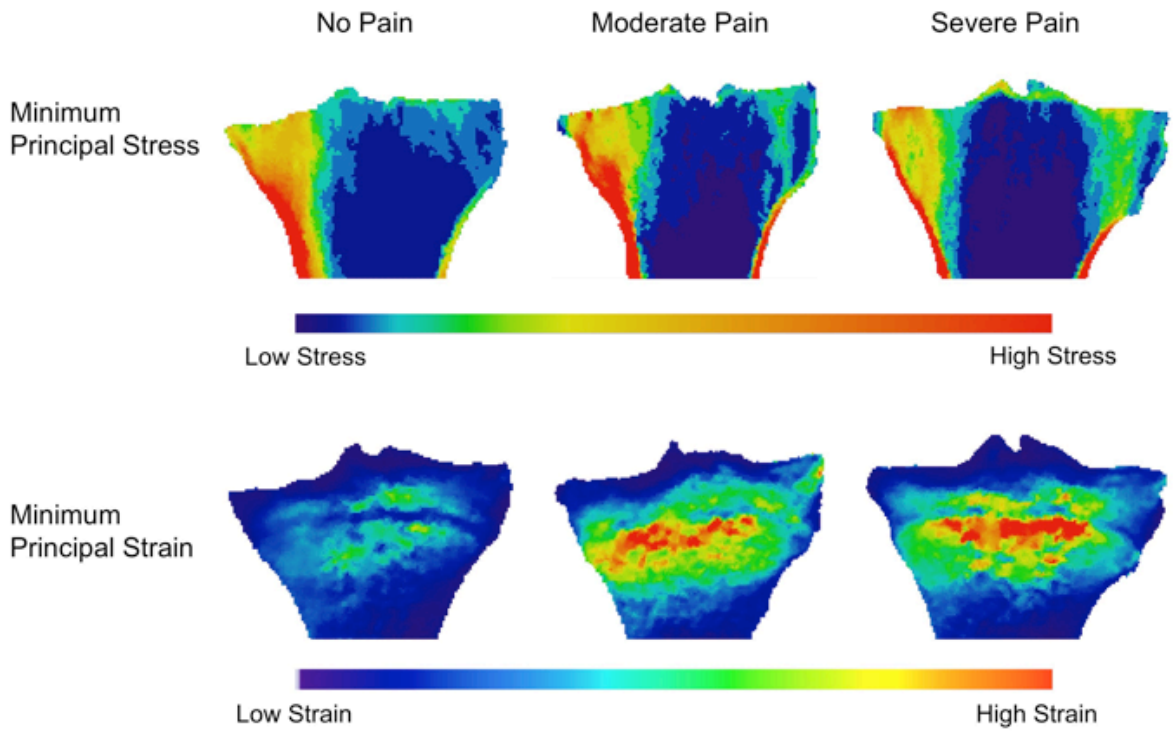

Figure 7-3. Representative finite element model outputs for principal compressive stress (top row) and principal compressive strain (bottom row) in one participant from each group.

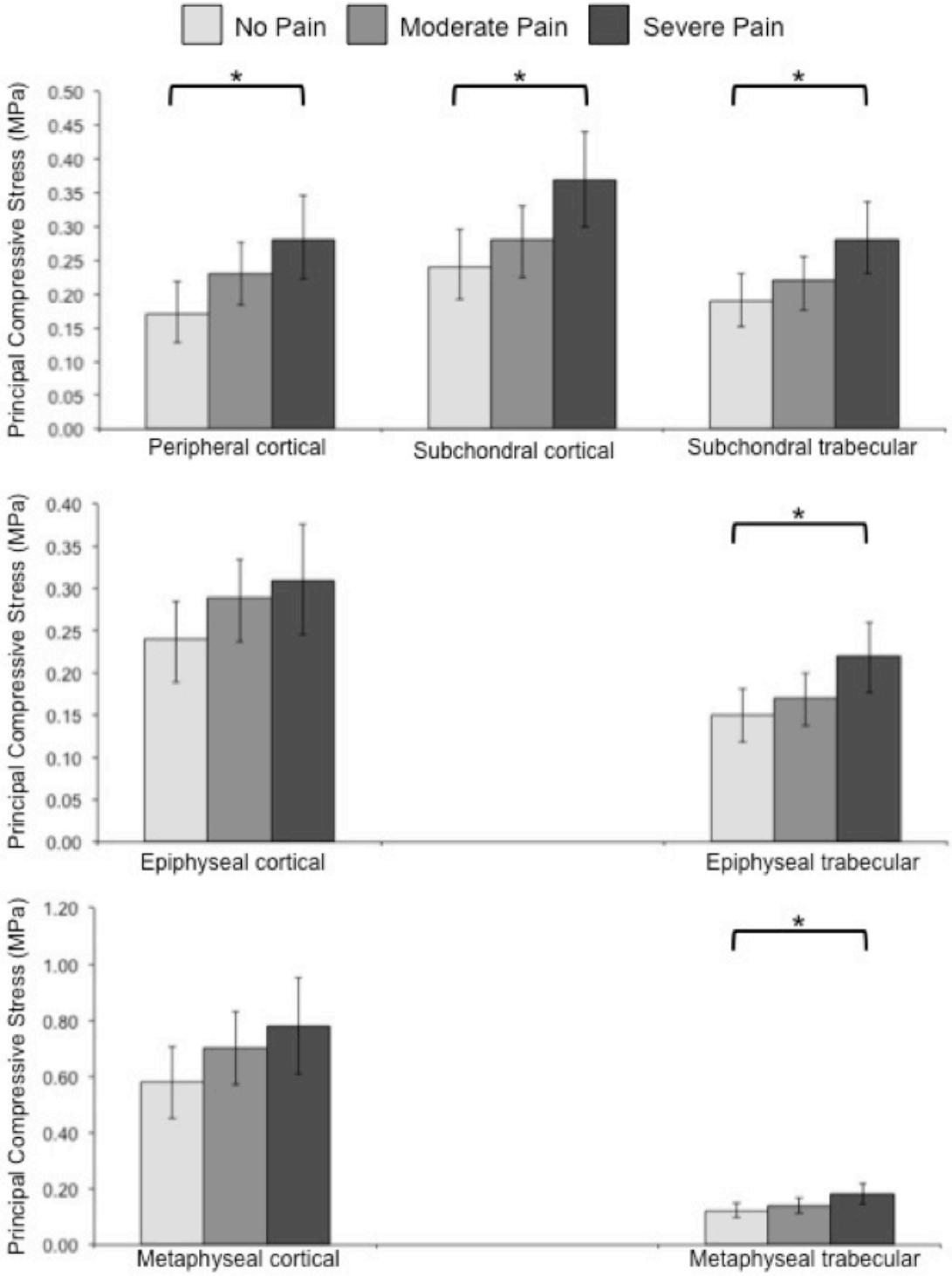

Figure 7-4. Adjusted mean principal compressive stress of each group ('no nocturnal pain', 'moderate nocturnal pain', and 'severe nocturnal pain') at subchondral, epiphyseal, and metaphyseal depths of the lateral region of the proximal tibia. Statistically significant differences ($p<0.05$) across groups are noted with brackets. Error bars represent 95% confidence intervals.

Table 7-5. Comparison of regional principal compressive stress in patients with knee OA with no pain and moderate pain, including mean ± standard deviation (SD), adjusted mean difference, percent difference from no pain, 95% confidence intervals (CI), and *p*-values. Bolded values indicate $p<0.05$.

Region	Minimum principal stress (MPa)		Mean Difference* from No Pain (%)	95% confidence interval		*p*-value
	No Pain	Moderate Pain		Lower limit	Upper limit	
	Mean ± SD	Mean ± SD				
Medial peripheral cortical	0.39 ± 014	0.43 ± 0.21	0.02 (5.0%)	-0.13	0.16	1.000
Medial epiphyseal cortical	0.60 ± 0.21	0.68 ± 0.29	0.04 (6.5%)	-0.18	0.26	1.000
Medial metaphyseal cortical	1.76 ± 0.62	1.80 ± 0.64	-0.03 (-1.1%)	-0.57	0.50	1.000
Medial subchondral cortical	0.41 ± 0.13	0.40 ± 0.11	-0.03 (-7.1%)	-0.14	0.07	1.000
Medial subchondral trabecular	0.37 ± 0.13	0.35 ± 0.11	-0.03 (-10.5%)	-0.14	0.07	1.000
Medial epiphyseal trabecular	0.36 ± 0.14	0.33 ± 0.11	-0.04 (-10.8%)	-0.14	0.07	1.000
Medial metaphyseal trabecular	0.40 ± 0.17	0.40 ± 0.20	-0.01 (-2.4%)	-0.17	0.15	1.000
Subchondral spine	0.23 ± 0.05	0.26 ± 0.10	0.03 (13.0%)	-0.04	0.10	1.000
Central epiphyseal trabecular	0.11 ± 0.03	0.12 ± 0.03	0.01 (0.0%)	-0.02	0.03	1.000
Central metaphyseal trabecular	0.09 ± 0.02	0.09 ± 0.02	-0.002 (0.0%)	-0.02	0.02	1.000
Lateral subchondral cortical	0.24 ± 0.06	0.28 ± 0.13	0.03 (16.7%)	-0.06	0.13	1.000
Lateral subchondral trabecular	0.19 ± 0.05	0.21 ± 0.09	0.02 (15.8%)	-0.05	0.10	1.000
Lateral epiphyseal trabecular	0.15 ± 0.04	0.17 ± 0.07	0.02 (13.3%)	-0.04	0.08	1.000
Lateral metaphyseal trabecular	0.12 ± 0.03	0.14 ± 0.06	0.02 (16.7%)	-0.03	0.07	1.000
Lateral peripheral cortical	0.17 ± 0.06	0.23 ± 0.11	0.06 (35.3%)	-0.02	0.14	0.261
Lateral epiphyseal cortical	0.23 ± 0.09	0.29 ± 0.16	0.05 (20.8%)	-0.04	0.14	0.496
Lateral metaphyseal cortical	0.57 ± 0.14	0.70 ± 0.29	0.12 (20.7%)	-0.11	0.35	0.565

*Mean values adjusted for age (64.1) and sex (1.6).

Table 7-6. Comparison of regional principal compressive stress in patients with knee OA with no pain and severe pain, including mean ± standard deviation (SD), adjusted mean difference, percent difference from no pain, 95% confidence intervals (CI), and *p*-values. Bolded values indicate $p<0.05$.

Region	Minimum principal stress (MPa)		Mean Difference* from No Pain (%)	95% confidence interval		*p*-value
	No Pain	Severe Pain		Lower limit	Upper limit	
	Mean ± SD	Mean ± SD				
Medial peripheral cortical	0.39 ± 0.14	0.28 ± 0.13	-0.13 (-30.0%)	-0.30	0.05	0.238
Medial epiphyseal cortical	0.60 ± 0.21	0.49 ± 0.27	-0.15 (-22.6%)	-0.40	0.11	0.481
Medial metaphyseal cortical	1.76 ± 0.62	1.38 ± 0.44	-0.46 (-25.0%)	-1.09	0.17	0.221
Medial subchondral cortical	0.41 ± 0.13	0.32 ± 0.11	-0.11 (-23.8%)	-0.23	0.01	0.098
Medial subchondral trabecular	0.37 ± 0.13	0.28 ± 0.11	-0.10 (-26.3%)	-0.23	0.02	0.122
Medial epiphyseal trabecular	0.36 ± 0.14	0.26 ± 0.11	-0.10 (-29.7%)	-0.23	0.02	0.141
Medial metaphyseal trabecular	0.40 ± 0.17	0.30 ± 0.13	-0.11 (-26.8%)	-0.30	0.08	0.436
Subchondral spine	0.23 ± 0.05	0.26 ± 0.07	0.03 (13.0%)	-0.06	0.11	1.000
Central epiphyseal trabecular	0.11 ± 0.03	0.13 ± 0.04	0.02 (18.2%)	-0.01	0.05	0.462
Central metaphyseal trabecular	0.09 ± 0.02	0.10 ± 0.03	0.01 (11.1%)	-0.01	0.04	0.645
Lateral subchondral cortical	0.24 ± 0.06	0.38 ± 0.13	0.13 (54.2%)	0.02	0.24	**0.020**
Lateral subchondral trabecular	0.19 ± 0.05	0.28 ± 0.10	0.09 (47.4%)	0.01	0.18	**0.026**
Lateral epiphyseal trabecular	0.15 ± 0.04	0.22 ± 0.08	0.07 (46.7%)	0.004	0.13	**0.034**
Lateral metaphyseal trabecular	0.12 ± 0.03	0.18 ± 0.07	0.06 (50.0%)	0.004	0.12	**0.034**
Lateral peripheral cortical	0.17 ± 0.06	0.28 ± 0.14	0.11 (64.7%)	0.02	0.21	**0.019**
Lateral epiphyseal cortical	0.23 ± 0.09	0.32 ± 0.13	0.07 (29.2%)	-0.03	0.18	0.233
Lateral metaphyseal cortical	0.57 ± 0.14	0.80 ± 0.39	0.20 (34.5%)	-0.07	0.47	0.208

*Mean values adjusted for age (64.1) and sex (1.6).

Table 7-7. Comparison of regional principal compressive strain in patients with knee OA with no pain and moderate pain, including mean ± standard deviation (SD), adjusted mean difference, percent difference from no pain, 95% confidence intervals (CI), and *p*-values.

Region	Minimum principal strain (microstrain)		Mean Difference* from No Pain (%)	95% confidence interval		*p*-value
	No Pain	Moderate Pain		Lower limit	Upper limit	
	Mean ± SD	Mean ± SD				
Medial peripheral cortical	878 ± 612	1076 ± 599	231 (26.4%)	-367	828	1.000
Medial epiphyseal cortical	1375 ± 684	1537 ± 644	234 (17.4%)	-386	855	1.000
Medial metaphyseal cortical	1420 ± 575	1625 ± 618	197 (13.7%)	-358	751	1.000
Medial subchondral cortical	436 ± 194	483 ± 205	52 (11.7%)	-136	239	1.000
Medial subchondral trabecular	780 ± 413	974 ± 603	264 (35.2%)	-252	780	0.623
Medial epiphyseal trabecular	2362 ± 1155	2798 ± 1209	554 (23.9%)	-566	1674	0.668
Medial metaphyseal trabecular	2362 ± 949	2673 ± 984	275 (11.5%)	-666	1216	1.000
Subchondral spine	565 ± 186	604 ± 228	58 (10.2%)	-133	249	1.000
Central epiphyseal trabecular	2511 ± 970	2809 ± 974	363 (14.6%)	-537	1263	0.956
Central metaphyseal trabecular	2005 ± 863	2193 ± 788	168 (8.3%)	-638	974	1.000
Lateral subchondral cortical	625 ± 190	656 ± 224	26 (4.0%)	-154	206	1.000
Lateral subchondral trabecular	1128 ± 423	1171 ± 543	48 (43.%)	-373	469	1.000
Lateral epiphyseal trabecular	2390 ±1049	2601 ± 990	256 (10.7%)	-640	1151	1.000
Lateral metaphyseal trabecular	2001 ± 1072	2106 ± 924	77 (3.8%)	-821	975	1.000
Lateral peripheral cortical	1141 ± 516	1292 ± 616	130 (11.2%)	-363	623	1.000
Lateral epiphyseal cortical	1136 ± 630	1193 ± 549	72 (6.1%)	-453	598	1.000
Lateral metaphyseal cortical	726 ± 472	824 ± 459	126 (17.5%)	-303	555	1.000

*Mean values adjusted for age (64.1) and sex (1.6).

Table 7-8. Comparison of regional principal compressive strain in patients with knee OA with no pain and severe pain, including mean ± standard deviation (SD), adjusted mean difference, percent difference from no pain, 95% confidence intervals (CI), and *p*-values. Bolded values indicate $p<0.05$.

Region	Minimum principal strain (microstrain)		Mean Difference* from No Pain (%)	95% confidence interval		*p*-value
	No Pain	Severe Pain		Lower limit	Upper limit	
	Mean ± SD	Mean ± SD				
Medial peripheral cortical	878 ± 612	1432± 958	534 (61.4%)	-167	1236	0.191
Medial epiphyseal cortical	1375 ± 684	1832 ± 994	466 (34.6%)	-262	1194	0.350
Medial metaphyseal cortical	1420 ± 575	1755 ± 640	309 (21.6%)	-342	960	0.726
Medial subchondral cortical	436 ± 194	539 ± 267	92 (21.1%)	-129	313	0.907
Medial subchondral trabecular	780 ± 413	1188 ± 893	430 (57.4%)	-176	1037	0.249
Medial epiphyseal trabecular	2362 ± 1155	3250 ± 1829	892 (38.5%)	-423	2207	0.292
Medial metaphyseal trabecular	2362 ± 949	3253 ± 1235	824 (34.5%)	-280	1929	0.207
Subchondral spine	565 ± 186	686 ± 246	128 (22.8%)	-97	352	0.486
Central epiphyseal trabecular	2511 ± 970	3229 ± 1397	690 (27.7%)	-367	1746	0.330
Central metaphyseal trabecular	2005 ± 863	2875 ± 1069	819 (40.5%)	-126	1765	0.109
Lateral subchondral cortical	625 ± 190	686 ± 148	-25 (-4.0%)	-154	206	1.000
Lateral subchondral trabecular	1128 ± 423	1010 ± 311	-118 (-10.6%)	-612	375	1.000
Lateral epiphyseal trabecular	2390 ±1049	2883 ± 1199	449 (18.8%)	-602	1500	0.871
Lateral metaphyseal trabecular	2001 ± 1072	2815 ± 1133	784 (38.5%)	-272	1836	0.212
Lateral peripheral cortical	1141 ± 516	1117 ± 407	-60 (-5.2%)	-638	519	1.000
Lateral epiphyseal cortical	1136 ± 630	1556 ± 698	386 (33.9%)	-231	1002	0.376
Lateral metaphyseal cortical	726 ± 472	1127 ± 645	386 (53.7%)	-117	890	0.186

*Mean values adjusted for age (64.1) and sex (1.6).

Table 7-9. Comparison of stiffness outcomes in patients with knee OA with no pain and moderate pain as well as severe pain including mean ± standard deviation (SD), adjusted mean difference, percent difference from no pain, 95% confidence intervals (CI), and *p*-values.

Region	Stiffness (N/mm)		Mean Difference* from No Pain (%)	95% confidence interval		*p*-value
	No Pain	Moderate Pain		Lower limit	Upper limit	
	Mean ± SD	Mean ± SD				
Lateral	4777 ± 1909	4804 ± 1651	-72 (-1.5%)	-1579	1434	1.000
Medial	7588 ± 3553	7202 ± 2678	-469 (-5.2%)	-2994	2056	1.000

Region	Stiffness (N/mm)		Mean Difference* from No Pain (%)	95% confidence interval		*p*-value
	No Pain	Severe Pain		Lower limit	Upper limit	
	Mean ± SD	Mean ± SD				
Lateral	4777 ± 1909	5260 ± 1481	-50 (-1.0%)	-1819	1719	1.000
Medial	7588 ± 3553	5260 ± 2538	-2132 (-28.2%)	-5096	831	0.238

*Mean values adjusted for age (64.1) and sex (1.6).

7.5. Discussion

In this study using subject-specific FE at the knee in patients with OA, we report associations between FE mechanical quantities (principal compressive stress, principal compressive strain, von Mises stress, von Mises strain, stiffness) and clinical OA characteristics (OA severity, total WOMAC pain, nocturnal pain, alignment). The results showed that higher principal compressive stress is associated with nocturnal pain at most lateral depths, valgus alignment was associated with higher lateral principal compressive stress, and varus alignment was associated with higher medial principal compressive stress. Higher principal compressive strain, both medially and centrally, was associated with valgus alignment. Our subject-specific FE study indicated higher principal compressive stress through cortical and trabecular regions at subchondral and epiphyseal depths at the lateral side of the proximal tibia in TKR patients with severe nocturnal pain, as compared to similar patients with no nocturnal pain. This exploratory study is the first to use QCT-based subject-specific FE techniques to investigate relationships between mechanical quantities at the proximal tibia and OA-related symptoms, such as pain, in a clinical sample of OA patients. These findings suggest that there may be previously unexplored associations between OA-related knee pain and mechanical quantities, such as principal compressive stress.

In participants with severe nocturnal pain, we observed 47% to 65% greater principal compressive stress at most depths at the lateral region of the proximal tibia than in participants with no nocturnal pain. These between-group differences are up to 10 times greater than associated precision errors, ranging from 4.6% to 5.9% at regions with significant between-group differences[30], lending credence to the comparison and observation that high principal compressive stress at the lateral proximal tibia may be explain OA-related knee pain in patients awaiting TKR. To further ensure that this effect was related to the mechanical environment and not differences in BMD, we calculated regional BMD values raised to the power of 2.1 to coincide with our E-BMD conversion equation[179] and performed between-group t-tests at each region. No differences were observed, with the exception of differences at the medial peripheral (p=0.048) and medial subchondral cortical (p=0.041) regions between participants with no pain and severe pain, as previously noted[209], proposing that these differences may be related to structural characteristics not captured in the tissue modulus. In our previous precision study evaluating FE outputs in healthy participants and participants with OA[30], OA participants had

higher stress in subchondral trabecular regions. We found similar trends in this study, where most participants with severe nocturnal pain had high principal compressive stress in trabecular regions at both lateral and medial plateaus. These findings further emphasize the importance of exploring mechanical behaviour in relation to pain, and that mechanical stress may be related to nocturnal pain, especially at trabecular regions deeper from the subchondral surface.

Our obtained mechanical quantities are within similar ranges as previously reported subject-specific FE outcomes at the knee[30, 131, 241]. Reported principal compressive stress and principal compressive strain values were within similar range as our previous precision study using this same technique, evaluating participants with and without OA[30]. Reported von Mises stress values were also within similar range as previous subject-specific modelling of the knee joint[131] and the proximal tibia[241]. Although there were no differences in von Mises strain between groups, qualitative strain patterns in this work show higher principal compressive strain and von Mises strain values at the epiphyseal depth, which is similar to previous parametric FE studies of the proximal tibia[166].

Study findings support our previous research using the same cohort, which investigated relationships between OA-related pain and subchondral BMD[209] and epiphyseal BMD[232]. Specifically, high lateral stress may be related to the combination of low medial epiphyseal BMD[232] and high lateral focal BMD[209]. First, in our previous work[232], we proposed that lower epiphyseal BMD may be a chondroprotective process to lower medial stiffness, thereby lessening medial cartilage stress[167]. Lower medial stiffness would naturally transfer more load to the lateral compartment, leading to higher lateral BMD and higher stress. To determine if this may be contributing to our observations, we performed *post hoc* analysis of relationships between medial stiffness and lateral stress at all depths, which showed significant relationships between lower medial stiffness and higher lateral stress at the subchondral cortical ($\rho = -0.35$, $p=0.023$), peripheral cortical ($\rho = -0.55$, $p<0.001$), and epiphyseal cortical ($\rho = -0.46$, $p=0.002$) regions. In addition, stress is inversely proportional to tibial plateau surface area, where changes in load distributed over smaller areas will result in higher changes in resulting stress. As the lateral tibial plateau generally has a smaller contact surface area than the medial plateau[245], any alterations in lateral loading may have a greater effect on lateral stress, than similar alterations in medial loading. In support of this, in this work there was a trend across all trabecular regions where participants with more severe nocturnal pain had higher stress at the lateral plateau and

lower stress at the medial plateau, showing that more load was being transferred laterally in participants with more severe pain, whereas participants with no nocturnal pain had more even stress between medial and lateral plateaus. Also, medial stiffness was quite low in participants with severe pain (about 2/3rds the stiffness of participants with no pain). Second, our prior work in this cohort identified that participants with severe nocturnal pain had ~30% higher focal BMD at the lateral region at the subchondral trabecular depth (2.5-10mm from the subchondral surface)[209]. Localized higher lateral BMD would equate with a higher elastic modulus, leading to localized loading, which would lead to more load being carried through the lateral regions of proximal tibia.

Our results indicate that high medial stress is related to varus alignment, high lateral stress is related to valgus alignment, and high medial and lateral strain are related to valgus alignment. Interestingly, alignment is not consistently associated with OA-related pain[94, 95, 217], and was not associated with either total WOMAC pain or nocturnal pain in this sample[114]. Although these are strong associations, our models did not include any ligaments or soft tissue, which have been shown to be the primary load-bearing structures in FE models simulating malalignment[246], thus we recommend further FE studies, which include ligaments and associated soft tissues at the knee to determine if our observed associations are still present when considering soft tissue.

We found no between-group differences in stiffness or principal compressive strain. Stiffness was highly variable in this sample, ranging from 2 046 MPa to 14 368 MPa at the medial plateau and 2 550 MPa to 8 913 MPa at the lateral plateau. That being said, mean medial stiffness tended to decrease as pain severity increased. Given this trend, combined with high stiffness variability, we believe we were underpowered to capture differences in stiffness between the groups. We recommend further studies including patients of varying degrees of OA severity to determine if stiffness is associated with disease progression, or able to discriminate pain severity at earlier stages of OA. Concerning minimum principal strain, the only between-group difference was between patients with no pain and severe pain at the central metaphyseal region. Although previous studies report relationships between higher strain and patellofemoral pain[183], there were few relationships between minimum principal strain and nocturnal knee pain in this study. This could be related to our model as associations between nocturnal pain and

strain occurred at regions adjacent to the constrained distal tibia, thus should be interpreted with caution.

Although speculative, it may be worthwhile hypothesizing how these study findings may relate to cartilage stresses within the OA joint. Recent work using FE to evaluate tibial cartilage[247] reported higher peak stress at the lateral tibial plateau in obese OA patients, compared to both OA patients with simulated weight loss and normal patients. These peak stresses were also associated with imaged cartilage defects at the lateral tibial plateau. As cartilage defects may result in higher subchondral bone stress levels[176, 248], there may be additional alterations within the OA joint contributing to higher lateral stress in this sample. Unfortunately, as previously mentioned, soft tissue data was not available for this study. Although associations between cartilage damage and OA-related pain are conflicting[66, 79, 249], it may be worthwhile including cartilage in future FE studies to consider the combined role of subchondral bone and cartilage and associated mechanical load transfer from one tissue to the other along with any potential relationships with OA-related pain.

This study has various merits. First, this study includes the largest known application of QCT-based subject-specific FE in patients with clinically diagnosed OA and will be valuable in guiding outcome and sample size selection for future FE studies. Second, our findings show that FE can discriminate differences in mechanical behaviour in patients with varying levels of nocturnal pain. Subject-specific FE is becoming a more widely used tool to evaluate the mechanical and loading behaviour of the knee, but the inclusion of clinical symptoms of OA, including pain, is limited. This study may aid in understanding the relationships between pain pathogenesis and related mechanical quantities. As these between-group differences are approximately 10 times larger than associated precision errors[30], these results are trustworthy. Third, by using nocturnal pain scores as our grouping variable, we are excluding potential factors, such as inflammation, which may affect pain scores or severity during weight-bearing activities. Fourth, we report both principal compressive stress and principal compressive strain (compressive stress and strain), as these are more representative metrics for inhomogeneous materials, such as bone. We've also included von Mises stress and von Mises strain to compare our results with previous subject-specific FE studies reporting these metrics. Fifth, we considered the heterogeneity of bone mechanical properties and used a density-modulus equation that has been shown to lead to accurate QCT-based FE models[176, 250]. Sixth, although we used non-

weight-bearing QCT scans in our model, a subject-specific re-alignment approach was used, resulting in similar 3D orientation based on individual knee landmarks and best-fit planes. This permitted similar comparisons of FE outcomes across all participants at various depths of the proximal tibia while still maintaining subject-specific alignment.

This study has certain limitations concerning both our sample, our FE technique, and multiple statistical tests. Pain severity and assessment was based on the entire knee joint, including multiple joint surfaces (tibiofemoral and patellofemoral) and tissues (e.g., bone, menisci, and synovium), and it is uncertain if pain originated within the proximal tibial bony structure, other tissues, or a combination of tissues. In our sample, although OA severity was homogeneous across participants, all were in late-stage OA (KL grade of 3 to 4), and it may not be possible to apply our findings to patients across all stages of OA. Concerning our model, we converted cortical and trabecular BMD to elastic moduli using a single E-BMD relationship (Supplemental Table 1). Applying cortical- or trabecular-specific E-BMD relationships may offer moderate improvements in stiffness predictions; however, in this work a single equation is justified to provide reasonable estimates of proximal tibial mechanical behaviour[30, 176, 242] without compromising the needs for additional computational resources. We were not able to include realistic subject-specific soft tissues, such as menisci, cartilage, or ligaments, as only CT images were available. To overcome this, we used a single homogeneous isotropic material to simulate simplified surrounding soft tissue in all FE models[30, 131], using the same material properties for all samples. Additionally, all participants were supine during scanning, thus our model may overestimate cartilage thickness or joint space narrowing. Thinner cartilage or cartilage defects associated with OA or OA-related pain may lead to higher bone stress[176, 248]. Accordingly, this analysis provides a conservative measurement, potentially underestimating proximal tibial stress. We opted not to include soft tissues in this model, as our focus was the role of bone in OA-related pain, though further research and development are needed in developing a full-knee FE model which incorporates subject-specific bone, cartilage, meniscal, and ligamentous structures while still maintaining short development and processing time. For our correlation analysis, we used an unadjusted $p < 0.05$ to identify associations between mechanical quantities at various regions and clinical characteristics of OA in this preliminary exploratory. For our across-group comparison, we chose a more conservative Bonferroni correction for multiple testing.

7.6. Conclusion

In conclusion, our exploratory subject-specific FE analysis of patients with OA demonstrated that higher medial stress was associated with varus alignment while higher lateral stress was associated with valgus alignment. Additionally, higher medial and lateral strain were associated with valgus alignment. Patients with severe nocturnal pain had higher lateral principal compressive stress at subchondral, epiphyseal, and metaphyseal depths in the proximal tibia than patients with no nocturnal pain. This study suggests that FE modelling has potential to identify mechanical quantities, especially stress and strain, related to pain in participants with OA and thus, may have a role in OA-related pain pathogenesis. As FE modelling is able to incorporate and evaluate the mechanical behaviour of the entire knee joint, mechanical stress may reflect a more comprehensive analysis or combined effect of bone-related structural changes associated with OA and OA-related pain, as compared to the analysis of individual or regional image-based features. These results emphasize on the importance of studying the combined effects of individual alterations in OA and suggest including metrics that represent these combined alterations, such as mechanical stress or strain. These preliminary results provide insight into the capabilities of FE analysis and identify mechanical quantities to target when investigating the role of bone in OA-related pain.

8. DISCUSSION

8.1. Overview of Findings

The key finding of **Chapter 4** was that local subchondral bone density appeared to have a role in OA-related pain pathogenesis. Specifically, this study identified that patients with severe nocturnal pain demonstrated higher lateral focal BMD at depths of 2.5-5mm (33% higher) and 5-10mm (32% higher) than patients with no nocturnal pain. These differences were approximately 7 times greater than associated precision errors[22], and suggest that there may be previously overlooked characteristics in deeper subchondral bone layers that may have a role in OA pain pathogenesis. Although not significant, there was also a trend for lower average medial BMD in patients with more severe pain. As the medial tibial compartment supports proportionally greater load through the proximal tibia[237], and OA more often affects the medial plateau[33], similar or higher BMD would be expected through the medial compartment. This unexpected and unusual finding was the driving motivation for further exploration in studies presented in Chapters 5 and 6.

The key finding of **Chapter 5** was a relationship between lower epiphyseal and metaphyseal BMD and higher total WOMAC pain. Specifically, we report that total epiphyseal BMD, medial epiphyseal BMD, and total metaphyseal BMD are independent predictors of total WOMAC pain. These findings suggest that there may be previously overlooked regions and characteristics in proximal tibial BMD that may have a role in OA-related pain. This research focuses on often overlooked epiphyseal and metaphyseal regions of the proximal tibia, whereas most research studying the role of bone in OA commonly evaluates the subchondral region. The results of this study may be clinically important for TKR preparation and planning. Based on the findings of this study, there may be lower amount of bone in individuals with higher OA-related pain, potentially placing them at risk for poor implant fixation[225], loosening[223, 226], or surgical revisions[224]. Given the results of this study, it may be beneficial to use imaging to evaluate preoperative bone density or volume fraction in TKR patients with high amounts of pain.

The key finding of **Chapter 6** was that lateral subchondral cyst number and volume were associated with lateral subchondral BMD and knee alignment, but were not associated with WOMAC pain. Specifically, we report that higher lateral BMD is associated with higher lateral cyst number and higher lateral cyst number per lateral proximal tibial volume. Higher lateral cyst

number and volume were also associated with valgus alignment; surprisingly, there were no relationships between cyst parameters and pain. Cyst size and presence were also associated with both JSN and alignment, providing evidence that cyst development may be a response to altered load distribution through the proximal tibia[218, 234]. In this work, we propose that higher lateral loading, as evidenced through lateral cyst presence and associated stress concentrations[131] and higher localized BMD[17], may be due to laterally shifted loading, either through disease progression or through patients' efforts to actively unload the medial compartment in effort to relieve initial knee pain[58], creating a precursor to lateral cyst formation. This study is important as there may be OA-associated changes in tibial load distribution leading to cyst presence and further joint deterioration. This study is also important as it indicates that cysts are not associated with OA-related pain, thereby ruling out potential pain initiators.

The key finding of **Chapter 7**, was that various mechanical outcomes are associated with clinical characteristics of OA. For example, higher principal compressive stress at various depths of the lateral region was associated with higher nocturnal pain. Specifically, patients with severe nocturnal pain had 47% to 65% higher principal compressive stress throughout trabecular and cortical bone at subchondral, epiphyseal, and metaphyseal depths of the lateral proximal tibial region than patients with no nocturnal pain. This study also noted a trend for lower medial stiffness in participants with high pain, which could be speculated reflecting a chondroprotective mechanism to lower medial cartilage stress. Prospective data is needed to assess if proposed lower medial stiffness would lead to lateral load transfer, resulting in higher lateral stress, higher remodelling and higher localized BMD. This lower medial stiffness may partially explain high lateral BMD found in individuals with high nocturnal pain. These results also emphasize the need for a more comprehensive 'whole-joint' or 'whole-tibia' approach when analyzing the role of bone in OA-related pain.

8.2. Comparison to Existing Findings

Direct comparisons between associations between these new findings (i.e., depth-specific BMD measurements or FE outcomes at the proximal tibia and OA-related pain) and existing findings are difficult given these are the only known existing works evaluating relationships between volumetric BMD, or FE outcomes, and pain at the proximal tibia; however, comparable studies

evaluating subchondral BMD exist at the patella[19, 20]. Additionally, BMD values can be compared to existing measures using pQCT[23], HR-pQCT[251], and QCT[21, 22, 162, 252, 253], while FE outcomes can compared to existing measures from FE-based studies at the proximal tibia[30, 131, 241].

Relationships between pain and subchondral trabecular BMD proximal tibia were similar to previously reported relationships at the patella[19]; although these results are from the same sample. With regards to high focal BMD, prior work has reported high BMD in locations adjacent to BMLs[15], which are strongly associated with pain[78, 136]. At epiphyseal depths, studies using animal models have reported associations between low bone density at locations further from the joint surface (epiphyseal and metaphyseal depths) and OA severity[254-256].

The findings of our study evaluating associations between subchondral cysts and pain are similar to prior *ex vivo* research exploring cyst characteristics at the tibia using micro-CT[17] where high cyst number per volume was associated with high trabecular thickness, and the hip using HR-pQCT[18] where high cyst number per volume was associated with high BV/TV. Concerning relationships between cyst parameters and OA-related pain, similar trends were reported in various studies using MRI, where cyst presence[104, 112] or size[10, 66, 106] were not associated with OA-related knee pain.

Mechanical outcomes from our study evaluating relationships between mechanical FE outcomes and OA-related pain are within similar range as previously reported von Mises stress and strain [30, 131, 241], principal compressive stress and strain[30], and stiffness[166]. Stress distributions from all participants in this study showed similar patterns as previously observed in patients with OA using similar techniques[30] where stress in participants with OA was distributed through both trabecular and cortical regions. These findings support and combine results from our studies evaluating BMD at various depths from the subchondral surface and subchondral cyst parameters. As BMD is connected to stress (e.g., high BMD leads to a high elastic modulus, which will support load and bear high stress), high lateral focal BMD would be able to support high stress, whereas low medial BMD would support lower stress. Additionally, as subchondral cysts act as stress risers[131], more numerous lateral subchondral cysts would lead to higher stress in lateral regions.

8.3. Strengths and Limitations

These combined studies have various strengths requiring further explanation. First, these studies combined present a 'whole-bone' approach to determining how BMD and mechanical outcomes are associated with OA-related pain. A key weakness of similar image-based studies is the individual analysis of relationships between bony features and OA-related pain[9, 10, 63, 66]. Although it may be valuable to determine if there is a single key feature associated with OA-related pain, these features are rarely observed in isolation in patients with more severe OA, i.e., osteophytes, sclerosis, and subchondral cysts may all be observed in the same patient and the severity of these features are combined to generate a single disease severity score. BMD is associated with various bony features associated with OA-related pain[13-18], as well as OA severity[21, 23], and is a key determinant of mechanical properties of bone[25, 171]. By including BMD analyses at various depths from the subchondral surface, along with associated FE outcomes, this work is able to evaluate bone across the entire proximal tibia. Additionally, this work is able to evaluate how bone characteristics at one region (e.g., medial epiphyseal region) may be associated with or influence bone characteristics at other regions or depths (e.g., lateral subchondral region), furthering our understanding of the structural role of bone in OA-related pain at the proximal tibia.

Second, and related to the first strength, the key findings of our FE study are reflective of our previous studies evaluating BMD at various depths and subchondral cyst characteristics. This would be expected, as mapped mechanical properties are directly proportional to BMD, but it is worth emphasizing as it enforces the importance of BMD and the role of structural and mechanical characteristics of bone at the proximal tibia in painful knee OA. This also demonstrates consistency and reliability between study outcomes and techniques, even though different metrics and processes are used. Each study provides outcomes that may reveal that patients with high OA-related pain may be shifting load to, or naturally over-loading, the lateral tibial plateau, as demonstrated through higher lateral focal subchondral BMD, lower medial trabecular BMD, larger and more numerous lateral subchondral cysts, and higher stress at most depths of the lateral compartment of the proximal tibia, each possibly contributing to increased chondroprotective bone remodelling processes. Combined, the results of these studies emphasize the need for further understanding in the structural role of bone in OA-related pain pathogenesis,

and may provide potential outcomes worth monitoring during OA-related pain progression to further develop targeted treatments.

Third, our imaging and modeling techniques are based on *in vivo* clinical QCT images from patients with clinically diagnosed OA, which provide a foundation for future clinical applications, such as patient-specific surgical planning (if sufficient resources and expertise are available). This combined work also provides evidence for potential previously overlooked target outcomes (e.g., density of epiphyseal and metaphyseal regions) for studies using similar QCT images in patients at various stages of knee OA and OA-related knee pain.

This thesis research has various limitations related to sample size and imaging or FE techniques warranting further discussion. First, the main limitation in this study is our sample size. Although previously discussed in each individual study, this also warrants discussion in relation to the collected studies. There were many noteworthy characteristics associated with total WOMAC and nocturnal pain, but some trends between studies were not consistent, possibly because we were underpowered to determine certain associations. For example, lower medial epiphyseal BMD was associated with total WOMAC pain, but subchondral cyst volume within the same region was not. Although low BMD is not completely analogous with cyst size, regions with larger cysts tend to have lower BMD than regions with smaller cysts. Future works with larger sample size and varying levels of OA-related pain will perhaps be able to elucidate and further understand these observations. Another limitation related to the sample of this study is the lack of a matched control group, either as a group of healthy participants or participants with moderate to severe OA but with little or no pain. A control group would allow for stronger analysis in determining the magnitude of the observed phenomena, and aid in reducing bias. Although the use of QCT doses patients with a small amount ionizing radiation, techniques are continuously improving and it may be worthwhile to consider and include healthy or control groups in future work evaluating BMD in patients with OA where possible. Second, these techniques have been developed for 0.625mm isotropic resolution, which may hinder the ability to translate these same techniques to CT images with smaller voxel sizes. Although 0.625mm isotropic voxel size is small enough to discriminate differences in BMD and FE outcomes in this work, improvements to CT imaging techniques have since been developed and it is possible to achieve CT images with smaller resolutions, e.g., to 0.3mm isotropic. The depth-specific image processing techniques used in this study may be easily transferrable to images with smaller voxel

size with minimal alterations, but transfer and mapping materials to FE models will require additional optimization and model validation. Similar techniques could be used with voxels measuring 0.5mm isotropic[176, 257], but further analysis is required for even smaller voxel sizes, with additional precision testing and optimization. Third, our FE models used a uniform elastic modulus for all bone tissue. This may be problematic for two reasons: differences in the roles and modulus of cortical and trabecular bone as discussed in Chapter 7, and the understanding that bone elastic modulus is dependent on the degree of mineralization[258, 259]. In patients with OA, the degree of mineralization can vary throughout the subchondral and epiphyseal regions[44], which may also lead to variations in structural orientation or tissue modulus distribution[260]. This is an inherent limitation in QCT imaging as QCT does not have the ability to distinguish alterations in bone volume fraction (BV/TV) from degree of mineralization (BM/BV) that occurs in different stages of OA[261, 262] ($\mathrm{BMD} = \mathrm{BV/TV} \times \mathrm{BM/BV}$). These characteristics may not be represented in CT images and thus, are inherent limitations of our FE model as well. Fourth, there are certain limitations to consider before these techniques can be applied in a clinical setting. Tibial segmentation and object map generation can be time-consuming. Although it may be possible to fully automate the segmenting process, object maps will still need correction before applying depth-specific image processing tools. As an example, our semi-automatic segmentation process with manual correction (described in Chapter 4) takes approximately 45 minutes to an hour to build and correct an object map for a single tibia. On object maps where splines are used to help expedite the segmenting process, manual correction at the subchondral surface is still required, and could take up to 30 to 45 minutes to correct an object map for a single tibia. Although this is the rate-limiting step, additional process streamlining is required before full implementation in clinical settings. Additionally, further analysis is required to determine the interrater precision of these imaging techniques. Precision errors are presented in each relevant chapter for each image processing technique, but as a single user performed most image processing and segmentations in this work, further analysis is required to determine precision between users before clinical implementation.

8.4. Clinical Significance

There is currently no cure for OA, the exact cause for disease initiation is unknown, and the exact mechanism of pain pathogenesis is also unknown. Bone is densely innervated[7, 8] and may

be a source of pain, but current reported relationships between image-based bony features and pain are conflicting[9, 10, 63, 105]. Overall, this work suggested that BMD at various depths from the subchondral surface of the proximal tibia is related to pain and may be a promising image-based feature worthwhile monitoring during disease or pain progression. As BMD may be modified, these studies also provide important preliminary information to aid in developing pain management strategies in patients with OA. Additionally, these studies help in identifying a potential mechanical role of bone in pain pathogenesis where previous works have suggested that mechanically driven bone remodelling may have a role in OA progression[45, 185, 193, 263] . This work further expands on this hypothesis by suggesting a mechanical component to pain, with a potential link to bone remodelling[57, 264] and clinical symptoms of OA. Accordingly, rational therapeutic approaches may benefit through monitoring bone density while targeting to maintain bone mineral and limit deterioration in bone structure and mechanical outcomes.

These results may be important for various types of patients at various stages of OA. Our studies evaluating BMD at various depths of the proximal tibia provide specific potential metrics to identify and monitor patients in early stages of OA, potentially leading to earlier intervention in developing patient-specific pain management strategies and treatments. In patients with OA, depth-specific imaging techniques combined with subject-specific FE analysis could provide a series of new *in vivo* metrics to help monitor the success of pain management treatments such as assistive devices, braces, joint distraction, or bone-modifying pharmaceuticals. Our study evaluating epiphyseal and metaphyseal BMD provides specific potential metrics to monitor in patients with late stages of painful OA awaiting joint replacement. Knowing which specific regions to monitor for low BMD, depth-specific imaging techniques could be used to evaluate pre-operative BMD, aiding surgical planning and patient preparation and complimenting current customized surgical approaches.

8.5. Conclusions

Four primary conclusions were generated from this thesis research:

1. QCT-based depth-specific imaging techniques demonstrated higher lateral maximum focal BMD in patients with severe nocturnal pain, compared to patients with no nocturnal pain at depths of 2.5-5mm (33% higher) and 5-10mm (32% higher) from the subchondral surface of the proximal tibia. There was also a non-significant trend for lower average

medial BMD in trabecular regions (2.5-5mm and 5-10mm from the subchondral surface) in patients with higher nocturnal pain.

2. QCT-based imaging techniques demonstrated that low tibial epiphyseal BMD at the total and medial regions, and low total metaphyseal BMD were associated with higher OA-related knee pain.
3. QCT-based measures of cyst parameters indicated that greater cyst number was associated with BMD, alignment, and JSN. Cyst parameters were not associated with OA severity scores or OA-related knee pain.
4. Subject-specific FE modeling of the proximal tibia in patients with OA, indicated that:
    a) Higher lateral principal compressive stress was associated with nocturnal pain. Specifically, OA patients with moderate nocturnal pain had 36% higher stress at the lateral peripheral cortical regions than patients with no nocturnal pain. OA patients with severe nocturnal pain had between 43% to 73% higher stress in lateral trabecular and cortical regions
    b) Higher medial stress was associated with varus alignment, higher lateral stress was associated with valgus alignment, and lower medial stiffness was associated with valgus alignment.

8.6. Contributions

This thesis research has generated many 'firsts', and many of the individual study results provided insights to the structural role of bone in pain pathogenesis in patients with knee OA:

1. First studies to use depth-specific QCT imaging techniques to assess relationships between OA-related knee pain and BMD at various depths from the subchondral surface of the proximal tibia in patients with clinically diagnosed OA.
2. First studies to demonstrate that QCT-derived BMD is associated with OA-related pain.
3. First studies to demonstrate that lower trabecular BMD at subchondral, epiphyseal, and metaphyseal depths are associated with OA-related pain.
4. First study to report that OA patients with severe nocturnal pain have higher localized lateral subchondral trabecular BMD, specifically at depths of 2.5-5mm (32% higher) and 5-10mm (33% higher) from the subchondral surface, than patients with no nocturnal pain.

5. First study to evaluate commonly overlooked trabecular epiphyseal and metaphyseal regions of the proximal tibia, and report lower BMD at these regions in TKR patients with more severe knee pain.
6. First *in vivo* study to use clinical QCT imaging at the proximal tibia to measure and evaluate associations between subchondral cyst parameters and OA-related pain, disease severity, and subchondral BMD.
7. First *in vivo* study to report associations between lateral cyst number and lateral subchondral BMD, as well as associations between lateral cyst parameters and valgus alignment.
8. First *in vivo* study to use subject-specific FE techniques at the proximal tibia in patients with clinically diagnosed OA to determine relationships between mechanical FE outcomes (stress, strain, stiffness) and OA-related pain. This study also currently reports the largest sample size of unique individuals (n=42) for any subject-specific QCT FE study of the knee.
9. First study to report associations between mechanical FE outcomes (stress, strain, stiffness) and clinical characteristics of OA (OA severity, pain, alignment). These findings suggest that there may be previously unexplored associations between OA-related knee pain and mechanical outcomes, emphasizing that bone may have a mechanical role in OA-related pain pathogenesis.

8.7. Future Research

This thesis research provides supporting rationale for future studies evaluating associations between bone and OA-related pain:

1. Depth-specific imaging techniques are currently being modified and developed to determine subchondral cortical and trabecular BMD at the distal femur. These techniques will first be used in a sample of healthy and OA participants to determine tool precision and any potential differences between healthy and OA distal femora. Once precision errors and any BMD differences are identified, these techniques will then be used in this sample to determine if distal femoral subchondral BMD is associated with OA-related knee pain.

2. Image processing tools are currently being developed to determine cyst parameters (number, volume, etc.) at the distal femur. These techniques will be applied to this sample to determine if femoral cyst characteristics are related to pain, and to determine how femoral cyst characteristics may be related to tibial cyst characteristics.
3. Currently, these depth-specific imaging and FE techniques are being used in the Multicenter Osteoarthritis Study (MOST), a longitudinal study at various locations in the USA consisting of over 5000 volunteers using MRI (for assessing cartilage) and CT (for assessing bone). This research will help us further understand the mechanical role of subchondral bone with cartilage degeneration in a larger sample over various stages of OA disease and symptomatic severity.
4. We are currently modifying and adapting regional stress and strain extraction algorithms to determine stress and strain surrounding subchondral cysts using our previously segmented cyst image volumes. This research will build on aspects from both our regional FE study and our subchondral cyst study, complimenting previous simulated works from McErlain et al.[131] and evaluating mechanical outputs in peri-cystic regions in patients with OA while incorporating OA-related pain.
5. We are currently modifying our FE models to investigate if element failure is associated with nocturnal knee pain. In addition to FE outcomes, it may be possible to assign failure criteria (safety factor) to the elements within the FE model to determine if mechanical failure is associated with OA-related pain. Failed elements would represent bone that has yielded, thus requiring remodeling. These criteria could explain, in part, why pain is occurring at night and potentially that nocturnal pain in patients with OA may be related to bone remodeling.
6. There may be additional FE outcomes worthwhile investigating that may be related to pain, such as hydrostatic stress, strain energy density, load distribution between medial and lateral plateaus, or fluid flow[265, 266] that may not be related to OA severity, but may be related to pain.
7. It may be possible to develop multi-modality co-registration techniques to co-register MRI and CT images to further determine relationships between bony features best analyzed using a single modality, such as BML on MRI and BMD on CT, and determine how these features are inter-related, along with OA-related pain. This work could

enhance the ability to further identify structures or bony changes related to pain in studies or centres with limited resources (i.e., if only CT or only MRI scanners were available in a clinical facility) and would also further our understanding of the mechanical role of bone in OA-related pain in relation to soft-tissue (cartilage) changes. These co-registration techniques could also ease the inclusion of soft tissues (cartilage, menisci, ligaments) in FE models with accurate subject-specific geometry.

8. Concerning FE modeling and computational simulations, there are always possibilities to improve modeling techniques and address limitations as computational resources become more available. For example, as processing speeds increase, it may be conveniently possible to map material properties from smaller voxels to smaller elements, and incorporate trabecular orientation.

REFERENCES

1. Felson DT. Clinical practice. Osteoarthritis of the knee. New England Journal of Medicine 2006;354:841-8.
2. Hunter DJ, Felson DT. Osteoarthritis. British Medical Journal 2006;332:639-42.
3. Canada S. Symptom onset, diagnosis and management of osteoarthritis: Research Article. In: Canada S, editor.2014. p. 10-7.
4. Gooberman-Hill R, Woolhead G, MacKichan F, Ayis S, Williams S, Dieppe P. Assessing chronic joint pain: Lessons from a focus group study. Arthritis & Rheumatism 2007;57:666-71.
5. Woolhead G, Gooberman-Hill R, Dieppe P, Hawker G. Night pain in hip and knee osteoarthritis: A focus group study. Arthritis Care & Research 2010;62:944-9.
6. Dye SF, Vaupel GL. The pathophysiology of patellofemoral pain. Sports Medicine and Arthroscopy Review 1994;2:203-10.
7. Bjurholm A, Kreicbergs A, Brodin E, Schultzberg M. Substance P- and CGRP-immunoreactive nerves in bone. Peptides 1988;9:165-71.
8. Buma P. Innervation of the patella: An immunohistochemical study in mice. Acta Orthopaedica Scandinavica 1994;65:80-6.
9. Javaid MK, Kiran A, Guermazi A, Kwoh CK, Zaim S, Carbone L, et al. Individual magentic resonance imaging and radiographic features of knee osteoarthritis in subjects with unilateral knee pain. Arthritis & Rheumatism 2012;64:3246-55.
10. Sowers M, Karvonen-Gutierrez CA, Jacobson JA, Jiang Y, Yosef M. Associations of anatomical measures from MRI with radiographically defined knee osteoarthritis score, pain, and physical functioning. Journal of Bone & Joint Surgery - American Volume 2011;93:241-51.
11. Barr AJ, Campbell TM, Hopkinson D, Kingsbury SR, Bowes MA, Conaghan PG. A systematic review of the relationship between subchondral bone features, pain and structural pathology in peripheral joint osteoarthritis. Arthritis Research & Therapy 2015;17:228.

12. Yusuf E, Kortekaas MC, Watt I, Huizinga TW, Kloppenburg M. Do knee abnormalities visualised on MRI explain knee pain in knee osteoarthritis? A systematic review. Annals of the Rheumatic Diseases. 2011;70:60-7.
13. Bousson V, Lowitz T, Laouisset L, Engelke K, Laredo JD. CT imaging for the investigation of subchondral bone in knee osteoarthritis. Osteoporos International 2012;23:S861-S5.
14. Lo G, Zhang Y, McLennan C, Niu J, Kiel D, McLean R, et al. The ratio of medial to lateral tibial plateau bone mineral density and compartment-specific tibiofemoral osteoarthritis1. Osteoarthritis and Cartilage 2006;14:984-90.
15. Lowitz T, Museyko O, Bousson V, Laouisset L, Kalendar WA, Laredo JD, et al. Bone marrow lesions identified by MRI in knee osteoarthritis are associated with locally increased bone mineral density measured by QCT. Osteoarthritis and Cartilage 2013;21:957-64.
16. Linde KN, Puhakka KB, Langdahl BL, Soballe K, Krog-Mikkelsen I, Madsen F, et al. Bone mineral density is lower in patients with severe knee osteoarthritis and attrition. Calcified Tissue International 2017;101:593-601.
17. Chen Y, Wang T, Guan M, Zhao W, Leung F-K-L, Pan H, et al. Bone turnover and articular cartilage differences localized to subchondral cysts in knees with advanced osteoarthritis. Osteoarthritis and Cartilage 2015;23:2174-83.
18. Chiba K, Burghardt AJ, Osaki M, Majumdar S. Three-dimensional analysis of subchondral cysts in hip osteoarthritis: An ex vivo HR-pQCT study. Bone 2014;66:140-5.
19. Burnett W, SA K, McLennan C, Hazel D, Talmo C, Hunter D, et al. Patella bone density is lower in knee osteoarthritis patients experiencing moderate-to-severe pain at rest. Journal of Musculoskeletal & Neuronal Interactions 2016;16:33-9.
20. Burnett WD, Kontulainen SA, McLennan CE, Wilson DR, Hunter DJ, Johnston JD. Regional depth-specific subchondral bone density measures in osteoarthritic and normal patellae: In vivo precision and preliminary comparisons. Osteoporosis International 2014;25:1107-14.
21. Johnston JD, Kontulainen SA, Masri BA, Wilson DR. A comparison of conventional maximum intensity projection with a new depth-specific topographic mapping technique in

the CT analysis of proximal tibial subchondral bone density. Skeletal Radiology 2010;39:867-76.

22. Johnston JD, McLennan CE, Hunter DJ, Wilson DR. In vivo precision of a depth-specific topographic mapping technique in the CT analysis of osteoarthritic and normal proximal tibial subchondral bone density. Skeletal Radiology 2010;40:1057-64.
23. Bennell KL, Creaby MW, Wrigley TV, Hunter DJ. Tibial subchondral trabecular volumetric bone density in medial knee joint osteoarthritis using peripheral quantitative computed tomography technology. Arthritis & Rheumatism 2008;58:2776-85.
24. Zysset PK, Sonny M, Hayes WC. Morphology-mechanical property relations in trabecular bone of the osteoarthritic proximal tibia. Journal of Arthroplasty 1994;9:203-16.
25. Keyak JH, Lee IY, Skinner HB. Correlations between orthogonal mechanical properties and density of trabecular bone: use of different densitometric measures. Journal of Biomedical Materials Research 1994;28:1329-36.
26. Hurwitz DE, Sumner DR, Andriacchi TP, Sugar DA. Dynamic knee loads during gait predict proximal tibial bone distribution. Journal of Biomechanics 1998;31:423-30.
27. Thorp LE, Wimmer MA, Block JA, Moisio KC, Shott S, Goker B, et al. Bone mineral density in the proximal tibia varies as a function of static alignment and knee adduction angular momentum in individuals with medial knee osteoarthritis. Bone 2006;39:1116-22.
28. Wada M, Maezawa Y, Baba H, Shimada S, Sasaki S, Nose Y. Relationships among bone mineral densities, static alignment and dynamic load in patients with medial compartment knee osteoarthritis. Rheumatology (Oxford, England) 2001;40:499-505.
29. Daheshia M, Yao JQ. The bone marrow lesion in osteoarthritis. Rheumatology International 2010;31:143-8.
30. Arjmand H. Quantitative Computed Tomography Based Finite Element Modeling of Normal and Osteoarthritic Knees: In vivo Precision and Preliminary Comparisons: University of Saskatchewan, Saskatoon, SK Canada; 2016.
31. Arjmand H, Nazemi M, Kontulainen SA, Milner JS, Holdsworth DW, McLennan CE, et al. Finite element modeling of proximal tibial stiffness in normal and osteoarthritic knees: In vivo precision and preliminary comparisons. Osteoarthritis and Cartilage 2016;24:S309-S10.

32. Duncan RC. Prevalence of radiographic osteoarthritis--it all depends on your point of view. Rheumatology 2006;45:757-60.
33. McAlindon TE, Snow S, Cooper C, Dieppe PA. Radiographic patterns of osteoarthritis in the knee joint in the community: The importance of the patellofemoral joint. Annals of the Rheumatic Diseases 1992;51:844-9.
34. Williams PL, Warwick R, Dyson M, Bannister LH. Gray's Anatomy. 37 ed. Williams PL, R. W, M. D, H. BL, editors. London: Churchill Livingstone; 1989.
35. Seedhom BB, Dowson D, Wright V. Proceedings: Functions of the menisci. A preliminary study. Annals of the Rheumatic Diseases 1974;33:111.
36. Walker PS, Erkman MJ. The role of the menisci in force transmission across the knee. Clinical Orthopaedics and Related Research 1975:184-92.
37. Schreppers GJ, Sauren AA, Huson A. A numerical model of the load transmission in the tibio-femoral contact area. Proceedings of the Institution of Mechanical Engineers Part H: Journal of Engineering in Medicine 1990;204:53-9.
38. Ahmed AM, Burke DL. In-vitro measurement of static pressure distribution in synovial joints--Part I: Tibial surface of the knee. Journal of Biomechanical Engineering 1983;105:216-25.
39. Fortier LA, Nixon AJ. Distributional change in substance P nociceptive fiber patterns in naturally osteoarthritic articulations. The Journal of Rheumatology 1997;24:7.
40. Madry H, van Dijk CN, Mueller-Gerbl M. The basic science of the subchondral bone. Knee Surgery, Sports Traumatology, Arthroscopy 2010;18:419-33.
41. Ljunggren AE. Variations in the relationship between the diaphysis and the epiphyses of the tibia. Acta Morphologica Neerlando-Scandinavica 1976;14:101-37.
42. Radin EL, Paul IL. Importance of bone in sparing articular cartilage from impact. Clinical Orthopaedics and Related Research 1971;78:3.
43. Burr DB. The importance of subchondral bone in the progression of osteoarthritis. Journal of Rheumatology Supplement 2004;70:77-80.
44. Burr DB, Schaffler MB. The involvement of subchondral mineralized tissues in osteoarthrosis: quantitative microscopic evidence. Microscopy Research and Technique 1997;37:343-57.

45. Dieppe P. Subchondral bone should be the main target for the treatment of pain and disease progression in OA. Osteoarthritis and Cartilage 1999;7:325-6.
46. Health Canada. Arthritis in Canada: An Ongoing Challenge. 2003.
47. Dieppe PA, Reichenbach S, Williams S, Gregg P, Watt I, Juni P. Assessing bone loss on radiographs of the knee in osteoarthritis. Arthritis & Rheumatism 2005;52:3536-41.
48. Felson DT, Lawrence RC, Dieppe PA, Hirsch R, Helmick CG, Jordan JM, et al. Osteoarthritis: new insights. Part 1: the disease and its risk factors. Annals of Internal Medicine 2000;133:635-46.
49. Brandt KD, Dieppe P, Radin EL. Etiopathogenesis of osteoarthritis. Rheumatic Disease Clinics of North America 2008;34:531-59.
50. Goldring SR. Role of Bone in Osteoarthritis Pathogenesis. Medical Clinics of North America 2009;93:25-35.
51. Hunter DJ, Guermazi A, Roemer F, Zhang Y, Neogi T. Structural correlates of pain in joints with osteoarthritis. Osteoarthritis and Cartilage 2013;21:1170-8.
52. Sowers MF, Hayes C, Jamadar D, Capul D, Lachance L, Jannausch M, et al. Magnetic resonance-detected subchondral bone marrow and cartilage defect characteristics associated with pain and X-ray-defined knee osteoarthritis. Osteoarthritis and Cartilage 2003;11:387-93.
53. Neogi T. Clinical significance of bone changes in osteoarthritis. Arthritis Research and Therapy Conference: International Congress on Bone Involvement in Arthritis, Osteorheumatology 2011;14.
54. Hunter DJ. Imaging Insights on the Epidemiology and Pathophysiology of Osteoarthritis. Rheumatic Disease Clinics of North America 2009;35:447-63.
55. Setton LA, Elliott DM, Mow VC. Altered mechanics of cartilage with osteoarthritis: human osteoarthritis and an experimental model of joint degeneration. Osteoarthritis and Cartilage 1999;7:2-14.
56. Li G, Ma Y, Cheng TS, Landao-Bassonga E, Qin A, Pavlos NJ, et al. Identical subchondral microarchitecture patterns with increased bone resorption in rheumatoid arthritis as compared to osteoarthritis. Osteoarthritis and Cartilage 2014;22:2083-92.
57. Frost HM. Bone's mechanostat: a 2003 update. Anatomical Record Part A: Discoveries in Molecular, Cellular, and Evolutionary Biology 2003;275:1081-101.

58. Hurwitz DE, Ryals AR, Block JA, Sharma L, Schnitzer TJ, Andriacchi TP. Knee pain and joint loading in subjects with osteoarthritis of the knee. Journal of Orthopaedic Research 2000;18:8.
59. Kellgren JH, Lawrence JS. Radiological assessment of osteo-arthrosis. Annals of the Rheumatic Diseases 1957;16:494-502.
60. Altman RD, Gold GE. Atlas of individual radiographic features in osteoarthritis, revised. Osteoarthritis and Cartilage 2007;15 Suppl A:A1-56.
61. Altman RD, Hochberg M, Murphy WA, Jr., Wolfe F, Lequesne M. Atlas of individual radiographic features in osteoarthritis. Osteoarthritis and Cartilage 1995;3 Suppl A:3-70.
62. Hannan MT, Felson DT, Pincus T. Analysis of the discordance between radiographic changes and knee pain in osteoarthritis of the knee. The Journal of Rheumatology 2000;27:1513-7.
63. Hayes CW, Jamadar DA, Welch GW, Jannausch ML, Lachance LL, Capul DC, et al. Osteoarthritis of the knee: Comparison of MR imaging findings with radiographic severity measurements and pain in middle-aged women. Radiology 2005;237:998-1007.
64. Chan WP, Lang P, Stevens MP, Sack K, Majumdar S, Stoller DW, et al. Osteoarthritis of the knee: Comparison of radiography, CT, and MR imaging to assess extent and severity. American Journal of Radiology 1991;157:799-806.
65. Peterfy CG, Guermazi A, Zaim S, Tirman PFJ, Miaux Y, White D, et al. Whole-Organ Magnetic Resonance Imaging Score (WORMS) of the knee in osteoarthritis. Osteoarthritis and Cartilage 2004;12:177-90.
66. Torres L, Dunlop DD, Peterfy C, Guermazi A, Prasad P, Hayes KW, et al. The relationship between specific tissue lesions and pain severity in persons with knee osteoarthritis. Osteoarthritis and Cartilage 2006;14:1033-40.
67. Kim IJ, Kim DH, Jung JY, Song YW, Guermazi A, Crema MD, et al. Association between bone marrow lesions detected by magnetic resonance imaging and knee pain in community residents in Korea. Osteoarthritis and Cartilage 2013;21:1207-13.
68. Wildi LM, Raynauld JP, Martel-Pelletier J, Abram F, Dorais M, Pelletier JP. Relationship between bone marrow lesions, cartilage loss and pain in knee osteoarthritis: Results from a randomised controlled clinical trial using MRI. Annals of the Rheumatic Diseases 2010;69:2118-24.

69. Neogi T, Felson D, Niu J, Nevitt M, Lewis CE, Aliabadi P, et al. Association between radiographic features of knee osteoarthritis and pain: Results from two cohort studies. British Medical Journal 2009;339:498-501.
70. Duncan R, Peat G, Thomas E, Wood L, Hay E, Croft P. How do pain and function vary with compartmental distribution and severity of radiographic knee osteoarthritis? Rheumatology 2008;47:1704-7.
71. Hunter DJ, McDougall JJ, Keefe FJ. The Symptoms of Osteoarthritis and the Genesis of Pain. Rheumatic Disease Clinics of North America 2008;34:623-43.
72. Hawker GA, Stewart L, French MR, Cibere J, Jordan JM, March L, et al. Understanding the pain experience in hip and knee osteoarthritis - an OARSI/OMERACT initiative. Osteoarthritis and Cartilage 2008;16:415-22.
73. Hensor EMA, Dube B, Kingsbury SR, Tennant A, Conaghan PG. Towards a clinical definition of early osteoarthritis: Onset of patient-reported knee pain begins on stairs. Data from the Osteoarthritis Initiative. Arthritis Care & Research 2015;67:40-7.
74. Haverkamp D, Brokelman RBG, van Loon CJM, van Kampen A. Timing of arthroplasty, what is the influence of nocturnal pain and pain at rest on the outcome? Knee Surgery, Sports Traumatology, Arthroscopy 2013;21:2590-4.
75. Bellamy N, Buchanan WW, Goldsmith CH, Campbell J, Stitt LW. Validation study of WOMAC: A health status instrument for measuring clinically important patient relevant outcomes to antirheumatic drug therapy in patients with osteoarthritis of the hip or knee. Journal of Rheumatology 1988;15:1833-40.
76. Roos EM, Toksvig-Larsen S. Knee injury and Osteoarthritis Outcome Score (KOOS): Validation and comparison to the WOMAC in total knee replacement. Health and Quality of Life Outcomes 2003;1.
77. Baliki MN, Schnitzer TJ, Bauer WR, Apkarian AV. Morphological signatures for chronic pain. PloS One 2011;6:e26010.
78. Lo GH, McAlindon TE, Niu J, Zhang Y, Beals C, Dabrowski C, et al. Bone marrow lesions and joint effusion are strongly and independently associated with weight-bearing pain in knee osteoarthritis: data from the osteoarthritis initiative. Osteoarthritis and Cartilage 2009;17:1562-9.

79. Wluka AE, Wolfe R, Stuckey S, Cicuttini FM. How does tibial cartilage volume relate to symptoms in subjects with knee osteoarthritis? Annals of the Rheumatic Diseases 2004;63:264-8.
80. Everhart JS, Siston RA, Flanigan DC. Tibiofemoral subchondral surface ratio (SSR) is a predictor of osteoarthritis symptoms and radiographic progression: Data from the Osteoarthritis Initiative (OAI). Osteoarthritis and Cartilage 2014;22:771-8.
81. Kumar DK, Wyatt CR, Lee S, Nardo L, Link TM, Majumdar S, et al. Association of cartilage defects, and other MR findings with pain and function in individuals with mild-moderate radiographic hip osteoarthritis and controls. Osteoarthritis and Cartilage 2013;21:1685-92.
82. Baum T, Joseph GB, Arulanandan A, Nardo L, Virayavanich W, Carballido-Gamio J, et al. Association of MRI-based knee cartilage T2 measurements and focal knee lesions with knee pain: Data from the Osteoarthritis Initiative. Arthritis Care & Research 2012;64:248-55.
83. Dor FJ, Ramirez ML, Parmar K, Altman EL, Huang CA, Down JD, et al. Primitive hematopoietic cell populations reside in the spleen: Studies in the pig, baboon, and human. Experimental Hematology 2006;34:1573-82.
84. Burr D. The importance of subchondral bone in osteoarthrosis. Current Opinion in Rheumatology 1998;10:256-62.
85. Lajeunesse D, Reboul P. Subchondral bone in osteoarthritis: A biologic link with articular cartilage leading to abnormal remodeling. Current Opinion in Rheumatology 2003;15:6.
86. Tanamas SK, Hanna FS, Cicutinni FM, Wluka AE, Berry PA, Urquhart DM. Does knee malalignment increase the risk of development and progression of knee osteoarthritis? A systematic review. Arthritis & Rheumatism 2009;61:459-67.
87. Schipplein OD, Andriacchi TP. Interaction between active and passive knee stabilizers during level walking. Journal of Orthopaedic Research 1991;9:113-9.
88. Tetsworth K, Paley D. Malalignment and degenerative arthroplasty. Orthopedic Clinics of North America 1994;25:367-77.
89. Sharma L, Song J, Dunlop D, Felson D, Lewis CE, Segal N, et al. Varus and valgus alignment and incident and progressive knee osteoarthritis. Annals of the Rheumatic Diseases 2010;69:1940-5.

90. Brouwer GM, van Tol AW, Bergink AP, Belo JN, Bernsen RMD, Reijman M, et al. Association between valgus and varus alignment and the development and progression of radiographic osteoarthritis of the knee. Arthritis & Rheumatism 2007;56:1204-11.
91. Lo GH, Harvey WF, McAlindon TE. Associations of varus thrust and alignment with pain in knee osteoarthritis. Arthritis & Rheumatism 2012;64:2252-9.
92. Chang CB, Koh IJ, Seo ES, Kang YG, Seong SC, Kim TK. The radiographic predictors of symptom severity in advanced knee osteoarthritis with varus deformity. The Knee 2011;18:456-60.
93. Miura H, Takasugi S-I, Kawano T, Manabe T, Iwamoto Y. Varus-valgus laxity correlates with pain in osteoarthritis of the knee. The Knee 2009;16:30-2.
94. Maly MR, Costigan PA, Olney SJ. Mechanical factors relate to pain in knee osteoarthritis. Clinical Biomechanics 2008;23:796-805.
95. Goulston LM, Sanchez-Santos MT, D'Angelo S, Leyland KM, Hart DJ, Spector TD, et al. A comparison of radiographic anatomic axis knee alignment measurements and cross-sectional associations with knee osteoarthritis. Osteoarthritis and Cartilage 2016;24:612-22.
96. Hicks-Little CA, Peindl RD, Hubbard-Turner TJ, Cordova ML. The relationship between early-stage knee osteoarthritis and lower-extremity alignment, joint laxity, and subjective scores of pain, stiffness, and function. Journal of Sport Rehabilitation 2016;25:213-8.
97. Kraus VB, McDaniel G, Worrell TW, Feng S, Vail TP, Varju G, et al. Association of bone scintigraphic abnormalities with knee malalignment and pain. Annals of the Rheumatic Diseases 2009;68:1673-9.
98. Neogi T, Nevitt M, Niu J, Sharma L, Roemer F, Guermazi A, et al. Subchondral bone attrition may be a reflection of compartment-specific mechanical load: The MOST study. Annals of the Rheumatic Diseases 2010;69:841-4.
99. Spector TD, Hart DJ, Byrne J, Harris PA, Dacre JE, Doyle DV. Definition of osteoarthritis of the knee for epidemiological studies. Annals of the Rheumatic Diseases 1993;52:790-4.
100. Boegård T, Rudling O, Petersson IF, Jonsson K. Correlation between radiographically diganosed osteophytes and magnetic resonance detected cartilage defects in the patellofemoral joint. Annals of the Rheumatic Diseases 1998;57:395-400.

101. Boegard T, Rudling O, Petersson IF, Jonsson K. Correlation between radiographically diagnosed osteophytes and magnetic resonance detected cartilage defects in the tibiofemoral joint. Annals of the Rheumatic Diseases 1998;57:401-7.
102. Cicuttini FM, Baker J, Hart DJ, Spector TD. Association of pain with radiological changes in different compartments and views of the knee joint. Osteoarthritis and Cartilage 1996;4:143-7.
103. Cicuttini FM, Baker J, Hart DJ, Spector TD. Choosing the best method for radiological assessment of patellofemoral osteoarthritis. Annals of the Rheumatic Diseases 1996;55:134-6.
104. Hayashi D, Xu L, Roemer FW, Hunter DJ, Li L, Katur AM, et al. Detection of osteophytes and subchondral cysts in the knee with use of tomosynthesis. Musculoskeletal Imaging 2012;263:206-15.
105. Kinds MB, Marijnissen ACA, Bijlsma JWJ, Boers M, Lafeber FPJG, Welsing PMJ. Quantitative radiographic features of early knee osteoarthritis: Development over 5 years and relationship with symptoms in the CHECK Cohort. Journal of Rheumatology 2013;40:58-65.
106. Kornaat PR, Bloem JL, Ceulemans RYT, Riyazi N, Rosendaal FR, Nelissen RG, et al. Osteoarthritis of the knee: Association between clinical findings and MR imaging findings. Radiology 2006;239:811-7.
107. Lanyon P, O'Reilly S, Jones A, Doherty M. Radiographic assessment of symptomatic knee osteoarthritis in the community:Definitions and normal joint space. Annals of Rheumatic Diseases 1998;57:7.
108. Szebenyi B, Hollander AP, Dieppe P, Quilty B, Buddy J, Clarke S, et al. Associations between pain, function, and radiographic features in osteoarthritis of the knee. Arthritis & Rheumatism 2006;54:230-5.
109. Ai F, Yu C, Zhang W, Morelli JN, Kacher D, Li X. MR Imaging of knee osteoarthritis and correlation of findings with reported patient pain. Journal of Huazhong University of Science and Technology 2010;30:248-54.
110. Dieppe PA, Cushnaghan J, Shepstone L. The Bristol 'OA500' study: progression of osteoarthritis (OA) over 3 years and the relationship between clinical and radiographic changes at the knee joint. Osteoarthritis and Cartilage 1997;5:87-97.

111. Chang CB, Han I, Kim SJ, Seong SC, Kim TK. Association between radiological findings and symptoms at the patellofemoral joint in advanced knee osteoarthritis. The Journal of Bone and Joint Surgery (Br) 2007;89-B:1324-8.
112. Link TM, Steinbach LS, Ghosh S, Ries M, Lu Y, Lane NE, et al. Osteoarthritis: MR imaging findings in different stages of disease and correlation with clinical findings. Radiology 2003;226:373-81.
113. Sanghi D, Avasthi S, Mishra A, Singh A, Agarwal S, Srivastava RN. Is radiology a determinant of pain, stiffness, and functional disability in knee osteoarthritis? A cross-sectional study. Journal of Orthopaedic Science 2011;16:719-25.
114. Burnett S, Hart DJ, Cooper C, Spector TD. A radiographic atlas of osteoarthritis. London: Springer-Veriag; 1994.
115. Felson D, Nevitt M, Yang M, Clancy M, Niu J, Torner J, et al. A new approach yields high rates of radiographic progression in knee osteoarthritis. Journal of Rheumatology 2008;35:2047-54.
116. Spector T, Cooper C, Cushnaghan J, Hart D, Dieppe PA. A radiographic atlas of knee osteoarthritis. London: Springer Verlag; 1992.
117. Day JS, Van Der Linden JC, Bank RA, Ding M, Hvid I, Sumner DR, et al. Adaptation of subchondral bone in osteoarthritis. Biorheology 2004;41:359-68.
118. Radin EL. Mechanical aspects of osteoarthrosis. Bulletin on the Rheumatic Diseases 1976;26:862-5.
119. Chappard C, Peyrin F, Bonnassie A, Lemineur G, Brunet-Imbault B, Lespessailles E, et al. Subchondral bone micro-architectural alterations in osteoarthritis: a synchrotron micro-computed tomography study. Osteoarthritis and Cartilage 2006;14:215-23.
120. Ding M, Odgaard A, Hvid I. Changes in the three-dimensional microstructure of human tibial cancellous bone in early osteoarthritis. The Journal of Bone and Joint Surgery 2003;85-B:906-12.
121. Bullough PG. Osteoarthritis and related disorders: pathology. In: Klippel JH, Dieppe PA, editors. Rheumatology. 2nd ed. London: Mosby; 1998. p. 8..1-8.
122. Neogi T. Clinical significance of bone changes in osteoarthritis. Therapeutic Advances in Musculoskeletal Disease 2012;4:259-67.

123. Neogi T, Felson D, Niu J, Lynch J, Nevitt M, Guermazi A, et al. Cartilage loss occurs in the same subregions as subchondral bone attrition: A within-knee subregion-matched approach from the multicenter osteoarthritis study. Arthritis & Rheumatism 2009;61:1539-44.
124. Reichenbach S, Dieppe PA, Nuesch E, Williams S, Villiger PM, Juni P. Association of bone attrition with knee pain, stiffness and disability: A cross-sectional study. Annals of the Rheumatic Diseases 2011;70:293-8.
125. Hernandez-Molina G, Neogi T, Hunter DJ, Niu J, Guermazi A, Reichenbach S, et al. The association of bone attrition with knee pain and other MRI features of osteoarthritis. Annals of the Rheumatic Diseases 2008;67:43-7.
126. Ahlback S. Osteoarthrosis of the knee: A radiographic investigation. Acta Radiologica Diagnosis 1968;277 Suppl:7-72.
127. Ondrouch AS. Cyst Formation in Osteoarthritis. Journal of Bone and Joint Surgery (Br) 1963;45:755-60.
128. Durr HD, Martin H, Pellengahr C, Schlemmer M, Maier M, Jansson V. The cause of subchondral bone cysts in osteoarthrosis: a finite element analysis. Acta Orthopaedica Scandinavica 2004;75:554-8.
129. Resnick D, Niwayama G, Coutts R. Subchondral cysts (geodes) in arthritic disorders: Pathologic and radiographic appearance of the hip joint. American Journal of Roentgenology and Radium Therapy 1977;128:345-50.
130. Freund E. The pathological significance of intra-articular pressure. Edinburgh Medical Journal 1940;47:192.
131. McErlain DD, Milner JS, Ivanov TG, Jencikova-Celerin L, Pollmann SI, Holdsworth DW. Subchondral cysts create increased intra-osseous stress in early knee OA: A finite element analysis using simulated lesions. Bone 2011;48:639-46.
132. Felson DT, McLaughlin S, Goggins J, LaValley MP, Gale E, Totterman S, et al. Bone marrow edema and its relation to progression of knee osteoarthritis. Annals of Internal Medicine 2003;139:330-6.
133. Driban JB, Price LL, Lo GH, Pang J, Hunter DJ, Miller E, et al. Evaluation of bone marrow lesion volume as a knee osteoarthritis biomarker - longitudinal relationships with

pain and structural changes: data from the Osteoarthritis Initiative. Arthritis Research & Therapy 2013;15:R112.

134. Guermazi A, Niu J, Hayashi D, Roemer FW, Englund M, Neogi T, et al. Prevalence of abnormalities in knees detected by MRI in adults without knee osteoarthritis: Population based observational study (Framingham Osteoarthritis Study). British Medical Journal 2012;345:7874.
135. Zanetti M, Bruder E, Romero J, Hodler J. Bone marrow edema pattern in osteoarthritic knees: Correlation between MR imaging and hostologic findings. Radiology 2000;215:835-40.
136. Felson DT, Chaisson CE, Hill CL, Totterman SM, Gale ME, Skinner KM, et al. The association of bone marrow lesions with pain in knee osteoarthritis. Annals of Internal Medicine 2001;134:541-9.
137. Ip S, Sayre EC, Guermazi A, Nicolaou S, Wong H, Thorne A, et al. Frequency of bone marrow lesions and association with pain severity: results from a population-based symptomatic knee cohort. The Journal of Rheumatology 2011;38:1079-85.
138. Felson DT, Callaghan MJ, Parkes M, Marjanovic EJ, Lunt M, Oldham JA, et al. Bone marrow lesions in knee osteoarthritis change in 6 to 12 weeks. Osteoarthritis and Cartilage 2011;19:S10.
139. Lo GH, Hunter DJ, Zhang Y, McLennan CE, LaValley MP, Kiel DP, et al. Bone marrow lesions in the knee are associated with increased local bone density. Arthritis & Rheumatism 2005;52:2814-21.
140. Seah S, Wheaton D, Li L, Dyke JP, Talmo C, Harvey WF, et al. The relationship of tibial bone perfusion to pain in knee osteoarthritis. Osteoarthritis and Cartilage 2012;20:1527-33.
141. Baert IAC, Staes F, Truijen S, Mahmoudian A, Noppe N, Vanderschueren G, et al. Weak associations between structural changes on MRI and symptoms, function and muscle strength in relation to knee osteoarthritis. Knee Surgery, Sports Traumatology, Arthroscopy 2014;22:2013-25.
142. Hunter DJ, Lo GH, Gale D, Grainger AJ, Guermazi A, Conaghan PG. The reliability of a new scoring system for knee osteoarthritis MRI and the validity of bone marrow lesion assessment: BLOKS (Boston-Leeds Osteoarthritis Knee Score). Annals of the Rheumatic Diseases 2008;67:206-11.

143. Bilgici A, Dogan C, Cil E, Sakarya S, Kuru O, Selcuk MB. Relationship between pain severity and magnetic resonance imaging features in patients with osteoarthritis of the knee. Turkish Journal of Rheumatology 2010;25:184-90.
144. Dore D, Quinn S, Ding C, Winzenberg T, Zhai G, Cicuttini F, et al. Natural history and clinical significance of MRI-detected bone marrow lesions at the knee: A prospective study in community dwelling older adults. Arthritis Research and Therapy 2010;12:6.
145. Felson DT, Niu J, Guermazi A, Roemer FW, Aliabadi P, Clancy M, et al. Correlation of the development of knee pain with enlarging bone marrow lesions on magentic resonance imaging. Arthritis & Rheumatism 2007;56:2986-92.
146. Kornaat PR, Kloppenburg M, Sharma R, Botha-Scheepers SA, Graverand M-PH, Coene LNJEM, et al. Bone marrow edema-like lesions change in volume in the majority of patients with osteoarthritis; associations with clinical features. European Radiology 2007;17:3073-8.
147. Ratzlaff C, Guermazi A, Collins J, Katz JN, Losina E, Vanwyngaarden C, et al. A rapid, novel method of volumetric assessment of MRI-detected subchondral bone marrow lesions in knee osteoarthritis. Osteoarthritis and Cartilage 2013;21:806-14.
148. Stefanik JJ, Gross KD, Guermazi A, Felson DT, Roemer FW, Zhang Y, et al. The relation of MRI-detected structural damage in the medial and lateral patellofemoral joint to knee pain: The Multicenter and Framingham Osteoarthritis Studies. Osteoarthritis and Cartilage 2015;23:565-70.
149. Dore D, Ding C, Jones G. A pilot study of the reproducibility and validity of measuring knee subchondral bone density in the tibia. Osteoarthritis and Cartilage 2008;16:1539-44.
150. Beattie KA, Boulus P, Duryea J, O'Neill J, Pui M, Gordon CL, et al. The relationships between bone mineral density in the spine, hip, distal femur and proximal tibia and medial minimum joint space width in the knees of healthy females. Osteoarthritis and Cartilage 2005;13:872-8.
151. Bruyere O, Dardenne C, Lejeune E, Zegels B, Pahaut A, Richy F, et al. Subchondral tibial bone mineral density predicts future joint space narrowing at the medial femoro-tibial compartment in patients with knee osteoarthritis. Bone 2003;32:541-5.

152. Madsen OR, Schaadt O, Bliddal H, Egsmose C, Sylvest J. Bone mineral distribution of the proximal tibia in gonarthrosis assessed in vivo by photon absorption. Osteoarthritis and Cartilage 1994;2:141-7.
153. Clarke S, Wakeley C, Duddy J, Sharif M, Watt I, Ellingham K, et al. Dual-energy X-ray absorptiometry applied to the assessment of tibial subchondral bone mineral density in osteoarthritis of the knee. Skeletal Radiology 2004;33.
154. Dore D, Quinn S, Ding C, Winzenberg T, Jones G. Correlates of subchondral BMD: A cross-sectional study. Journal of Bone and Mineral Research 2009;24:2007-15.
155. Messent EA, Ward RJ, Tonkin CJ, Buckland-Wright C. Tibial cancellous bone changes in patients with knee osteoarthritis. A short-term longitudinal study using Fractal Signature Analysis. Osteoarthritis and Cartilage 2005;13:463-70.
156. Messent EA, Buckland-Wright JC, Blake GM. Fractal analysis of trabecular bone in knee osteoarthritis (OA) is a more sensitive marker of disease status than bone mineral density (BMD). Calcified Tissue International 2005;76:419-25.
157. Watts NB. Fundamentals and pitfalls of bone densitometry using dual-energy X-ray absorptiometry (DXA). Osteoporosis International 2004;15:847-54.
158. Akamatsu Y, Mitsugi N, Taki N, Ashi HK, Saito T. Medial versus lateral condoyle bone mineral density ratios in a cross-sectional study: A potential marker for medial knee osteoarthritis severity. Arthritis Care & Research 2012;64:1036-45.
159. Lo GH, Tassinari AM, Driban JB, Price LL, Schneider E, Majumdar LS, et al. Cross-sectional DXA and MR measures of tibial periarticular bone associate with radiographic knee osteoarthritis severity. Osteoarthritis and Cartilage 2012;20:686-93.
160. Speirs AD, Beaulé PE, Rakhra KS, Schweitzer ME, Frei H. Increased acetabular subchondral bone density is associated with cam-type femoroacetabular impingement. Osteoarthritis and Cartilage 2013;21:551-8.
161. Wright DA, Meguid M, Lubovsky O, Whyne CM. Subchondral bone density distribution in the human femoral head. Skeletal Radiology 2011;41:677-83.
162. Johnston JD, Masri BA, Wilson DR. Computed tomography topographic mapping of subchondral density (CT-TOMASD) in osteoarthritic and normal knees: methodological development and preliminary findings. Osteoarthritis and Cartilage 2009;17:1319-26.

163. Intema F, Thomas TP, Anderson DD, Elkins JM, Brown TD, Amendola A, et al. Subchondral bone remodeling is related to clinical improvement after joint distraction in the treatment of ankle osteoarthritis. Osteoarthritis and Cartilage 2011;19:668-75.
164. Engelke K, Libanati C, Fuerst T, Zysset PK, Genant HK. Advanced CT based in vivo methods for the assessment of bone density, structure, and strength. Curr Osteoporos Rep 2013;11:246-55.
165. Johnston JD, Kontulainen SA, Masri BA, Wilson DR. Predicting subchondral bone stiffness using a depth-specific QCT topographic mapping technique in normal and osteoarthritic proximal tibiae. Clinical Biomechanics (Bristol, Avon) 2011.
166. Amini M, Nazemi SM, Lanovaz J, Kontulainen S, Masri BA, Wilson DR, et al. Individual and combined effects of OA-related subchondral bone alterations on proximal tibial surface stiffness: A parametric finite element modeling study. Medical Engineering and Physics 2015;37:783-91.
167. Venäläinen MS, Mononen ME, Jurvelin JS, Töyräs J, Virén T, Korhonen RK. Importance of material properties and porosity of bone on mechanical response of articular cartilage in human knee joint: A two-dimensional finite element study. . Journal of Biomechanical Engineering 2014;136:121005.
168. Austman RL, Milner JS, Holdsworth DW, Dunning CE. The effect of the density-modulus relationship selected to apply material properties in a finite element model of long bone. Journal of Biomechanics 2008;41:3171-6.
169. Fang J, Gong H, Kong L, Zhu D. Simulation on the internal structure of three-dimensional proximal tibia under different mechanical environments. BioMedical Engineering Online 2013;12:130.
170. Helgason B, Perilli E, Schileo E, Taddei F, Brynjólfsson S, Viceconti M. Mathematical relationships between bone density and mechanical properties: A literature review. Clinical Biomechanics 2008;23:135-46.
171. Keaveny TM, Morgan EF, Niebur GL, Yeh OC. Biomechanics of trabecular bone. Annu Rev Biomed Eng 2001;3:307-33.
172. Keaveny TM, Borchers RE, Gibson LJ, Hayes WC. Theoretical analysis of the experimental artifact in trabecular bone compressive modulus. Journal of Biomechanics 1993;26:599-607.

173. Linde F, Hvid I, Madsen F. The effect of specimen geometry on the mechanical behaviour of trabecular bone specimens. Journal of Biomechanics 1992;25:10.
174. Keaveny TM, Pinilla TP, Crawford RP, Kopperdahl DL, Lou A. Systematic and random errors in compression testing of trabecular bone. Journal of Orthopaedic Research 1997;15:10.
175. Odgaard A, Linde F. The underestimation of Young's modulus in compressive testing of cancellous bone specimens. Journal of Biomechanics 1991;24:691-8.
176. Nazemi SM, Amini M, Kontulainen SA, Milner JS, Holdsworth DW, Masri BA, et al. Prediction of local proximal tibial subchondral bone structural stiffness using subject-specific finite element modeling: Effect of selected density-modulus relationship. Clinical Biomechanics 2015;30:703-12.
177. Morgan EF, Bayraktar HH, Keaveny TM. Trabecular bone modulus-density relationships depend on anatomic site. Journal of Biomechanics 2003;36:897-904.
178. Anderson MJ, Keyak JH, Skinner HB. Compressive mechanical properties of human cancellous bone after gamma irradiation. Journal of Bone and Joint Surgery (Am) 1992;74:747-52.
179. Goulet RW, Goldstein SA, Ciarelli MJ, Kuhn JL, Brown MB, Feldkamp LA. The relationship between the structural and orthogonal compressive properties of trabecular bone. Journal of Biomechanics 1994;27:375-89.
180. Rho JY, Hobatho MC, Ashman RB. Relations of mechanical properties to density and CT numbers in human bone. Medical Engineering and Physics 1995;17:347-55.
181. Hodgskinson R, Currey JD. Young's modulus, density and material properties in cancellous bone over a large density range. Journal of Materials Science: Materials in Medicine 1992;3:377-81.
182. Snyder SM, Schneider E. Estimation of mechanical properties of cortical bone by computed tomography. Journal of Orthopaedic Research 1991;9:422-31.
183. Farrokhi S, Piva SR, Gil AB, Oddis CV, Brooks MM, Fitzgerald GK. Association of severity of coexisting patellofemoral disease with increased impairments and functional limitations in patients with knee osteoarthritis. Arthritis Care & Research 2013;65:544-51.
184. Cooper C, McAlindon T, Coggon D, Egger P, Dieppe PA. Occupational activity and osteoarthritis of the knee. Annals of the Rheumatic Diseases 1994;53:90-3.

185. Dieppe P, Lohmander L. Pathogenesis and management of pain in osteoarthritis. The Lancet 2005;365:965-73.
186. Chen B, Pei G-x, Jin D, Wei K-h, Qin Y, Qing-si L. Distribution and property of nerve fibers in human long bone tissue. Chinese Journal of Traumatology 2007;10:3-9.
187. Buckland-Wright C. Subchondral bone changes in hand and knee osteoarthritis detected by radiography. Osteoarthritis and Cartilage 2004;12:10.
188. Bobinac D, Spanjol J, Zoricic S, Maric I. Changes in articular cartilage and subchondral bone histomorphometry in osteoarthritic knee joints in humans. Bone 2003;32:284-90.
189. Kamibayashi L, Wyss UP, Cooke TD, Zee B. Trabecular microstructure in the medial condyle of the proximal tibia of patients with knee osteoarthritis. Bone 1995;17:27-35.
190. Ding M, Danielsen CC, Hvid I. Bone density does not reflect mechanical properties in early-stage arthrosis. Acta Orthopaedica Scandinavica 2001;72:181-5.
191. Burt-Pichat B, Lafage-Proust MH, DuBoeuf F, Laroche N, Itzstein C, Vico L, et al. Dramatic decrease of innervation density in bone after ovariectomy. Endocrinology 2005;146:503-10.
192. Mach DB, Rogers SD, Sabino MC, Luger NM, Schwei MJ, Pomonis JD, et al. Origins of skeletal pain: Sensory and sympathetic innervation of the mouse femur. Neuroscience 2002;113:155-66.
193. Radin EL, Paul IL, Rose RM. Role of mechanical factors in pathogenesis of primary osteoarthritis. Lancet 1972;1:519-22.
194. Lo GH, Niu J, McLennan CE, Kiel DP, McLean RR, Guermazi A, et al. Meniscal damage associated with increased local subchondral bone mineral density: a Framingham study. Osteoarthritis and Cartilage 2007;16:261-7.
195. Milz S, Eckstein F, Putz R. The thickness of the subchondral plate and its correlation with the thickness of the uncalcified articular cartilage in the human patella. Anatomy and Embryology (Berlin) 1995;192:437-44.
196. Kontulainen SA, Johnston JD, Liu D, Leung C, Oxland TR, McKay HA. Strength indices from pQCT imaging predict up to 85% of variance in bone failure properties at tibial epiphysis and diaphysis. Journal of Musculoskeletal and Neuronal Interactions 2008;8:401-9.

197. Lyyra T, Jurvelin J, Pitkanen P, Vaatainen U, Kiviranta I. Indentation instrument for the measurement of cartilage stiffness under arthroscopic control. Medical Engineering and Physics 1995;17:395-9.
198. Kontulainen S, Liu D, Manske S, Jamieson M, Sievänen H, McKay H. Analyzing cortical bone cross-sectional geometry by peripheral QCT: comparison with bone histomorphometry. Journal of Clinical Densitometry 2007;10:86-92.
199. Spoor CF, Zonneveld FW, Macho GA. Linear measurements of cortical bone and dental enamel by computed tomography: Applications and Problems. American Journal of Physical Anthropology 1993;91:469-84.
200. Frank AW, Labas MC, Johnston JD, Kontulainen SA. Site-specific variance in radius and tibia bone strength as determined by muscle size and body mass. Physiotherapy Canada 2012;64:292-301.
201. Hulet C, Sabatier JP, Souquet D, Locker B, Marcelli C, Vielpeau C. Distribution of bone mineral density at the proximal tibia in knee osteoarthritis. Calcified Tissue International 2002;71:315-22.
202. Ahlborg HG, Nguyen ND, Nguyen TV, Center JR, Eisman JA. Contribution of hip strength indices to hip fracture risk in elderly men and women. Journal of Bone and Mineral Research 2005;20:1820-7.
203. Hunter DJ, Sharma L, Skaife T. Alignment and osteoarthritis of the knee. The Journal of Bone and Joint Surgery 2009;91:85-9.
204. Sabokbar A, Crawford R, Murray DW, Athanasou NA. Macrophage-osteoclast differentiation and bone resorption in osteoarthrotic subchondral acetabular cysts. Acta Orthopaedica Scandinavica 2000;71:255-61.
205. von Rechenberg B, Leutenegger C, Zlinsky K, McIlwraith CW, Akens MK, Auer JA. Upregulation of mRNA of interleukin-1 and -6 in subchondral cystic lesions of four horses. Equine Veterinary Journal 2001;33:143-9.
206. McErlain DD, Ulici V, Darling M, Gati JS, Pitelka V, Beier F, et al. An in vivo investigation of the initiation and progression of subchondral cysts in a rodent model of secondary osteoarthritis. Arthritis Research & Therapy 2012;14:R26.
207. Fondi C, Franchi A. Definition of bone necrosis by the pathologist. Clinical Cases of Mineral and Bone Metabolism 2007;4:21-6.

208. Theodorou SJ, Theodorou DJ, Resnick D. Osteonecrosis of the patella: diagnostic imaging perspective. Journal of Computer Assisted Tomography 2005;29:87-93.
209. Burnett WD, Kontulainen SA, McLennan CE, Hazel D, Talmo C, Hunter DJ, et al. Knee osteoarthritis patients with severe nocturnal pain have altered proximal tibial subchondral bone mineral density. Osteoarthritis and Cartilage 2015;23:1483-90.
210. Day JS, Ding M, van der Linden JC, Hvid I, Sumner DR, Weinans H. A decreased subchondral trabecular bone tissue elastic modulus is associated with pre-arthritic cartilage damage. Journal of Orthopaedic Research 2001;19:914-8.
211. Carter DR, Hayes WC. The compressive behavior of bone as a two-phase porous structure. Journal of Bone and Joint Surgery (Am) 1977;59:954-62.
212. Sangha O, Stucki G, Liang MH, Fossel AH, Katz JN. The Self-Admininstered Comorbidity Questionnaire: A new method to assess comorbidity for clinical and health services research. Arthritis & Rheumatism 2003;49:156-63.
213. Glüer CC, Blake G, Lu Y, Blunt BA, Jergas M, Genant HK. Accurate assessment of precision errors: how to measure the reproducibility of bone densitometry techniques. Osteoporosis International 1995;5:262-70.
214. Chen Y, Huang Y-C, Lu WW. Is subchondral bone mineral density associated with nocturnal pain in knee osteoarthritis patients? Osteoarthritis and Cartilage 2015;23:2297-8.
215. Schneider A, G H, Blettner. Linear Regression Analysis. Deutsches Ârzteblatt International 2010;107:776-82.
216. Thompson R. A note on restricted maximum likelihood estimation with an alternative outlier model. Journal of the Royal Statistical Society Series B (Methodological) 1985;47:53-5.
217. Burnett W, Kontulainen S, McLennan C, Hazel D, Talmo C, Hunter D, et al. Response to Letter to the Editor: 'Is subchondral bone mineral density associated with nocturnal pain in knee osteoarthritis patients?'. Osteoarthritis and Cartilage 2015;23:2299-301.
218. Hertz VHH. Uber die Berührung fester elastischer Körper. Journal für die reine und angewandte Mathematik 1882;92:156-71.
219. Peduzzi P, Concato J, Kemper E, Holford TR, Feinstein AR. A simulation study of the number of events per variable in logistic regression analysis. Journal of Clinical Epidemiology 1996;49:1373-9.

220. Rantalainen T, Nikander R, Daly RM, Heinonen A, Sievanen H. Exercise loading and cortical bone distribution at the tibial shaft. Bone 2011;48:786-91.
221. Wasserstein R, Lazar N. The ASA's statements on p-values: context, process, and purpose. The American Statistician 2016;70:129-33.
222. Angst F, Aeschlimann A, Stucki G. Smallest detectable and minimal clinically important differences of rehabilitation intervention with their implications for required sample sizes using WOMAC and SF-36 Quality of Life measurement instruments in patients with osteoarthritis of the lower extremities. Arthritis Care & Research 2001;45:384-91.
223. Petersen MM, Nielsen PT, Lebech A, Toksvig-Larsen S, Lund B. Preoperative bone mineral density of the proximal tibia and migration of the tibial compartment after uncemented total knee arthroplasty. Journal of Arthroplasty 1999;14:77-81.
224. Levitz CL, Lotke PA, Karp JS. Long-term changes in bone mineral density following total knee replacement. Clinical Orthopaedics and Related Research 1995;321:68-72.
225. Mavrogenis AF, Dimitriou R, Parvizi J, Babis GC. Biology of implant osseointegration. Journal of Musculoskeletal and Neuronal Interactions 2009;9:61-71.
226. Sharkey PF, Hozack WJ, Rothman RH, Shastri S, Jacoby SM. Why are total knee arthroplasties failing today? Clinical Orthopaedics and Related Research 2002;404:7-13.
227. Ritter MA, Davis KE, Small SR, Merchun JG, Farris A. Trabecular bone density of the proximal tibia as it relates to failure of a total knee replacement. The Bone & Joint Journal 2014;96-B:1503-9.
228. Crema MD, Roemer FW, Marra MD, Niu J, Lynch JA, Felson DT, et al. Contrast-enhanced MRI of subchondral cysts in patients with or at risk for knee osteoarthritis: The MOST study. European Journal of Radiology 2010;75:e92-e6.
229. Tanamas SK, Wluka AE, Pelletier JP, Martel-Pelletier J, Abram F, Wang Y, et al. The association between subchondral bone cysts and tibial cartilage volume and risk of joint replacement in people with knee osteoarthritis: a longitudinal study. Arthritis Research & Therapy 2010;12:R58.
230. Roemer FW, Eckstein F, Guermazi A. Magnetic Resonance Imaging-Based Semiquantitative and Quantitative Assessment in Osteoarthritis. Rheumatic Disease Clinics of North America 2009;35:521-55.

231. UNSCEAR 2000 Report to the General Assembly - Volume 1. United Nations Scientific Committee on the Effects of Atomic Radiation2000.
232. Burnett W, Kontulainen S, McLennan C, Hazel D, Talmo C, Wilson D, et al. Proximal tibial trabecular bone mineral density is related to pain in patients with osteoarthritis. Arthritis Research & Therapy 2017;19:200.
233. Frazer LL, Santschi EM, Fischer KJ. The impact of subchondral bone cysts on local bone stresses in th emedial femoral condyle of the equine stifle joint. Medical Engineering and Physics 2017;48:158-67.
234. Machado M, Flores P, Ambrosio J, Completo A. Influence of the contact model on the dynamic response of the human knee joint. Proceedings of the Institution of Mechanical Engineers Part K: Journal of Multi-body Dynamics 2011;225:344-58.
235. Werner FW, Ayers DC, Maletsky LP, Rullkoetter PJ. The effect of valgus/varus malalignment on load distribution in total knee replacements. Journal of Biomechanics 2005;38:349-55.
236. Hsu H-P, Garg A, Walker PS, Spector M, Ewald FC. Effect of knee compartment alignment on tibial load distribution with clinical correlation. Clinical Orthopaedics and Related Research 1989;248:135-44.
237. Johnson F, Leitl S, Waugh W. The distribution of load across the knee. The Journal of Bone and Joint Surgery 1980;62:346-9.
238. Mercadante S. Malignant bone pain: Pathophysiology and treatment. Pain 1997;69:1-18.
239. Lerner ZF, DeMers MS, Delp SL, Browning RC. How tibiofemoral alignment and contact locations affect predictions of medial and lateral tibiofemoral contact forces. Journal of Biomechanics 2015;48:644-50.
240. Buckland-Wright JC, Macfarlane DG, Lynch JA, Jasani MK, Bradshaw CR. Joint space width measures cartilage thickness in osteoarthritis of the knee: high resolution plain filmand double contrast macroradiographic investigation. Annals of Rheumatic Diseases 1995;54:263-8.
241. Tuncer M, Hansen UN, Amis AA. Prediction of the structural failure of tibial bone models under physiological loads: Effect of CT density-modulus relationships. Medical Engineering and Physics 2014;36:991-7.

242. Vijayakumar V, Quenneville CE. Quantifying the regional variations in the mechanical properties of cancellous bone of the tibia using indentation testing and quantitative computed tomographic imaging. Proceedings of the Institution of Mechanical Engineers Part H, Journal of Engineering in Medicine 2016;230:588-93.
243. Carey RE, Zheng L, Aiyangar AK, Harner CD, Zhang X. Subject-specific finite element modeling of the tibiofemoral joint based on CT, magnetic resonance imaging and dynamic stereo-radiography data in vivo. Journal of Biomechanical Engineering 2014;136:041004--8.
244. Kazemi M, Dabiri Y, Li LP. Recent advances in computational mechanics of the human knee joint. Computational and Mathematical Methods in Medicine 2013;2013:718423.
245. Wang Y, Wluka AE, Cicuttini FM. The determinants of change in tibial plateau bone area in osteoarthritic knees: a cohort study. Arthritis Research & Therapy 2005;7:R687.
246. Bendjaballah MZ, Shirazi-Adl A, Zukor DJ. Finite element analysis of human knee joint in varus-valgus. Clinical Biomechanics 1997;12:139-48.
247. Klets O, Mononen ME, Liukkonen ML, Nevalainen MT, Nieminen MT, Saarakkala S, et al. Estimation of the effect of body weight on the development of osteoarthritis based on cumulative stresses in cartilage: Data from the Osteoarthritis Initiative. Annals of Biomedical Engineering 2018;34:334-44.
248. Dar FH, Aspden RM. A finite element model of an idealized diarthrodial joint to investigate the effects of variation in the mechanical properties of the tissues. Proceedings of the Institution of Mechanical Engineers Part H, Journal of Engineering in Medicine 2003;217:341-8.
249. Katz JN, Meredith DS, Lang P, Creel AH, Yoshioka H, Neumann G, et al. Associations among preoperative MRI features and functional status following arthroscopic partial meniscectomy. Osteoarthritis and Cartilage 2006;14:418-22.
250. Baca V, Horak Z, Mikulenka P, Dzupa V. Comparison of an inhomogeneous orthotropic and isotrapic material models used for FE analyses. Medical Engineering and Physics 2008;30:924-30.
251. Kroker A, Zhu Y, Manske SL, Barber R, Mohtadi N, Boyd SK. Quantitative in vivo assessment of bone microarchitecture in the human knee using HR-pQCT. Bone 2017;97:43-8.

252. Muller-Gerbl M, Putz R, Hodapp N, Schulte E, Wimmer B. Computed tomography-osteoabsorptiometry for assessing the density distribution of subchondral bone as a measure of long-term mechanical adaptation in individual joints. Skeletal Radiology 1989;18.
253. Hoechel S, Wirz D, Müller-Gerbl M. Density and strength distribution in the human subchondral bone plate of the patella. International Orthopaedics 2012;36:1827-34.
254. Brandt KD, Myers SL, Burr D, Albrecht M. Osteoarthritic changes in canine articular cartilage, subchondral bone, and synovium fifty-four months after transection of the anterior cruciate ligament. Arthritis & Rheumatism 1991;34:1560-70.
255. Dedrick DK, Goldstein SA, Brandt KD, O'Connor BL, Goulet RW, Albrecht M. A longitudinal study of subchondral plate and trabecular bone in cruciate-deficient dogs with osteoarthritis followed up for 54 months. Arthritis & Rheumatism 1993;36:1460-7.
256. Boyd SK, Matyas JR, Wohl GR, Kantzas A, Zernicke RF. Early regional adaptation of periarticular bone mineral density after anterior cruciate ligament injury. Journal of Applied Physiology 2000;89:2359-64.
257. Nazemi M, Amini M, Kontulainen SA, Milner JS, Holdsworth DW, Masri BA, et al. Optimizing finite element predictions of local subchondral bone structural stiffness using neural network-derived density-modulus relationships for proximal tibial subchondral cortical and trabecular bone. Clinical Biomechanics 2017;41:1-8.
258. Van Der Linden JC, Birkenhäger-Frenkel DH, Verhaar JA, Weinans H. Trabecular bone's mechanical properties are affected by its non-uniform mineral distribution. Journal of Biomechanics 2001;34:1573-80.
259. Zebaze RM, Jones AC, Pandy M, Knackstedt M, Seeman E. Differences in the degree of bone tissue mineralization account for little of the difference in tissue elastic properties. Bone 2011;48:1246-51.
260. van Ruijven LJ, Mulder L, van Eijden TM. Variation in mineralization affect the stress and strain distributions in cortical and trabecular bone. Journal of Biomechanics 2007;40:1211-8.
261. Burr D. Anatomy and physiology of the mineralized tissues: Role in the pathogenesis of osteoarthrosis. Osteoarthritis and Cartilage 2004;12:S20-30.

262. Burr DB, Forwood MR, Fyhrie DP, Martin RB, Schaffler MB, Turner CH. Bone microdamage and skeletal fragility in osteoporotic and stress fractures. Journal of Bone and Mineral Research 1997;12:6-15.
263. Radin EL, Martin RB, Burr DB, Caterson B, Boyd RD, Goodwin C. Effects of mechanical loading on the tissues of the rabbit knee. Journal of Orthopaedic Research 1984;2:221-34.
264. Frost HM. The pathomechanics of osteoporoses. Clinical Orthopaedics and Related Research 1985;200:198-225.
265. Simkin PA. Bone pain and pressure in osteoarthritic joints. In: Chadwick DJ, Goode J, editors. Osteoarthritis Joint Pain. Chichester: John Wiley & Sons Ltd.; 2004. p. 179-90.
266. Simkin PA. Osteoarthritis and knee pain. Annals of Internal Medicine. 2002;136:630.
267. Keyak JH, Rossi SA, Jones KA, Skinner HB. Prediction of femoral fracture load using automated finite element modeling. Journal of Biomechanics 1998;31:125-33.

APPENDIX

Supplemental Tables for von Mises stress and strain from finite element analysis.

Table A-1. Goulet's density-modulus conversion relationships used in FE models

Relationship	Citation
$E=6310\left(BV/TV\right)^{2.1}$	Goulet et al.[179]
$\rho_{ash}=0.55\rho_{app}$	Helgason et al.[170]
$\rho_{real}=1.8\ g/cm^3$	Carter et al.[211]
$\rho_{app}=\rho_{real}\times BV/TV$	Helgason et al.[170]
$\rho_{ash}=1.06\ BMD+0.0389$	Keyak et al.[267]

Table A-2. Spearman's rank correlation coefficients (ρ) for relationships between regional von Mises stress and OA characteristics (OA severity, total WOMAC pain, nocturnal pain, and alignment). For alignment, positive relationships represent associations with valgus alignment, and negative relationships represent associations with varus alignment. Bolded values indicate $p < 0.05$.

Region	OA severity (KL score)		Total WOMAC pain		Nocturnal pain		Alignment	
	ρ	*p*-value	ρ	*p*-value	ρ	*p*-value	ρ	*p*-value
Medial peripheral cortical	**0.32**	**0.048**	0.01	0.942	-0.18	0.266	**-0.54**	**<0.001**
Medial epiphyseal cortical	**0.37**	**0.018**	0.20	0.205	0.004	0.980	**-0.50**	**0.001**
Medial metaphyseal cortical	0.13	0.435	0.13	0.406	-0.15	0.341	**-0.57**	**<0.001**
Medial subchondral cortical	-0.18	0.261	-0.14	0.365	-0.20	0.202	**-0.38**	**0.012**
Medial subchondral trabecular	-0.04	0.831	-0.08	0.608	-0.19	0.230	**-0.59**	**<0.001**
Medial epiphyseal trabecular	0.06	0.726	0.02	0.880	-0.23	0.152	**-0.66**	**<0.001**
Medial meatphyseal trabecular	0.01	0.931	-0.05	0.771	-0.23	0.150	**-0.61**	**<0.001**
Subchondral spine	0.12	0.477	0.27	0.087	0.27	0.079	**0.40**	**0.009**
Epiphyseal central	-0.10	0.534	0.17	0.292	0.21	0.179	**0.31**	**0.045**
Metaphyseal central	**-0.31**	**0.049**	-0.04	0.780	0.11	0.481	0.21	0.188
Lateral subchondral cortical	-0.04	0.791	0.19	0.223	**0.44**	**0.003**	**0.71**	**<0.001**
Lateral subchondral trabecular	0.01	0.957	0.20	0.204	**0.42**	**0.006**	**0.68**	**<0.001**
Lateral epiphyseal trabecular	0.04	0.787	0.20	0.211	**0.35**	**0.023**	**0.59**	**<0.001**
Lateral metaphyseal trabecular	-0.05	0.773	0.18	0.249	**0.32**	**0.036**	**0.66**	**<0.001**
Lateral peripheral cortical	0.05	0.781	**0.44**	**0.004**	**0.50**	**0.001**	**0.60**	**<0.001**
Lateral epiphyseal cortical	0.18	0.268	**0.48**	**0.001**	**0.40**	**0.009**	**0.48**	**0.001**
Lateral metaphyseal cortical	0.25	0.121	0.28	0.076	**0.32**	**0.036**	**0.60**	**<0.001**

Table A-3. Spearman's rank correlation coefficients (ρ) for relationships between regional von Mises strain and OA characteristics (OA severity, total WOMAC pain, nocturnal pain, and alignment). For alignment, positive relationships represent associations with valgus alignment, and negative relationships represent associations with varus alignment. Bolded values indicate $p < 0.05$.

Region	OA Severity (KL Score)		Total WOMAC pain		Nocturnal pain		Alignment	
	ρ	*p*-value	ρ	*p*-value	ρ	*p*-value	ρ	*p*-value
Medial peripheral cortical	-0.15	0.355	0.20	0.126	0.26	0.102	**0.55**	**<0.001**
Medial epiphyseal cortical	-0.001	0.996	0.16	0.301	0.22	0.170	**0.50**	**0.001**
Medial metaphyseal cortical	0.25	0.114	0.16	0.306	0.23	0.137	**0.40**	**0.009**
Medial subchondral cortical	-0.19	0.249	0.15	0.341	0.13	0.425	**0.58**	**<0.001**
Medial subchondral trabecular	-0.06	0.701	0.20	0.202	0.17	0.284	**0.56**	**<0.001**
Medial epiphyseal trabecular	0.01	0.977	0.21	0.173	0.22	0.171	**0.52**	**<0.001**
Medial meatphyseal trabecular	0.19	0.251	0.20	0.196	0.28	0.074	**0.47**	**0.002**
Subchondral spine	-0.19	0.239	0.11	0.507	0.15	0.356	**0.39**	**0.010**
Epiphyseal central	0.02	0.913	0.20	0.195	0.17	0.278	**0.51**	**0.001**
Metaphyseal central	0.12	0.475	0.28	0.072	**0.33**	**0.032**	**0.55**	**<0.001**
Lateral subchondral cortical	0.05	0.779	0.10	0.513	0.003	0.985	-0.05	0.736
Lateral subchondral trabecular	0.002	0.992	0.14	0.384	0.04	0.802	0.04	0.824
Lateral epiphyseal trabecular	0.03	0.861	0.26	0.098	0.17	0.283	**0.48**	**0.001**
Lateral metaphyseal trabecular	0.02	0.906	0.30	0.053	0.27	0.077	**0.53**	**<0.001**
Lateral peripheral cortical	-0.03	0.872	0.18	0.247	0.001	0.994	0.10	0.538
Lateral epiphyseal cortical	-0.07	0.683	0.28	0.070	0.20	0.201	**0.49**	**0.001**
Lateral metaphyseal cortical	-0.01	0.947	0.19	0.219	0.24	0.135	**0.66**	**<0.001**

Table A-4. Comparison of regional von Mises stress in patients with knee OA with no pain and moderate pain, including mean ± standard deviation (SD), adjusted mean difference, percent difference from no pain, 95% confidence intervals (CI), and *p*-values. Bolded values indicate $p<0.05$.

Region	von Mises stress (MPa)		Mean Difference* from No Pain (%)	95% confidence interval		*p*-value
	No Pain	Moderate Pain		Lower limit	Upper limit	
	Mean ± SD	Mean ± SD				
Medial peripheral cortical	0.46 ± 0.14	0.50 ± 0.20	0.02 (21.%)	-0.13	0.16	1.000
Medial epiphyseal cortical	0.69 ± 0.23	0.81 ± 0.33	0.06 (8.3%)	-0.18	0.30	1.000
Medial metaphyseal cortical	1.84 ± 0.62	1.87 ± 0.63	-0.04 (-2.6%)	-0.58	0.49	1.000
Medial subchondral cortical	0.62 ± 0.15	0.60 ± 0.13	-0.04 (-6.3%)	-0.16	0.08	1.000
Medial subchondral trabecular	0.49 ± 0.15	0.48 ± 0.13	-0.04 (-8.0%)	-0.16	0.08	1.000
Medial epiphyseal trabecular	0.38 ± 0.14	0.35 ± 0.11	-0.04 (-10.3%)	-0.16	0.07	1.000
Medial metaphyseal trabecular	0.42 ± 0.18	0.42 ± 0.20	-0.01 (-2.4%)	-0.17	0.16	1.000
Subchondral spine	0.28 ± 0.07	0.32 ± 0.10	0.03 (14.3%)	-0.05	0.11	0.955
Central epiphyseal trabecular	0.12 ± 0.03	0.13 ± 0.03	0.01 (0.0%)	-0.02	0.04	1.000
Central metaphyseal trabecular	0.09 ± 0.03	0.09 ± 0.02	-0.001 (0.0%)	-0.02	0.02	1.000
Lateral subchondral cortical	0.40 ± 0.09	0.49 ± 0.23	0.09 (22.5%)	-0.08	0.27	0.590
Lateral subchondral trabecular	0.26 ± 0.07	0.31 ± 0.16	0.05 (19.2%)	-0.07	0.17	0.849
Lateral epiphyseal trabecular	0.16 ± 0.04	0.18 ± 0.08	0.02 (12.5%)	-0.04	0.08	1.000
Lateral metaphyseal trabecular	0.14 ± 0.03	0.15 ± 0.06	0.02 (15.4%)	-0.03	0.07	1.000
Lateral peripheral cortical	0.23 ± 0.08	0.30 ± 0.13	0.07 (30.4%)	-0.03	0.17	0.298
Lateral epiphyseal cortical	0.28 ± 0.10	0.36 ± 0.14	0.06 (20.0%)	-0.04	0.16	0.471
Lateral metaphyseal cortical	0.68 ± 0.15	0.81 ± 0.32	0.12 (15.7%)	-0.13	0.36	0.721

*Mean values adjusted for age (64.1) and sex (1.6)..

Table A-5. Comparison of regional von Mises stress in patients with knee OA with no pain and severe pain, including mean ± standard deviation (SD), adjusted mean difference, percent difference from 'no pain', 95% confidence intervals (CI), and *p*-values. Bolded values indicate $p<0.05$.

Region	von Mises stress (MPa)		Mean Difference* from No Pain (%)	95% confidence interval		*p*-value
	No Pain	Severe Pain		Lower limit	Upper limit	
	Mean ± SD	Mean ± SD				
Medial peripheral cortical	0.46 ± 0.14	0.35 ± 0.13	-0.13 (-27.1%)	-0.30	0.04	0.192
Medial epiphyseal cortical	0.69 ± 0.23	0.58 ± 0.29	-0.15 (-20.8%)	-0.44	0.13	0.560
Medial metaphyseal cortical	1.84 ± 0.62	1.51 ± 0.45	-0.41 (-21.7%)	-1.04	0.22	0.334
Medial subchondral cortical	0.62 ± 0.15	0.55 ± 0.15	-0.09 (-14.3%)	-0.23	0.06	0.427
Medial subchondral trabecular	0.49 ± 0.15	0.38 ± 0.15	-0.12 (-24.0%)	-0.27	0.02	0.125
Medial epiphyseal trabecular	0.38 ± 0.14	0.28 ± 0.12	-0.11 (-28.2%)	-0.24	0.03	0.163
Medial metaphyseal trabecular	0.42 ± 0.18	0.32 ± 0.14	-0.11 (-23.8%)	-0.30	0.09	0.521
Subchondral spine	0.28 ± 0.07	0.33 ± 0.10	0.04 (17.9%)	-0.05	0.14	0.762
Central epiphyseal trabecular	0.12 ± 0.03	0.14 ± 0.04	0.02 (16.7%)	-0.01	0.06	0.274
Central metaphyseal trabecular	0.09 ± 0.03	0.11 ± 0.03	0.01 (22.2%)	-0.01	0.04	0.472
Lateral subchondral cortical	0.40 ±0.09	0.66 ± 0.27	0.25 (62.5%)	0.05	0.48	**0.011**
Lateral subchondral trabecular	0.26 ±0.07	0.44 ± 0.17	0.09 (65.4%)	0.08	0.27	**0.010**
Lateral epiphyseal trabecular	0.16 ± 0.04	0.24 ± 0.08	0.08 (50.0%)	0.01	0.15	**0.028**
Lateral metaphyseal trabecular	0.14 ± 0.03	0.20 ± 0.08	0.06 (53.8%)	0.003	0.12	**0.038**
Lateral peripheral cortical	0.23 ± 0.08	0.37 ± 0.16	0.13 (56.5%)	0.02	0.25	**0.021**
Lateral epiphyseal cortical	0.28 ± 0.10	0.39 ± 0.14	0.08 (26.7%)	-0.04	0.20	0.272
Lateral metaphyseal cortical	0.68 ± 0.15	0.95 ± 0.40	0.24 (32.9%)	-0.05	0.53	0.142

*Mean values adjusted for age (64.1) and sex (1.6).

Table A-6. Comparison of regional von Mises strain in patients with knee OA with no pain and moderate pain, including mean ± standard deviation (SD), adjusted mean difference, percent difference from no pain, 95% confidence intervals (CI), and *p*-values. Bolded values indicate $p<0.05$.

Region	von Mises strain (microstrain)		Mean Difference* from No Pain (%)	95% confidence interval		p-value
	No Pain	Moderate Pain		Lower limit	Upper limit	
	Mean ± SD	Mean ± SD				
Medial peripheral cortical	840 ± 590	1021 ± 567	210 (25.2%)	-364	784	1.000
Medial epiphyseal cortical	1281 ± 638	1437 ± 590	217 (17.2%)	-360	794	1.000
Medial metaphyseal cortical	1284 ± 524	1470 ± 540	179 (13.8%)	-320	678	1.000
Medial subchondral cortical	446 ± 204	495 ± 229	55 (12.3%)	-150	259	1.000
Medial subchondral trabecular	767 ± 407	935 ± 546	226 (30.3%)	-255	707	0.741
Medial epiphyseal trabecular	2079 ± 1010	2454 ± 1032	465 (24.7%)	-506	1436	0.713
Medial metaphyseal trabecular	2073 ± 837	2349 ± 860	249 (11.9%)	-578	1075	1.000
Subchondral spine	550 ± 171	589 ± 218	55 (10.1%)	-127	237	1.000
Central epiphyseal trabecular	2238 ± 872	2493 ± 855	301 (13.5%)	-497	1098	1.000
Central metaphyseal trabecular	1769 ± 770	1938 ± 702	155 (8.7%)	-559	869	1.000
Lateral subchondral cortical	649 ± 195	684 ± 229	32 (4.9%)	-156	220	1.000
Lateral subchondral trabecular	1085 ± 402	1133 ± 493	52 (4.8%)	-339	443	1.000
Lateral epiphyseal trabecular	2149 ± 939	2338 ± 875	213 (9.9%)	-578	1005	1.000
Lateral metaphyseal trabecular	1786 ± 937	1883 ± 832	77 (4.2%)	-715	870	1.000
Lateral peripheral cortical	1121 ± 498	1249 ± 583	104 (9.1%)	-366	575	1.000
Lateral epiphyseal cortical	1089 ± 580	1143 ± 506	67 (6.1%)	-416	551	1.000
Lateral metaphyseal cortical	714 ± 446	796 ± 428	107 (15.3%)	-292	507	1.000

*Mean values adjusted for age (64.1) and sex (1.6).

Table A-7. Comparison of regional von Mises strain in patients with knee OA with no pain and severe pain, including mean ± standard deviation (SD), adjusted mean difference, percent difference from no pain, 95% confidence intervals (CI), and *p*-values. Bolded values indicate $p<0.05$.

Region	von Mises strain (microstrain)		Mean Difference* from No Pain (%)	95% confidence interval		*p*-value
	No Pain	Severe Pain		Lower limit	Upper limit	
	Mean ± SD	Mean ± SD				
Medial peripheral cortical	840 ± 590	1377 ± 924	516 (62.1%)	-158	1190	0.187
Medial epiphyseal cortical	1281 ± 638	1720 ± 923	440 (35.0%)	-237	1118	0.335
Medial metaphyseal cortical	1284 ± 524	1624 ± 596	314 (25.6%)	-271	900	0.559
Medial subchondral cortical	446 ± 204	569 ± 289	112 (25.1%)	-128	352	0.743
Medial subchondral trabecular	767 ± 407	1150 ± 823	396 (53.3%)	-169	961	0.260
Medial epiphyseal trabecular	2079 ± 1010	2859 ± 1580	771 (37.7%)	-369	1911	0.295
Medial metaphyseal trabecular	2073 ± 837	2882 ± 1100	751 (37.5%)	-219	1721	0.180
Subchondral spine	550 ± 171	676 ± 241	130 (23.9%)	-83	344	0.405
Central epiphyseal trabecular	2238 ± 872	2869 ± 1227	594 (26.7%)	-342	1530	0.360
Central metaphyseal trabecular	1769 ± 770	2548 ± 954	732 (51.8%)	-105	1570	0.104
Lateral subchondral cortical	649 ± 195	632 ± 172	-15 (-2.3%)	-235	206	1.000
Lateral subchondral trabecular	1085 ± 402	1006 ± 310	-84 (-7.7%)	-543	376	1.000
Lateral epiphyseal trabecular	2149 ± 939	2599 ± 1048	397 (18.5%)	-532	1326	0.873
Lateral metaphyseal trabecular	1786 ± 937	2570 ± 1009	699 (44.8%)	-231	1629	0.202
Lateral peripheral cortical	1121 ± 498	1097 ± 393	-62 (-5.4%)	-614	491	1.000
Lateral epiphyseal cortical	1089 ± 580	1478 ± 646	354 (32.4%)	-213	921	0.378
Lateral metaphyseal cortical	714 ± 446	1101 ± 595	372 (41.9%)	-98	842	0.163

*Mean values adjusted for age (64.1) and sex (1.6).